INFORMATION TO USERS

This manuscript has been reproduced from the microfilm master. UMI films the text directly from the original or copy submitted. Thus, some thesis and dissertation copies are in typewriter face, while others may be from any type of computer printer.

The quality of this reproduction is dependent upon the quality of the copy submitted. Broken or indistinct print, colored or poor quality illustrations and photographs, print bleedthrough, substandard margins, and improper alignment can adversely affect reproduction.

In the unlikely event that the author did not send UMI a complete manuscript and there are missing pages, these will be noted. Also, if unauthorized copyright material had to be removed, a note will indicate the deletion.

Oversize materials (e.g., maps, drawings, charts) are reproduced by sectioning the original, beginning at the upper left-hand corner and continuing from left to right in equal sections with small overlaps.

Photographs included in the original manuscript have been reproduced xerographically in this copy. Higher quality 6" x 9" black and white photographic prints are available for any photographs or illustrations appearing in this copy for an additional charge. Contact UMI directly to order.

Bell & Howell Information and Learning
300 North Zeeb Road, Ann Arbor, MI 48106-1346 USA
800-521-0600

UMI®

KINETICS AND MECHANISMS OF THE FORMATION AND DISSOLUTION OF NICKEL(II) SURFACE PRECIPITATES ON CLAY MINERALS AND METAL OXIDES USING MACROSCOPIC, SPECTROSCOPIC, MICROSCOPIC, AND THERMOGRAVIMETRIC TECHNIQUES

by

Kirk Gerald Scheckel

A dissertation submitted to the Faculty of the University of Delaware in partial fulfillment of the requirements for the degree of Doctor of Philosophy with a major in Plant and Soil Sciences

Spring 2000

UMI Number: 9965811

UMI Microform9965811

Bell & Howell Information and Learning Company
300 North Zeeb Road
P.O. Box 1346
Ann Arbor, MI 48106-1346

KINETICS AND MECHANISMS OF THE FORMATION AND DISSOLUTION OF NICKEL(II) SURFACE PRECIPITATES ON CLAY MINERALS AND METAL OXIDES USING MACROSCOPIC, SPECTROSCOPIC, MICROSCOPIC, AND THERMOGRAVIMENTRIC TECHNIQUES

by

Kirk Gerald Scheckel

Approved: Donald L. Sparks
Donald. L. Sparks, Ph.D.
Chairman, Department of Plant and Soil Sciences

Approved: John C Nye
John C. Nye, Ph.D.
Dean, College of Agriculture and Natural Resources

Approved:
Conrado M. Gempesaw II, Ph.D.
Vice Provost for Academic Programs and Planning

I certify that I have read this dissertation and that in my opinion it meets the academic and professional standard required by the University as a dissertation for the degree of Doctor of Philosophy.

Signed: Donald L. Sparks

Donald L. Sparks, Ph.D.
Professor in charge of dissertation

I certify that I have read this dissertation and that in my opinion it meets the academic and professional standard required by the University as a dissertation for the degree of Doctor of Philosophy.

Signed: Yan Jin

Yan Jin, Ph.D.
Member of dissertation committee

I certify that I have read this dissertation and that in my opinion it meets the academic and professional standard required by the University as a dissertation for the degree of Doctor of Philosophy.

Signed: George W. Luther III

George W. Luther, III, Ph.D.
Member of dissertation committee

I certify that I have read this dissertation and that in my opinion it meets the academic and professional standard required by the University as a dissertation for the degree of Doctor of Philosophy.

Signed: David R. Veblen

David R. Veblen, Ph.D.
Member of dissertation committee

EPIGRAPH

To laugh often and much; to win the respect of intelligent people and affection of children; to earn the appreciation of honest critics and endure the betrayal of false friends; to appreciate beauty, find the best in others; to leave the world a bit better, whether by a healthy child, a garden patch or a redeemed social condition; to know even one life has breathed easier because you have lived. This is to have succeeded!

-- Ralph Waldo Emerson

ACKNOWLEDGMENTS

My parents, Gerald, Betty, Nathan, and Neta, for their love, support, and understanding in achieving this goal. Their thoughts and prayers were always felt and held close to my heart.

Donald L. Sparks, Ph.D., for his fatherly advice and counsel. I truly appreciate his efforts to help me become the best in my career endeavors and for starting me down the path of professional growth and development.

The Environmental Soil Chemistry Group at the University of Delaware for bringing a family atmosphere into the work environment.

My Ph.D. committee, professional friends, colleagues, and instructors, who have supported and helped me throughout my undergraduate and graduate education.

This manuscript is dedicated to:

My daughter, Madeline, for her precious smile and bright eyes that make me realize that my first and most important duty in life is to be "da-da-da-da-da".

My wife, Christina, to whom I owe a debt of sincere gratitude for her unconditional love, encouragement, and support over the past five years. I wish to thank her for her many sacrifices and providing a hand to hold in times of joy and sadness. I could not have accomplished this dream without her.

The memory of my father, Gerald (d. 3/4/2000). Though I miss his smile, jokes, and encouraging words, knowing that his pain does not endure while embraced by God in Heaven comforts my soul. Thank you, dad, for teaching me so much more than I could ever learn in books. I will treasure our memories forever!

TABLE OF CONTENTS

LIST OF TABLES x
LIST OF FIGURES xii
ABSTRACT xix

Chapter

1 **INTRODUCTION** 1

1.1 Rationale and Scope of Research 1
1.2 Literature Review 5

1.2.1 Metal Sorption 5
1.2.2 Dissolution Processes 18
1.2.3 Kinetics of Sorption and Desorption 26

1.2.3.1 Kinetic Models 30
1.2.3.2 Multiple Site Models 33
1.2.3.3 Dissolution Models 36

1.3 Research Objectives and Justification 37

2 **SORPTION OF NI(II) ON CLAY MINERALS AND OXIDES** 45

2.1 Abstract 45
2.2 Introduction 46
2.3 Materials and Methods 52

2.3.1 Materials 52
2.3.2 Ni Sorption Kinetics 53

2.4 Spectroscopic, Microscopic, and Thermogravimetric Characterization of Surface Precipitates 54

2.4.1 X-Ray Absorption Fine Structure (XAFS) Spectroscopy 55
2.4.2 Diffuse Reflectance Spectroscopy (DRS) 57
2.4.3 High Resolution Thermogravimetric Analysis (HRTGA) 57
2.4.4 Atomic Force Microscopy (AFM) 58
2.4.5 High Resolution Transmission Electron Microscopy (HRTEM) 60

2.5 Results 61

2.5.1 Macroscopic Sorption Kinetic Data 61
2.5.2 XAFS Analysis of Sorption Samples 66
2.5.3 DRS Analysis of Sorption Samples 80
2.5.4 HRTGA Investigation of Sorption Samples 83
2.5.5 AFM Analysis of Sorption Samples 88
2.5.6 HRTEM Analysis of Sorption Samples 92

2.6 Conclusions 95

3 INFLUENCE OF TEMPERATURE ON NI(II) SORPTION 99

3.1 Abstract 99
3.2 Introduction 100
3.3 Materials and Methods 107

3.3.1 Materials 107
3.3.2 Temperature and Kinetic Studies 108

3.4 Results and Discussion 109
3.5 Conclusions 121

4 DISSOLUTION OF NI(II) PRECIPITATES ON CLAY MINERALS AND OXIDES 124

4.1 Abstract 124
4.2 Introduction 126
4.3 Materials and Methods 134

4.3.1 Materials 134
4.3.2 Ni Sorption and Kinetics of Dissolution 136
4.3.3 Synthesis of Ni Reference Compounds 138

4.4 Spectroscopic, Microscopic, and Thermogravimetric Characterization of Surface Precipitates 140

4.4.1 X-Ray Absorption Fine Structure (XAFS) Spectroscopy 140
4.4.2 Diffuse Reflectance Spectroscopy (DRS) 142
4.4.3 High Resolution Thermogravimetric Analysis (HRTGA) 143
4.4.4 Atomic Force Microscopy (AFM) 144

4.5 Results 146

4.5.1 Macroscopic Dissolution Kinetic Data 146
4.5.2 XAFS Analysis of Dissolution Samples 156
4.5.3 DRS Analysis of Dissolution Samples 160
4.5.4 HRTGA Investigation of Dissolution Samples 163
4.5.5 AFM Analysis of Dissolution Samples 167

4.6 Discussion 170
4.7 Conclusions 176

5 CONCLUSIONS 178

5.1 Summary of Research 178
5.2 Future Research 182

REFERENCES 186

LIST OF TABLES

2.1 Percent Ni removed from solution during kinetic studies prior to XAFS analysis for each surface. 67

2.2 EXAFS structural parameters of Ni sorbed on pyrophyllite. 75

2.3 EXAFS structural parameters of Ni sorbed on talc. 75

2.4 EXAFS structural parameters of Ni sorbed on gibbsite. 76

2.5 EXAFS structural parameters of Ni sorbed on silica. 76

2.6 EXAFS structural parameters of Ni sorbed on gibbsite/silica mixture. 77

3.1 Summary of energy of activation values for the formation of various surfaces and their formulas. 105

3.2 Apparent first-order forward sorption rate coefficients (k_a') for Ni sorption at three temperatures on clay mineral and oxide surfaces. 114

3.3 Summary of reaction parameters derived from the Arrhenius and Eyring equations for Ni sorption on clay mineral and oxide surfaces. 118

4.1 Relative Ni remaining (%) on one month aged samples after 14 dissolution replenishments. 152

4.2 Structural parameters derived from XAFS analysis for dissolution of nickel precipitates aged for one month on pyrophyllite and talc employing EDTA (pH 7.5) and HNO_3 (pH 4.0). 159

4.3 Solid-state transformation products of Ni precipitates with aging time 173

LIST OF FIGURES

2.1 Ni sorption and Si release kinetics on (a) pyrophyllite, (b) talc, (c) gibbsite, (d) silica, and (e) gibbsite/amorphous silica mixture at pH 7.5, I = 0.1 M $NaNO_3$, $[Ni]_o$ = 3 mM, solid:solution = 10 g/L. 62

2.2 Ni sorption and Si release kinetics on pyrophyllite at (a) pH 7.5, (b) pH 7.0, (c) pH 6.5, (d) pH 6.0, and (e) pH 5.5. I = 0.1 M $NaNO_3$, $[Ni]_o$ = 3 mM, solid:solution = 10 g/L. 63

2.3 Relationship between Si release and Ni sorption on (a) the various sorbents and (b) pyrophyllite at various solution pH values. Data extracted from Figures 2.1 and 2.2. 64

2.4 Measured (solid lines) and fitted (dotted lines) radial structure functions (RSFs) produced by forward Fourier transforms of Ni sorbed on pyrophyllite with time. The spectra are uncorrected for phase shift. 68

2.5 Measured (solid lines) and fitted (dotted lines) radial structure functions (RSFs) produced by forward Fourier transforms of Ni sorbed on talc with time. The spectra are uncorrected for phase shift. 69

2.6 Measured (solid lines) and fitted (dotted lines) radial structure functions (RSFs) produced by forward Fourier transforms of Ni sorbed on gibbsite with time. The spectra are uncorrected for phase shift. 70

2.7 Measured (solid lines) and fitted (dotted lines) radial structure functions (RSFs) produced by forward Fourier transforms of Ni sorbed on silica with time. The spectra are uncorrected for phase shift. 71

2.8 Measured (solid lines) and fitted (dotted lines) radial structure functions (RSFs) produced by forward Fourier transforms of Ni sorbed on gibbsite/silica mixture with time. The spectra are uncorrected for phase shift. 72

2.9 The k^3 weighted χ functions of one month aged Ni reacted pyrophyllite, talc, gibbsite, silica, and gibbsite/silica mixture samples. The circles show key identification for Ni-Al LDH versus α-Ni hydroxide (Scheinost and Sparks, 1999). 78

2.10 The DRS $\nu 2$ bands for the Ni surface precipitates on the gibbsite/amorphous silica mixture for various aging times. (a) All spectra collected; note that the three smaller curves for the early reaction times are unmarked. (b) Spectra were collected for reaction times of 1 to 7 days with an expanded y-axis. 82

2.11 Changes in the thermal stability of Ni-Al LDH precipitates on pyrophyllite with aging. The derivative of the weight loss curve is shown for (A) aged Ni-pyrophyllite samples and (B) reference precipitates physically diluted with pyrophyllite to match surface loading in sorption samples. Weight loss events: (1) expulsion of H_2O and nitrate from LDH interlayer, (2) dehydroxylation of nitrate-bearing LDH, (3) decomposition of the precursor Ni-Al phyllosilicate, and (4) dehydroxylation of pyrophyllite. Adapted from Ford et al. (1999). 84

2.12 Changes in the thermal stability of the Ni surface precipitates on the mixture showing the conversion from α-$Ni(OH)_2$ to a Ni phyllosilicate with aging. The derivative weight loss curves are background subtracted from an unreacted sample to show only weight loss events associated with the precipitate phases. The identification markers are derived from reference compounds. 86

2.13 Atomic force micrographs (AFM) of pyrophyllite unreacted and reacted with Ni (pH 7.5, $[Ni]_o$ = 3 mM) for times of 3 hours, 1 day, and 1 month. The scan size was 1 μm by 1 μm with a maximum Z-range of 60 nm. The scans were collected in TappingMode™ AFM. 89

2.14 Atomic force micrographs (AFM) of talc unreacted and reacted with Ni (pH 7.5, $[Ni]_o$ = 3 mM) for times of 1 day, 3 days, and 1 month. The scan size was 1 μm by 1 μm with a maximum Z-range of 40 nm. The scans were collected in TappingMode™ AFM. 90

2.15 Atomic force micrographs (AFM) of silica unreacted and reacted with Ni (pH 7.5, $[Ni]_o$ = 3 mM) for times of 1 day, 3 days, and 1 month. The scan size was 1 μm by 1 μm with a maximum Z-range of 40 nm. The scans were collected in TappingMode™ AFM. 91

2.16 High magnification HRTEM (a) and EDX (b) of 1-year aged Ni-pyrophyllite. Ni precipitates are noted with arrows. 93

2.17 High magnification HRTEM (a) and EDX (b) of 1-year aged Ni-talc. Ni precipitates are noted with arrows. 94

3.1 Macroscopic sorption of percent Ni sorbed on (a) pyrophyllite, (b) talc, (c) gibbsite, (d) silica, and (e) gibbsite/silica mixture at three different temperatures versus time. 111

3.2 Apparent first-order kinetic plots of Ni sorption on (a) pyrophyllite, (b) talc, (c) gibbsite, (d) silica, and (e) gibbsite/silica mixture at three different temperatures. 113

3.3 Comparison showing the near parallel relationship of Arrhenius and Eyring plots for data collected for Ni sorption on pyrophyllite at three various temperatures. 115

3.4 Compiled Arrhenius plots of Ni sorption on clay mineral and oxide surfaces at three different temperatures. 116

3.5 Compiled Eyring plots of Ni sorption on clay mineral and oxide surfaces at three different temperatures. 117

3.6 Relationship of energy of activation (E_a) and enthalpy of activation ($\Delta H^{\ddagger}$) by $\Delta H^{\ddagger} = E_a - RT$. 120

4.1 Macroscopic dissolution behavior of aged Ni precipitates on pyrophyllite showing the relative amount of Ni remaining on the surface following extraction with (a) 1 mM EDTA at pH 4.0, (b) 1 mM EDTA at pH 7.5, (c) 3 mM oxalate at pH 4.0, (d) 3 mM acetylacetone at pH 6.0, (e) HNO_3 at pH 4.0, and (f) HNO_3 at pH 6.0 plotted against the total number of replenishments. The stability of the Ni precipitates increases with aging time. 147

4.2 Macroscopic dissolution behavior of aged Ni precipitates on talc showing the relative amount of Ni remaining on the surface following extraction with (a) 1 mM EDTA at pH 4.0, (b) 1 mM EDTA at pH 7.5, (c) 3 mM oxalate at pH 4.0, (d) 3 mM acetylacetone at pH 6.0, (e) HNO_3 at pH 4.0, and (f) HNO_3 at pH 6.0 plotted against the total number of replenishments. The stability of the Ni precipitates increases with aging time. 148

4.3 Macroscopic dissolution behavior of aged Ni precipitates on gibbsite showing the relative amount of Ni remaining on the surface following extraction with (a) 1 mM EDTA at pH 4.0, (b) 1 mM EDTA at pH 7.5, (c) 3 mM oxalate at pH 4.0, (d) 3 mM acetylacetone at pH 6.0, (e) HNO_3 at pH 4.0, and (f) HNO_3 at pH 6.0 plotted against the total number of replenishments. The stability of the Ni precipitates increases with aging time. 149

4.4 Macroscopic dissolution behavior of aged Ni precipitates on silica showing the relative amount of Ni remaining on the surface following extraction with (a) 1 mM EDTA at pH 4.0, (b) 1 mM EDTA at pH 7.5, (c) 3 mM oxalate at pH 4.0, (d) 3 mM acetylacetone at pH 6.0, (e) HNO_3 at pH 4.0, and (f) HNO_3 at pH 6.0 plotted against the total number of replenishments. The stability of the Ni precipitates increases with aging time. 150

4.5 Macroscopic dissolution behavior of aged Ni precipitates on gibbsite/silica mixture showing the relative amount of Ni remaining on the mixture surface following extraction with (a) 1 mM EDTA at pH 4.0, (b) 1 mM EDTA at pH 7.5, (c) 3 mM oxalate at pH 4.0, (d) 3 mM acetylacetone at pH 6.0, (e) HNO_3 at pH 4.0, and (f) HNO_3 at pH 6.0 plotted against the total number of replenishments. The stability of the Ni precipitates increases with aging time. 151

4.6 Dissolution of one-month aged Ni-Al LDH precipitates on pyrophyllite comparing replenishment and stirred-flow methods using (a) EDTA at pH 7.5 and (b) HNO_3 at pH 4.0. 154

4.7 Release of Si and Al during dissolution from Ni-Al LDH precipitates on pyrophyllite aged for 1 hour, 1 month, and 1 year using EDTA at pH 7.5. ... 155

4.8 Ni-K_α XAFS spectra of pyrophyllite (a and b) and talc (c and d) aged with Ni for one month and subsequently treated with EDTA (pH 7.5) for 1, 3, and 7 days. The k^3 weighted χ functions are shown on the left side, the measured (solid lines) and fitted (dotted lines) radial structure functions on the right side (uncorrected for phase shifts). The circle shows a key identification for Ni-Al LDH versus α-Ni hydroxide. 157

4.9 Ni-K_α XAFS spectra of pyrophyllite (a and b) and talc (c and d) aged with Ni for one month and subsequently treated with HNO_3 (pH 4.0) for 1, 7, and 14 days. The k^3 weighted χ functions are shown on the left side, the measured (solid lines) and fitted (dotted lines) radial structure functions on the right side (uncorrected for phase shifts). The circle shows a key identification for Ni-Al LDH versus α-Ni hydroxide. 158

4.10 The DRS ν2 bands for the Ni surface precipitates on (a) pyrophyllite (EDTA, pH 7.5), (b) pyrophyllite (HNO_3, pH 4.0), (c) talc (EDTA, pH 7.5), and (d) gibbsite (EDTA, pH 7.5) aged for one month ("untreated") and subsequently extracted with EDTA for 1, 3, and 7 days or with HNO_3 for 1, 7, and 14 days. The relative amount of Ni remaining on the clay mineral is also given. 161

4.11 High-resolution thermogravimetric analysis (HRTGA) of the Ni surface precipitate on pyrophyllite aged for one month ("untreated") following extraction with HNO_3 (pH 4) for 1, 7, and 14 days. The weight loss event at about 280 °C is indicative of Ni-Al LDH (Ford et al., 1999), while the weight loss between 450 and 600 °C is due to pyrophyllite. 165

4.12 Background subtracted HRTGA of Ni surface precipitates on the gibbsite/amorphous silica mixture aged for one month ("untreated") and following extraction with HNO_3 (pH 4) for 1, 7, and 14 days. The weight loss events at about 332, 438, and 533 °C are indicative of α-$Ni(OH)_2$, Si-exchanged α-$Ni(OH)_2$, and Ni phyllosilicate. 166

4.13 Atomic force micrographs (AFM) of pyrophyllite unreacted and reacted with 1 mM EDTA (pH 7.5) for times of 24 and 240 hours. The scan size was 1 μm by 1 μm with a maximum Z-range of 60 nm. The scans were collected in Fluid TappingMode™ AFM. 168

4.14 Atomic force micrographs (AFM) of pyrophyllite unreacted and reacted with HNO_3 (pH 4.0) for times of 24 and 240 hours. The scan size was 1 μm by 1 μm with a maximum Z-range of 60 nm. The scans were collected in Fluid TappingMode™ AFM. 169

4.15 Ni release by HNO_3 at pH 4.0 from homogeneous synthetic Ni-Al LDH and α-Ni hydroxide, both with either predominantly nitrate or silicate in the interlayer. 174

ABSTRACT

Retention of heavy metals at the mineral-water interface is an important process in maintaining environmental health and quality. Therefore, knowledge of the kinetics and mechanisms of heavy metal sorption and desorption on clay mineral and oxide surfaces is necessary in order to accurately predict the fate and mobility of these environmental contaminants. This study examines the kinetics and mechanisms of the formation and dissolution of Ni(II) surface precipitates on pyrophyllite, talc, gibbsite, amorphous silica, and a gibbsite/silica mixture using macroscopic, spectroscopic (XAFS, DRS and EDS), microscopic (AFM and HRTEM), and thermogravimetric (HRTGA) techniques.

Macroscopic batch studies demonstrated that Ni sorption reactions were initially rapid and the rate then slowed until relatively no Ni was in solution. Initial product formation of Ni-sorbent reactions, confirmed through spectroscopic and microscopic methods, resulted in mixed Ni-Al layered double hydroxides (LDH) phases on pyrophyllite and gibbsite, and α-$Ni(OH)_2$ precipitates on talc, amorphous silica, and the gibbsite/silica mixture. The source of Al in the LDH phase is believed to have dissolved from the pyrophyllite and gibbsite surfaces and substituted for Ni in the brucite-like hydroxide layers of the precipitate. As aging time progressed,

experimental evidence showed that the precipitates on the Si-containing sorbents (pyrophyllite, talc, silica, and mixture) transformed from a nitrate-containing interlayer to a Si-containing interlayer which underwent further conversion to a Ni-phyllosilicate precursor. Additionally, temperature sorption studies suggest that these mineral-like precipitate reactions are surface-controlled and an associative mechanism that consume energy based on E_a, $\Delta H^{\ddagger}$, $\Delta S^{\ddagger}$, and $\Delta G^{\ddagger}$ values.

Formation of these precipitate phases drastically reduces metal concentration in soil and sediment solutions, and effectively competes with adsorption onto soil minerals. However, an important question that has been left unanswered is the stability of the precipitates and the potential long-term release of the metal back into the environment. Proton- and ligand-promoted dissolution via a batch replenishment technique of Ni-Al LDH and α-$Ni(OH)_2$ precipitates aged from one hour to two years showed that as aging time increased, the amount of Ni removed from the precipitate phase decreased, indicating an increase in stability with residence time. The aging effect may be attributed partly to the solid-state transformation of the precipitate phases (silication of Ni-Al LDH and α-$Ni(OH)_2$), and partly to crystal growth due to Ostwald ripening. The differences in stability between Ni-Al LDH and α-$Ni(OH)_2$ could be explained by a combination of Al-for-Ni substitution in the hydroxide layers and silicate-for-nitrate substitution in the interlayer. Spectroscopic, microscopic, and thermogravimetric analyses show that during dissolution, the chemical structure of the precipitate was not changed, however, quantitative changes were evident as observed in the macroscopic studies.

Chapter 1

INTRODUCTION

1.1 Rationale and Scope of Research

Surely, a concern for the average person is their overall health and well being. Worries about the quality of air one breaths and of water one drinks has caused some to equip homes with air purifiers and water filtration systems. These concerns stem from the ever-growing fear of pollution. However, threats of contaminated soil and sediment environments do not trouble the general public as severely as air and water pollution even though air and water quality often times are affected by terrestrial impurity. Municipalities that serve their consumers from aquifers should be concerned with possible transport of contaminants, whether organic or inorganic, within soils to underground water supplies. Metals, such as Ni(II) employed in this study, can have devastating effects on animal and plant health even in micro-quanities.

One of the recent interests in soil chemistry has been the formation of metal surface precipitates on the surfaces of soil components. By using state-of-the-art *in-situ* spectroscopic, microscopic, and thermogravimetric techniques, researchers have definitively determined that these 3-dimensional deposits occur on an array of surfaces and with a number of environmentally important metals. This has been observed for Ni sorption on natural materials. Such product formation invalidates many of the sorption reaction models proposed to date that assume that sorption of metals onto surfaces results in adsorption phenomena only. Prior to the recent research, surface precipitation was believed to occur at only high sorbate levels and at times much slower than typical adsorption processes ($\leq$ 24 hours). The present studies have observed the formation of metal surface precipitates at sorbate levels and time scales that coincide with adsorption. These neoteric findings further emphasize the need to employ a combination of macroscopic, microscopic and spectroscopic methods to elucidate the kinetics and the mechanisms of metal reactions that occur in the natural environment. Research in this area has been quite limited and further studies are very necessary.

While metal precipitate formation is an important topic, it is also incumbent that one investigates the dissolution of surface precipitates. Such studies are rare in the literature. The fate and bioavailability of the metals in these surface complexes

have great environmental significance. Questions such as "How tightly held are the metals?" and "How long will the precipitates remain stable or are they stable?" and "How are the surface precipitates distributed on the surface with time?" have not been answered yet. Answers to these questions will aid in the remediation of contaminated sites. Recent studies have shown that Si substitution into the interlayer of the surface precipitates results in the formation of extremely stable metal phyllosilicate precursors with time. If the stability of the metal precipitates is very high, it may be prudent to leave the site untouched and leave the metal sequestered in the natural environment.

As mentioned earlier, it is necessary to employ an array of macroscopic, spectroscopic, and microscopic methods to identify and quantify reaction products associated with metal precipitation on clay mineral and oxide surfaces. Macroscopic kinetic studies can provide basic information to researchers such as rates of reactions and activation energy, however, such information does not yield a reaction mechanism. Mechanisms, such as adsorption vs. precipitation or desorption vs. dissolution, can only be confirmed by the use of spectroscopic, microscopic, or thermogravimetric techniques. X-ray absorption fine structure (XAFS) spectroscopy can determine identity, bond distances, coordination numbers, and oxidation states of neighboring atoms relative to an element of interest being probed. XAFS has been used extensively in the literature to allow soil and environmental scientists to

discriminate between adsorption and precipitation. Diffuse reflectance spectroscopy (DRS) can identify oxidation state and coordination of transition metals. High-resolution thermogravimetric analysis (HRTGA) has been utilized to observe and identify weight loss events by temperature decomposition of materials. Although HRTGA does not provide chemical information, it can be used successfully as a fingerprinting technique when data are compared to known references. Relatively new surface probing microscopies such as atomic force microscopy (AFM) are able to scan a reacting surface in-situ and in real-time. Unfortunately, AFM can lead to many artifacts but through careful training and sample preparation, one can produce exciting results. With recent advances in high-resolution transmission electron microscopy (HRTEM), one can view reactions at the mineral/water interface at the angstrom level.

With the variety of spectroscopic and microscopic methods available, one must be cautious to use tools that will be helpful in the research. As with employing only macroscopic methods to determine a reaction mechanism, using the wrong analytical technique for a reaction system will lead to mistakes. That is why many scientists employ a combination of spectroscopic and microscopic analyses to examine reactions in order to find an agreement among the multiple techniques.

1.2 Literature Review

1.2.1 Metal Sorption

Classically, adsorption has been defined as the accumulation of a substance or material at an interface between the solid surface and the bathing solution. Adsorption does not include surface precipitation or polymerization processes. Collectively, all three can be defined as sorption (Sparks, 1995). When a metal cation adsorbs onto a mineral surface it can do so by one of two means, either inner-sphere or outer-sphere complexation. If a water molecule is located between the surface functional group and the bound metal ion, the surface complex is defined as outer-sphere. Likewise, if the water molecule is not present between the sorbed ion and the surface, an inner-sphere complex is the result (Sposito, 1989). Additionally, inner-sphere complexes can be further defined by the number of bonds that attach the metal to the surface. A monodentate inner-sphere complex consolidates a single bond between the metal ion and a surface oxygen whereas a bidentate complex, generally more tightly held than monodentate species, incorporates two direct bonds of the metal to separate surface oxygens (Hayes, 1987). It is important to acknowledge that outer- and inner-sphere complexes often evolve simultaneously on a surface.

Inner-sphere complexation is usually slower than outer-sphere complexation; it is often not reversible and adsorption by this mechanism is weakly affected by the ionic strength of the aqueous solution. Inner-sphere complexation can increase, reduce, neutralize, or reverse the charge on the sorptive regardless of the original charge. Adsorption of ions via inner-sphere complexation can occur on a surface indifferent of the surface charge and involves a ligand exchange process where the metal or metalloid exchanges with OH^- or H_2O and becomes directly bound to the metal in the mineral's crystalline structure (Sparks, 1995).

Outer-sphere complexation involves electrostatic coulombic interactions and ions retained via this mechanism are weakly held compared to inner-sphere complexes in which the binding is covalent or ionic. Outer-sphere complexes usually form rapidly and adsorption of these complexes is affected by the solution ionic strength. Additionally, adsorption via outer-sphere complexation is reversible and can only occur on surfaces that are of opposite charge to the complexes (Sparks, 1995). Some anions are adsorbed as outer-sphere complexes on positively charged surfaces, however, some anions, particularly oxyanions such as sulfate, phosphate and arsenate, can be sorbed both as inner-sphere and outer-sphere complexes (Zhang and Sparks, 1990; Hayes et al., 1987). Strawn and Sparks (1999) also observed this by employing

XAFS to distinguish between inner- and outer-sphere lead adsorption on montmorillonite.

Many kinetic studies have shown that sorption of metal cations onto soil, clay mineral and metal oxide surfaces is described by a two step process comprising a rapid stage and a slow stage (Burns, 1976; Kinniburgh and Jackson, 1981; Kou, 1986; Brümmer et al., 1988; Ainsworth et al., 1994). The rapid initial stage, occurring on time scales of seconds, minutes or hours, has been interpreted as an adsorption phenomenon (Kinniburgh and Jackson, 1981; Sparks, 1995). However, the slow reaction stage, associated with time scales on the order of days, weeks or months is not clearly understood. Three possible mechanisms have been attributed to the slow sorption stage which include: 1) adsorption onto sites of lower reactivity (Benjamin and Leckie, 1981; Dzombak and Morel, 1986), 2) diffusion of the adsorbate into the adsorbent via micropores and/or directly in the solid material (absorption) (Ogwada and Sparks, 1986b; Steinberg et al., 1987; Brümmer et al., 1988; Comans and Hockley, 1992; Pignatello and Xing, 1995), and 3) surface precipitation formation (Sposito, 1984; Farley et al., 1985; Davis et al., 1987; Chisholm-Brause et al., 1990; Charlet and Manceau, 1992; Fendorf et al., 1994; O'Day et al., 1994; Fendorf et al., 1996; Scheidegger et al., 1996a,b; 1997; 1998; Scheidegger and Sparks, 1996; O'Day et al., 1996; Towle et al., 1997; Xia et al., 1997; Thompson, 1998; Scheinost et al.,

1999; Scheckel and Sparks, 2000a). However, until recently, the proposed mechanisms for slow metal sorption were based strictly on macroscopic measurements through sorption isotherms and kinetic studies. To definitively prove the suggested mechanisms one must employ molecular approaches. With the advent of in-situ spectroscopic and microscopic techniques, it is possible to identify the cause of slow sorption mechanisms.

While adsorption has been characterized as a two-dimensional surface feature, surface precipitation has been depicted as three-dimensional growth. According to Sposito (1986), precipitation is the formation of a solid mixture either by inclusion or by coprecipitation or on the surface of a pre-existing solid phase (surface precipitate). Precipitation is initiated by either homogeneous or heterogeneous nucleation. Surface precipitation follows a process which involves 1) adsorption of the metal onto the surface, 2) surface nucleation, and 3) crystalline growth outward from the surface (Stumm, 1992). Site saturation is manifested in pH edges by a plateauing of the curve at some level below 100 percent sorption. However, it is difficult to detect site saturation for metal cations because of the formation of hydroxide precipitates either in solution or on the surface, occurring at both high- and low-affinity binding sites, prior to bulk solution precipitation (James and Healy, 1972; Farley et al., 1985). Contribution of surface precipitates to overall sorption increases as sorbate/sorbent

ratios increase and may become the dominant sorption mechanism at very high ratios (Harvey and Linton, 1984; Farley et al., 1985). However, recent studies on the formation of surface precipitates indicate that high sorbate/sorbent ratios are not necessary and that site saturation is not achieved (Chisholm-Brause et al., 1990; Charlet and Manceau, 1992; Fendorf et al., 1994; O'Day et al., 1994; Fendorf et al., 1996; Scheidegger et al., 1996a,b; 1997, 1998; Scheidegger and Sparks, 1996; O'Day et al., 1996; Towle et al., 1997; Xia et al., 1997; Thompson, 1998; Scheinost et al., 1999; Scheinost and Sparks, 1999; Thompson et al., 1999a and b).

In considering surface precipitation of cations, simplified surface complexation reactions should be rewritten to better describe surface precipitation reactions, as follows:

$$\equiv XOH^0 + M^{2+} + H_2O = X(OH)_{3(S)} \equiv MOH_2^+ + H^+ \qquad {}^*K_M^{app}$$

$$\equiv MOH_2^+ + M^{2+} + H_2O = M(OH)_{2(S)} + MOH_2^+ + 2H^+ \qquad K_{spM}$$

$$\equiv XOH^0 + X^{3+} + 3H_2O = X(OH)_{3(S)} + \equiv XOH^0 + 3H^+ \qquad 1/K_{spX}$$

where $X(OH)_{3(S)}$ is the sorbent metal hydroxide, M^{2+} is the sorbing cation (Dzombak and Morel, 1990), ${}^*K_M^{app}$ is the apparent equilibrium constant, K_{spM} is the bulk solution solubility product of $M(OH)_{2(S)}$ (the sorbing metal cation hydroxide

precipitate), and K_{spX} is the bulk solution solubility product of $X(OH)_{3(S)}$. The symbols ≡ and = denote bonds at the surface and have different meanings for X^{3+} and M^{2+}: $\equiv XOH^0$ represents $[X(OH)_3]_n$ and $=MOH_2^+$ represents $[M(OH)_2]_n$ (Dzombak and Morel, 1986).

Furthermore, the equilibrium constant for surface precipitation is given as:

$$*K_M^{app} = K_M^{app} \{X(OH)_{3(S)}\}$$

where { } represents activity and since $\{X(OH)_{3(S)}\}$ is equal or very close to 1.0 (except for very high sorbate concentrations), the two constants $*K_M^{app}$ and K_M^{app} are thus equal or nearly equal.

Additionally, the activity of each solid species is assumed to be equal to its mole fraction in the surface phase so that this constraint may be given as:

$$\{M(OH)_{2(S)}\} = (M(OH)_{2(S)})/T_S$$

$$\{X(OH)_{3(S)}\} = (X(OH)_{3(S)})/T_S \text{ , so that}$$

$T_S = (M(OH)_{2(S)}) + (X(OH)_{3(S)})$, where T_S is the total mass of solid material in solid solution.

Pioneering work by Scheidegger et al. (1996a,b; 1997; 1998) and Scheidegger and Sparks (1996) helped to explain the kinetic reactions of Ni(II) sorption on the surfaces of pyrophyllite and metal oxides by showing the formation of a mixed cation (Ni-Al) hydroxide phase. They demonstrated that surface precipitation can occur at: 1) low sorbate concentrations, much less than monolayer coverage, 2) short time scales, within 15 minutes, and 3) pH values lower than where one would expect the precipitation of a metal's hydroxide phase according to its thermodynamic solubility product. This is contrary to the previous equilibrium equations for a mononuclear surface hydroxide precipitate. Surface clusters formed within 15 minutes, an extremely short time in comparison to traditional theory (Scheidegger et al., 1998). Scheidegger et al. (1998) noted that the bond distances for Ni-Ni were distinctly shorter in the polynuclear precipitates than in $Ni(OH)_{2(S)}$ indicating that the complexes are not $Ni(OH)_{2(S)}$. The nucleation of the heterogeneous solid at the surface interface has not been positively identified but the authors submit that the structure of the precipitate is similar to takovite ($Ni_6Al_2(OH)_{16}CO_3 \bullet H_2O$), based on XAFS data analysis and using natural takovite as a reference compound. It appears that Al plays an important part in the formation of these surface precipitates but its role is not fully

understood nor have the roles of other trivalent cations been studied vis a´ vis precipitation. In fact, O'Day et al. (1994), observing Co (II) reactions on kaolinite, Charlet and Manceau (1992), studying Cr (III) interactions with hydrous ferric oxides, Roe et al. (1991) examing Pb(II) reactions on goethite, and Chisholm-Brause et al. (1990), working with Pb on γ-Al_2O_3, also determined that the respective metal that they were studying formed multinuclear complexes on the surface of clay minerals and metal oxides. The above research demonstrates the necessity to recognize that surface precipitates form on clay mineral and metal oxide surfaces and that these surface precipitates may form over short reaction times. However, additional XAFS Pb studies on γ-Al_2O_3 by Strawn et al. (1998) and on α-Al_2O_3 by Bargar et al. (1997) demonstrated that surface precipitation is not the dominant sorption mechanism.

The formation of polynuclear hydroxide complexes in solution has been noted in the literature (Allmann, 1970; Taylor, 1984). The common chemical formula for the mixed-cation compounds is

$$[Me^{2+}_{1-x}\, Me^{3+}_{x}\, (OH)_2]^{+x} \bullet (x/n)A^{-n} \bullet mH_2O\,,$$

where Me^{2+} could be Co(II), Fe(II), Mg(II), Mn(II), Ni(II), or Zn(II) , and

Me^{3+} is Al(III), Cr(III), or Fe(III). Interlayer anions, A^{-n}, can be represented as Br^-, Cl^-, ClO_4^-, I^-, NO_3^-, or OH^-. The net positive charge, x, is counterbalanced by an equal negative charge, n. The remaining interlayer space is occupied by water molecules, m.

The divalent and trivalent cations are distributed within the brucite-like octahedral hydroxide structure. Brindley and Brown (1984) noted that the octahedral hydroxide layers are arranged with two layers per unit cell in hexagonal symmetry, with three layers per unit cell in rhombohedral symmetry, or with reduced symmetrical sequences. Induced hydrolysis causes the formation of mixed-cation hydroxide complexes. When a suspension of a fully hydrolyzed cation (Me^{3+}) is placed in solution with another cation (Me^{2+}) and the pH is constantly held below the pH value for which the Me^{2+}-hydroxide would precipitate, hydrolysis of Me^{2+} occurs and the precipitation of the polynuclear hydroxide phase is accomplished (Taylor, 1984).

However, other XAFS spectroscopic studies examining surfaces that do not contain Al or other trivalent cations have concluded that the sorbing trivalent or divalent cation employed in the studies formed $Me^{(+3)+2}$-(oxy)hydroxide phases and not the multinuclear complexes noted above. Fendorf et al. (1994) observed the formation of γ-CrOOH due to interactions of Cr(III) with silica. The Cr-Cr bond

distances of 2.99 Å were indicative of edge-sharing Cr octrahedra. Research by O'Day et al. (1996) using XAFS spectroscopy examined the sorption complexes of Co(II) on amorphous silica (α-SiO_2) and rutile (TiO_2). The complexes that formed on the surface of amorphous silica were the same, $Cr(OH)_{2\,(S)}$, regardless of the surface coverage and incubation time. The rutile sorption products varied depending on surface coverage. At low Co(II) coverages, Co apparently sorbed directly to the rutile surface to form monodentate or small mononuclear complexes occupying Ti-equivalent sites at the rutile surface. Higher coverages yielded an increase in Co second-neighbor backscattering indicating larger multinuclear complexes believed to be similar to anatase, a TiO_2 polymorph, and not $Cr(OH)_{2\,(S)}$, possibly due to the comparable bond distances of Cr-Cr to Ti-Ti. Scheinost et al. (1999) and Scheinost and Sparks (1999) employed XAFS and DRS to study the role of Al in the formation of secondary Ni precipitates on pyrophyllite, gibbsite, talc, and amorphous silica. Scheinost and coworkers found similar results to those of Scheidegger and coworkers for the Ni-pyrophyllite and -gibbsite sorption systems in which mixed Ni-Al LDH (layered double hydroxide) precipitates formed. However, using XAFS, Scheinost and Sparks (1999) determined that Ni sorption on Al-free talc and silica resulted in the formation of α-$Ni(OH)_2$ precipitates with a Ni-Ni bond distance of 3.08 Å, which is distinctly different than the 3.06 Å bond distance for Ni-Al LDH. These findings

coincided with DRS work by Scheinost et al. (1999) that found v2 band positions of 15,300 cm^{-1} and 14,900 cm^{-1} for Ni-Al LDH and α-$Ni(OH)_2$, respectively.

Despite an available Al source in gibbsite, Scheckel and Sparks (2000a) observed the formation of α-$Ni(OH)_2$ precipitates in a mixture of gibbsite and amorphous silica using XAFS, DRS, and HRTGA. It was speculated that the silica surface dominated due to the low solubility of gibbsite ($K_{so} = 9.61$) coupled with the rapid sorption kinetics ($k_a \sim 10^{-5}$ s^{-1}) of Ni on silica. Scheckel and Sparks (2000a), using spectroscopic and thermogravimetric techniques examined the sorption products for aging times up to one year and observed a conversion of the initial α-$Ni(OH)_2$ surface product to a Ni phyllosilicate precursor phase. This aging process was driven by Si substitution for nitrate into the interlayer of the brucite-like structure of α-$Ni(OH)_2$.

Electron spin resonance (ESR) spectroscopy, also defined as electron paramagnetic resonance (EPR) spectroscopy, is often used to study chemical species which have one or more unpaired electrons. Direct evidence for surface coordination of metals can be obtained from ESR spectra of sorbed paramagnetic ions. McBride et al. (1984) observed the sorption of Cu^{2+} on the surfaces of gibbsite and boehmite at

various pH values. They demonstrated that at low pH gibbsite chemisorbs small amounts of monomeric Cu^{2+}. However, at pH >5, the ESR spectra indicate the possibility of hydrolyzed and polymerized forms of Cu^{2+} on the surface of gibbsite. They rationalized that Cu^{2+} formed a complex with NH_3 while bound to the surface. Electron spin resonance results also indicated that Cu^{2+} sorbed to a surface hydroxyl O to form ternary complexes (McBride, 1985). Clark and McBride (1984) applied ESR to Cu^{2+} sorption on allophanes and imogolite. They showed that NH_3 was able to displace H_2O and OH-ligands from the sorbed Cu^{2+} to form Cu^{2+}-NH_3-surface complexes.

Johnsson et al. (1992) proposed a simple explanation for precipitate formation. They studied the dissolution of muscovite in water and noticed a secondary phase developing during the process. During dissolution of the muscovite surface, release of Al, Si, K and C were analyzed by X-ray photoelectron spectroscopy (XPS) and all were present. Johnsson et al. (1992) concluded that the secondary phase precipitate was an Al hydroxide based on the morphology of the structures and the increase in the Al/Si ratio as determined by XPS. One thing to note about this study is that the dissolution reaction products were not removed which could explain how Al was available for secondary phase formation.

Fendorf et al. (1996), Fendorf et al. (1994), and Fendorf and Sparks (1994), applied scanning force microscopy (SFM), high resolution transmission electron microscopy (HRTEM), and X-ray absorption fine structure (XAFS) spectroscopy to investigate Cr(III) sorption on SiO_2 and goethite. At high surface coverage (> 20%), Cr(III) formed cone-like cluster surface precipitates. Fendorf et al. (1996) investigated Cr(III) sorption on goethite. In contrast to SiO_2, Cr(III) precipitation on goethite was evenly distributed across the surface causing a "smoothing" or "coating" effect of the goethite topography. These results were similar to those of Junta and Hochella (1994). They studied Mn(II) oxidation on hematite, goethite and albite. The conversion of Mn(II) to Mn(III) resulted in discrete Mn surface clusters. Interestingly, after a 5 month incubation on the albite surface, the precipitates became more ordered and appeared similar to a honeycomb structure. The complexes on the other surfaces were not changed after 5 months. Fendorf et al. (1996), Fendorf et al. (1994), and Junta and Hochella (1994) concluded that the respective Me(III) formed a Me-oxyhydroxide type precipitate, i.e., γ-CrOOH with Cr(III) and β-MnOOH with Mn(II).

Although the mechanism(s) for the formation of these surface precipitates has not been clearly identified, it has been postulated that they can not form without the presence of a surface interface in solution (James and Healy, 1972). O'Day et al. (1994) theorized that the mechanism(s) for surface complex formation could be related

to: 1) cluster size and structural misregistry, assuming the formation of critical-sized clusters of atoms from supersaturated solutions as the first step in the growth of a new phase (Stumm and Morgan, 1981); 2) enhanced surface concentration of the sorbed metal contained within a perturbed interfacial volume at the surface (Cases and François, 1982); 3) reduced dielectric constant of water due to influences of the reaction surface which then results in a decrease in ΔG (James and Healy, 1972; Cases and François, 1982; Sposito, 1984).

1.2.2 Dissolution Processes

Dissolution of minerals involves several key steps which are either rate-limiting or not depending on whether the dissolution is transport (diffusion)- or surface-controlled. A transport-controlled rate-determining step involves the movement of a reactant or a weathering product through a layer of the surface of the mineral. Likewise, surface-controlled processes are generally slower than transport-controlled reactions so that concentrations adjacent to the surface build up to values essentially identical to those in the surrounding bulk solution. The possible rate-limiting steps are: 1) mass transfer of the reactants in the bulk solution to the surface, 2) adsorption of the reactants, 3) interlattice transfer of reacting species, 4) chemical reactions at the surface, 5) movement of the reactants away from the surface, and 6)

mass transfer of products and excess reactants into the bulk solution. Under normal system conditions, Steps 1 and 6 (transport-controlled) are not usually rate-limiting while Steps 3, 4, and 5 (surface-controlled) are often rate-limiting (Stumm and Wollast, 1990).

Mineral dissolution is one of the major processes influencing the overall cycle of elements within the subsurface environment. Dissolution is known to occur by interactions of surfaces with ligands, protons, deprotonation of surfaces, water, and recent studies indicate that metals may play a part in surface dissolution. The surface protonation of O and OH lattice sites is the mechanism of dissolution of silicates and accelerates with decreasing pH (Stumm and Morgan, 1996). The points of attack of the protons in layered silicates are the O atoms that interlink the Al-oxide groups with the Si-oxide structures for layer silicates. The protonation slowly releases Al from the silicate surface followed by the subsequent detachment of $Si(OH)_4$ species. Ligands, including environmentally important low molecular weight organic acids of biological decomposition and root exudates, are known to promote the dissolution of Al silicates (Brady and Walther, 1992). Dissolution of silicates and other minerals have been widely studied on a macroscopic scale: kaolinite and muscovite as a function of pH (Stumm and Wieland, 1990), δ-Al_2O_3 as influenced by pH (Furrer and Stumm, 1986), orthosilicates by divalent metal-oxygen bonds (Casey and Westrich, 1992), α-FeOOH

as a function of pH (Zinder et al., 1986), Fe (III) (hydr)oxides via reductive dissolution (Biber et al.,1994), albite promoted by temperature and pressure (Chou and Wollast, 1984), and biotite with acids (Grandstaff, 1986) to name a few.

One can express the rate of ligand-promoted dissolution, R_L, as

$$R_L = k'_L (\equiv ML) = k'_L C^s_L , \qquad [1]$$

where k'_L is the rate constant for ligand-promoted dissolution ($time^{-1}$), $\equiv ML$ represents the metal-ligand complex, and C^s_L is the surface concentration of the ligand complex (mol m^{-2}) (Furrer and Stumm, 1986). The proton-promoted dissolution rate, R_H, can be expressed as

$$R_H = k'_H (\equiv MOH_2^+)^j = k'_H (C^s_H)^j \qquad [2]$$

where k'_H is the rate constant for proton-promoted dissolution, $\equiv MOH_2^+$ represents the metal-proton complex, C^s_H is the concentration of the surface proton complex (mol m^{-2}), and j is the oxidation state of the metal ion in the surface structure (Stumm, 1992). The overall rate of dissolution is the sum of ligand-promoted, proton-

promoted, deprotonation-promoted, and pH-independent dissolution which is expressed as

$$R = R_L + R_H + R_{OH} + R_{H_2O} \qquad [3]$$

where, R_L and R_H were defined earlier. R_{OH} is the deprotonation-promoted dissolution rate and R_{H_2O} is defined as the pH-independent dissolution rate.

The overall rate of dissolution can be expressed as

$$R = k'_L C^s_L + k'_H (C^s_H)^j + k'_{OH} (C^s_{OH})^i + k'_{H_2O} \qquad [4]$$

where, $k'_L C^s_L$ and $k'_H (C^s_H)^j$ were defined earlier, k'_{OH} is the rate constant for deprotonation-promoted dissolution, C^s_{OH} is the concentration of the surface deprotonation complex and i is the oxidation state of the metal ion in the surface structure. The pH-independent dissolution rate is represented by k'_{H_2O}.

Furrer and Stumm (1986) investigated the rate of ligand-promoted and proton-promoted dissolution of γ-Al_2O_3. The ligand-promoted dissolution of γ-Al_2O_3 by the

aliphatic ligands oxalate, malonate, and succinate was observed to follow a linear relationship between the ligand-promoted dissolution rate, R_L, and the surface concentration of the ligand complexes, C^s_L. Proton-promoted dissolution of γ-Al_2O_3 exhibited a linear dependence with the slope (j) equal to the oxidation state of Al(III) when plotted as log R_H, rate of proton-promoted dissolution, versus log C^s_H, the surface concentration of the proton complexes.

The influence of ligands and oxyanions on dissolution was studied by Bondietti et al. (1993) who examined the effects of EDTA, phosphate, arsenate and selenite on the reactivity of Fe(III) (hydr)oxides. Dissolution was severely inhibited by phosphate, arsenate and selenite at near neutral pH values. At pH < 5, dissolution was accelerated by the presence of phosphate, arsenate and selenite.

A metal-promoted dissolution mechanism has also been proposed which suggests that sorbing cations may induce the dissolution of cations held within the sorbent and that these released cations then become incorporated to form multinuclear surface precipitates with the sorbing cation in the bulk solution (Scheidegger et al., 1997;Sparks et al., 1998; Scheidegger et al., 1998).

While it is evident from the literature surface precipitates often form on mineral surfaces, investigations on the dissolution of surface precipitates are not common (Scheidegger and Sparks, 1996; Fendorf et al., 1996; Ford et al., 1999; Scheckel et al., 2000; Scheckel and Sparks, 2000a and b). There is a veritable need, in view of the common formation of polynuclear metal complexes on natural materials, to better understand the degree and mechanism(s) of metal dissolution from surface precipitates. Such information is vital if one is to better assimilate the fate of metals in the subsurface environment.

Fendorf et al. (1996) examined the ligand-promoted dissolution of Cr(III) precipitates from silica and goethite surfaces with oxalate, a common plant root exudate. Ligand-promoted dissolution involves the formation of a surface complex with a ligand (e.g., oxalate, EDTA, PO_4^{3-}, etc.) via a ligand exchange mechanism. In this mechanism, a surface hydroxyl exchanges with the organic or inorganic ligand which adds a negative charge to the Lewis acid center coordination sphere and lowers the Lewis acid acidity. This reaction polarizes the metal-oxygen bonds and the metal is released from the surface into the solution (Sparks, 1995). Fendorf et al. (1996) noted from AFM studies that the morphologies of the hydrous chromium oxides on the two surfaces were very different. The silica surface exhibited small cone-shaped clusters while the goethite material revealed a "smoothing" effect from the

precipitates. Therefore, one can conclude that the surface area of the precipitates on silica is greater than those on goethite; thus, the metal is more likely released at a higher rate. In fact, after one hour of reaction, 17% of the sorbed Cr(III) on silica was released while < 1% of the Cr(III) from the goethite was dissolved. A solution of a pure hydrous chromium oxide solid resulted in the most rapid dissolution with 20% dissolved within one hour. After 29 hours, Cr (III) dissolution was 35%, 22.4% and 6.6% for pure hydrous chromium oxide, silica, and goethite, respectfully. Overall, Cr(III) detachment from goethite was approximately 70% less than that from silica.

Scheidegger and Sparks (1996) examined the dissolution of polynuclear Ni(II) surface complexes from pyrophyllite via proton-promoted dissolution with HNO_3 at pH = 4 and pH = 6. Proton-promoted dissolution occurs when protons bind to surface oxide ions, which causes the bonds to weaken. Thereafter, the metal is detached into the solution phase (Sparks, 1995). This study (Scheidegger and Sparks, 1996) was unique in that it examined the kinetics of precipitation and dissolution of the mixed Ni-Al hydroxide phases from the surface. Nickel detachment from surface complexes was rapid initially at both pH values (with < 10% of total Ni released) and was attributable to desorption of specifically adsorbed, mononuclear bound Ni. Dissolution then slowed tremendously, primarily due to the gradual dissolution of the multinuclear surface precipitates. A reference compound, crystalline $Ni(OH)_2$, was

also examined for its dissolution potential. The replenishment method was employed to simulate steady-state flow and a conventional batch method was also used to compare the influence of reaction products present in solution on dissolution. The replenishment method was more effective in removing Ni from the surface precipitates (~ 12% at pH = 6 and ~ 48 % at pH = 4). Compared to the dissolution of crystalline $Ni(OH)_2$ (~ 96% dissolved), Ni release from pyrophyllite was extremely slow.

Ford et al. (1999) investigated the dissolution of Ni-Al LDH surface precipitates on pyrophyllite using an EDTA solution at pH 7.5. Detachable Ni drastically decreased when the age of the precipitate increased from one hour to one year. By employing high-resolution thermogravimetric analysis, which is sensitive to changes in the interlayer composition of LDH, and by paralleling the results of the surface precipitates with those of reference compounds, the authors could show that a substantial part of the aging effect was due to replacement of interlayer nitrate by silicate which transformed the initial Ni-Al LDH into a Ni-Al phyllosilicate precursor. The source of the silicate was the dissolving surface of the pyrophyllite. Scheckel et al. (2000) and Scheckel and Sparks (2000a and b) investigated the dissolution of Ni-Al LDH phases on pyrophyllite and gibbsite and α-$Ni(OH)_2$ precipitates on talc, silica, and a mixture of gibbsite/amorphous silica employing EDTA (pH 7.5 and 4.0), oxalate, acetylacetone, and nitric acid (pH 6.0 and 4.0) for sorption aging times

ranging from one hour to two years. In these studies, an array of analytical techniques was applied to examine the dissolution of one-month aged Ni surface precipitates formed on pyrophyllite, talc, gibbsite, and the mixture. The differences in stability due to aging of the surface precipitates could be explained by a combination of Al-for-Ni substitution in the hydroxide layers (for pyrophyllite and gibbsite) and silicate-for-nitrate substitution in the interlayer (for pyrophyllite, talc, silica, and mixture). The macroscopic dissolution studies demonstrated increased stability in Ni surface precipitates with aging. The aging effect may be attributed partially to the solid-state transformation of the precipitate phases (silication of Ni-Al LDH and α-Ni hydroxide), and to crystal growth due to Ostwald ripening.

1.2.3 Kinetics of Sorption and Desorption

Determination of rate laws, reaction orders, and rate constants or rate coefficients can be elucidated in three general ways (Bunnett, 1986; Skopp, 1986; Sparks, 1989; Sparks, 1995): 1) initial rates, 2) using integrated rate equations and plotting the kinetic data, and 3) using non-linear least squares computation.

For an elementary reaction between reactants A and B yielding product Y one obtains,

$$A + B = Y \qquad [5]$$

The forward reaction rate law for Eq. [5] may be written as

$$v_f = d[A]/dt = - k_f [A][B] \qquad [6]$$

where k_f is the forward rate constant and the reverse reaction rate law is

$$v_r = d[A]/dt = k_r [Y] \qquad [7]$$

where k_r is the reverse rate constant.

In order for Eqs. [6] and [7] to be valid, the reaction(s) must be far from equilibrium such that either the forward or reverse reaction is insignificant. However, if both Eqs. [6] and [7] are occurring, they would be combined to generate the net reaction,

$$d[A]/dt = - k_f [A][B] + k_r [Y] \qquad [8]$$

which implies that the net reaction rate is the difference between the forward reaction and reverse reaction rates.

The limit of the reaction rate as time approaches zero is the initial rate. Measurement of initial rates is a way to assure that reverse reactions are not significant. In order to examine initial rates, one needs to employ a technique that can measure rapid reactions and quantify the products, e.g., a relaxation method and ICP spectroscopy, respectfully. One can then plot the concentration of product versus time from a short reaction period that minimally affected the instantaneous rate. By measuring initial rates, one can assume that only the forward reaction (Eq. [6]) dictates the overall reaction.

Integrated rate equations are often used to determine rate constants/coefficients. The first-order rate law can be written as:

$$d[\mathrm{A}]/dt = -k_f[\mathrm{A}] \qquad [9]$$

If [A] is first-order dependent, it can be evaluated by integrating Eq. [9] assuming the initial conditions, $t = 0$, $A = A_o$, resulting in,

$$\log[A] = \log[A_o] - k_f t/2.303 \qquad [10]$$

By plotting log[A] vs. t, a straight line should result if the reaction is first-order. The slope would be equal to $- k_f/2.303$ and the intercept would equal $\log[A_o]$.

Least squares analysis can also be employed to determine rate constants and rate coefficients. This method fits the best line to a set of data points with the basic linear equation, $y = mx + b$ where y and x are the ordinate and abscissa coordinates, respectfully. Additionally, the slope, m, and intercept, b, can also be computed. Error in least squares analysis generally stems from 1) an incorrect assumption of reaction order, 2) the reaction from which the data were collected was not at equilibrium, and 3) temperature fluctuations during the study.

Extreme caution should be practiced when examining integrated rate equations and least squares analysis to determine reaction orders and rate constants/coefficients. It is imprudent to conclude that a reaction order is correct, based merely on the conformity of the data to an integrated rate equation. One should determine if the rate is independent of initial concentration and should also investigate several integrated equations to fully determine the reaction order. Likewise, it is not advisable to resolve

mechanistic information simply based on multiple rate constants determined from several slopes of linearly plotted kinetic data. Mechanisms can be confirmed in various ways with one of the best being the application of molecular and atomic level spectroscopic and microscopic techniques.

1.2.3.1 Kinetic Models

For the most part, non-linear least squares computation are used to determine reaction parameters. Some linearized rate equations are listed below:

Ordered Model Equations

Zero-Order

$$C = C_o - kt \qquad [11]$$

First-Order

$$\ln C = \ln C_o - kt \qquad [12]$$

Second-Order

$$1/C = 1/C_o + kt \qquad [13]$$

n Order ($n > 1$)

$$1/C^{n-1} = 1/C_o^{n-1} + (n-1)kt \qquad [14]$$

Eqs. [11] through [14], k is the rate constant and t is time. C is defined as the concentration in solution and C_o is the initial concentration so that at $t = 0$, $C = C_o$. Ordered models, especially first-order kinetic models, have been widely used to describe reactions at the mineral/water interface (Sparks, 1989; Sparks, 1991; Sparks et al., 1993; Sparks, 1995). Multiple first-order reactions may occur during the same experiment as seen in previously mentioned biphasic kinetics. Some investigators have attempted to conclude mechanistic information from multiple first-order slopes, however, as stated earlier, it is unsound to draw such conclusions without other evidence.

Elovich Equation

$$q_t = (1/\beta) \ln (\alpha^*\beta) + (1/\beta) \ln t \qquad [15]$$

The Elovich equation was developed to describe the heterogeneous chemisorption kinetics of gases on solid surfaces. It has been employed to describe a

multitude of reaction mechanisms such as activation and deactivation of catalytic surface reactions and bulk and surface diffusion into solid matrixes. The Elovich equation has been applied to the sorption and desorption of many environmentally important inorganic reactions in soil chemistry (Sparks, 1989). It is written in linear form as Eq. [15], where q_t is the quantity of sorbate per unit mass of sorbent at time t and α and β are parameter constants. By plotting q_t vs ln t, a linear relationship should result with a slope of $(1/\beta)$ and an intercept of $(1/\beta)$ ln $(\alpha\beta)$.

Parabolic Diffusion Equation

$$q_t / q_\infty = R_D t^{1/2} \qquad [16]$$

The parabolic diffusion equation suggests that diffusion-controlled mechanisms are rate-limiting. It was first developed to describe radial diffusion in a cylindrical object where the ion concentrations on the surface and in the volume of the object are constant and uniform. The parabolic diffusion equation is most simply expressed as in Eq. [16] where q_t is the amount of sorbate per unit mass of sorbent at time t, q_∞ is the concentration of sorbate at equilibrium at time t_∞, and R_D is the overall

diffusion coefficient. A linear dependence results from a plot of q_t / q_∞ vs $t^{1/2}$ (Sparks, 1995).

Power Function or Fractional Power Equation

$$\ln q = \ln k + v \ln t \qquad [17]$$

The power function or fractional power equation is often modified when applied to soil chemical reactions. It can be expressed as Eq. [17] where q is the quantity of sorbate per unit mass of sorbent at time t, and k and v (always positive and < 1) are constants. In the situation when v is equal to 0.5, Eq. [17] is analogous to the parabolic diffusion equation, Eq. [16].

1.2.3.2 Multiple Site Models (Chemical Nonequilibrium Models)

Multiple site models consider the complexity of heterogeneous systems such as soils, soil components, and sediments. These heterogeneous systems involve chemical kinetic reactions and transport phenomena occurring simultaneously in the presence of varying particle sizes and multiple reaction sites. The overall reaction often consists of a rapid reaction phase followed by a slower reaction (Sparks et al., 1998).

To fully understand the multiple site models, one needs to consider the meaning(s) of "sites" with respect to sorption/desorption processes: 1) specific, molecular scale reaction sites; 2) sites of differing degrees of accessibility; 3) sites of differing sorbent type (i. e. organic matter and inorganic mineral surfaces); and 4) sites with different sorption/desorption mechanisms (Sparks et al., 1998).

One-Site Model

$$S \overset{k_d}{\leftrightarrow} C \qquad [18]$$

The one-site model assumes that the all sites are time-dependent and the rate is limited by one mechanism reacting with identical sites. The biggest limitation of the one-site model is that it cannot describe biphasic (rapid and slow stages) sorption/ desorption. The one-site model poorly predicts sorption in heterogeneous systems since multiple sites exist.

Two-Site Model

$$S_1 \overset{X_1K_p^c}{\leftrightarrow} C \overset{k_d}{\leftarrow} S_2 \qquad [19]$$

The two-site model assumes that biphasic reactions are proceeding with one attaining a rapid equilibrium and the other a slow, continuous reaction over a long time period (Karickhoff and Morris, 1985). The adjustable parameters involved with the two-site model are the fraction of sites at local equilibrium (X_1) and the rate constant (k). Sorption/desorption isotherms are employed to determine the partition coefficient (K_p). This model also infers that there are two different types of reaction sites, one for each reaction phase period (fast and slow). The two-site model often does not describe slow, nonequilibrium desorption well (Brusseau and Rao, 1989).

Multi-Site Model

$$F(t) = 1 - [M(t) / M] = 1 - [\beta /(\beta + t)]^{\alpha} \qquad [20]$$

Developed by Connaughton et al. (1993), the multi-site model accounts for the multiple sites that may occur in heterogeneous systems. This model requires the determination of two fitting parameters α, a shape parameter, and $1/\beta$, the mean standard deviation of the rate coefficients. The multi-site model was designed for sorption data and, unfortunately, over-predicts the amount of desorption when compared to desorption experiments in many cases.

1.2.3.3 Dissolution Models

Surface Ligand Complex Concentration vs. Dissolution Rate

$$R_L = k'_L (\equiv ML) = k'_L C^s_L , \qquad [21]$$

The rate of ligand-catalyzed dissolution, R_L, possesses a linear dependence on the surface concentration of the ligand complexes, C^s_L. By plotting C^s_L (mol m^{-2}), determined experimentally, versus R_L (mol m^{-2} h^{-1}), a linear relationship results with k'_L (h^{-1}) equal to 1/slope. Furrer and Stumm (1986) applied this model to the dissolution of γ-Al_2O_3 by oxalate, malonate, and succinate.

Surface Proton Complex Concentration vs. Dissolution Rate

$$R_H = k'_H (\equiv MOH_2^+)^\gamma = k'_H (C^s_H)^\gamma \qquad [22]$$

The proton-promoted dissolution rate is constant for each pH. The dissolution rate, R_H, is related to the surface protonation concentration, C^s_H, and to the numerical power of the oxidation state of the metal observed in the dissolution process. By

plotting log C^s_H (mol m^{-2}), determined experimentally, versus log R_H (mol m^{-2} h^{-1}), a linear relationship results with the slope equal to, j, the oxidation state of the metal and k'_H (h^{-1}) is the intercept. Furrer and Stumm (1986) applied this model to the dissolution of γ-Al_2O_3.

1.3 Research Objectives and Justification

The objectives of this dissertation research were to examine the kinetics and mechanisms of the formation and dissolution of Ni(II) surface precipitates on pyrophyllite, talc, gibbsite, amorphous silica, and a gibbsite/silica mixture using macroscopic, spectroscopic (XAFS and DRS), microscopic (AFM and HRTEM), and thermogravimetric (HRTGA) techniques. The sorption studies address the influence of Al-bearing and Al-free sorbents on product formation as affected by time, pH, and temperature. The dissolution investigations assess the effect of residence time on stability of the Ni precipitates and how a number of environmentally important dissolution agents influence precipitate stability.

Pyrophyllite ($Al_2Si_4O_{10}(OH)_2$), talc ($Mg_3Si_4O_{10}(OH)_2$), gibbsite ($Al(OH)_3$) and amorphous silica (SiO_2) were used as single model soil components to study the kinetics and mechanisms of Ni sorption/dissolution. A mixture of 40% gibbsite and

60% amorphous silica, by weight, was also employed to more closely mimic heterogeneous systems in natural environments.

Pyrophyllite (Robbins, NC, USA; Ward's) was employed in this research because it shows very little deviation from the chemical formula ($Al_2Si_4O_{10}(OH)_2$) of an ideal 2:1 clay. The dioctahedral structure of pyrophyllite consists of neutral tetrahedral-octahedral-tetrahedral layers and is the basic structure of the smectite and illite phyllosilicate groups which are very important and prominent in soils throughout the world. Sorption of ions is primarily limited to edge sites of pyrophyllite since the near neutral layer charge obviates planar permanent charge sites. The pyrophyllite was prepared by grinding the clay in a ceramic ball mill for approximately 14 days, centrifuging to collect the < 2 μm fraction in the supernatant, Na^+ saturating the < 2 μm fraction, and then removing excess salts by dialysis followed by freeze drying of the clay. The pyrophyllite was carefully characterized using diffuse reflectance infrared Fourier transform (DRIFT) spectroscopy and x-ray diffraction (XRD) with both methods exhibiting the expected normal peaks for pyrophyllite. The specific surface area of the clay was determined using N_2-BET (96.3 $m^2 g^{-1}$) and ethylene glycol monoethyl ether (EGME) (95 $m^2 g^{-1}$) methods.

Talc ($Mg_3Si_4O_{10}(OH)_2$) (Cherokee Co., NC, USA; Excalibur) also consists of neutral tetrahedral-octahedral-tetrahedral layers and is the prototype structure of the smectite and illite phyllosilicate groups which are prominent in soils. Sorption of ions is primarily limited to edge sites of talc, as in pyrophyllite, since the near neutral layer charge dismisses planar permanent charge sites. The structural difference between talc and pyrophyllite is that talc possesses three Mg^{2+} in its octahedral position while pyrophyllite has two Al^{3+} in the octahedral position. Therefore, talc is considered a trioctahedral clay and pyrophyllite a dioctahedral clay. By using talc, Al^{3+} would not be present in solution which is believed to be the driving mechanism behind the formation of multinuclear surface precipitates. The talc was prepared in the same manner as the pyrophyllite and characterized by the same methods. Surface area, determined by N_2-BET analysis, was 75 $m^2\ g^{-1}$.

Gibbsite ($Al(OH)_3$) (Arkansas, USA; Ward's) is a common component of soils and is composed of two planes of close-packed OH^- with Al^{3+} between them. The Al^{3+} reside in two-thirds of the octahedral holes, and they are distributed in hexagonal rings. In the interior, each Al^{3+} shares six OH^- with three other Al^{3+}, and each OH^- is bridged between two Al^{3+}. At the edge, however, each Al^{3+} shares only four OH^- and one H_2O molecule; neither is bridged between Al^{3+} (Hsu, 1995). The surface area, determined by N_2-BET analysis, was 25 $m^2\ g^{-1}$.

Precipitated amorphous silica was provided from the Chemicals Division of J. M. Huber Corporation under the copyright name of Zeofree® 5112. The amorphous silica was characterized by XRD to confirm its identity and surface area, as determined by N_2-BET analysis, was 90 $m^2 g^{-1}$. The average particle size is 8 μm.

The metal used in the studies was Ni(II) in the form of $Ni(NO_3)_2$. The largest use of nickel is in the manufacturing of Monel metal, stainless steels, and nickel-chrome resistance wire in electronic equipment. Nickel is a common contaminant in industrial wastes from tanneries, sewage sludge and mining activities. Nickel is common in meteorites and is found in many ores as sulfides, arsenides, antimonides and oxides or silicates. Additionally, nickel accumulation in ground water has increased tremendously over the past several decades. It possesses ferromagnetic properties. Nickel has the ability to form stable inner-sphere complexes and/or surface precipitates of a mixed cation hydroxide composition on the surfaces of clay minerals and metal oxides depending on the pH and surface loading of the system (Scheidegger and Sparks, 1996; Scheidegger et al., 1996 a,b; 1997; 1998).

Nickel is a common element studied by chemists in aquatic, sediment and soil environments. Most often in these situations, Ni(II) is octahedrally bound and in a

high spin state (d^8). Ni tends to have a slow water exchange rate (10^4) in comparison to most transition metals. As with most first row transition metals, Ni (II) is a Class III metal meaning that it is labile and has a modest ligand (H_2O) exchange rate. It will be held tightly by a variety of chelating ligands such as EDTA (Class II ligand). Within the natural environments listed above, Ni is not typically abundant. Its appearance in these places is generally the result of human inputs. As with any substance, too much Ni(II) can be harmful although it is an essential micronutrient for both plants and animals and many believe that it is a serious carcinogen.

Sorption on Ni(II) in aquatic and soil environments is dependent on pH, temperature and type of sorbent (minerals or OM). Ionic strength plays a small part as well. Ni is often found as $Ni(H_2O)_6^{2+}$ (octahedrally bound) is these environments prior to sorption reactions. Ni(II) follows the typical metal sorption edge in regards to pH in which little is sorbed at low pH and most is sorbed at a higher pH and the curve is "S" shaped. The kinetics of Ni(II) sorption is relatively rapid depending on the comparison. Ni(II) tends to form inner-sphere bidentate bonds at lower pH values (< 7) and will form surface precipitates on an array of sorbents quite easily at pH values above 7. $Ni(H_2O)_6^{2+}$ hydrolysis tends to occur at about pH 8. Surface precipitation of Ni on clay mineral and oxide surfaces results in the formation of $Ni(OH)_2$-like precipitates depending on the composition on the sorbent. Octahedrally bound Ni(II)

($Ni(H_2O)_6^{2+}$) sorption to reactive sites within the environment will result in the formation of the chemical bond, loss of two of its water molecules, and release of protons from the surface. Therefore, the pH of the system will decrease. Transfer of an electron is from Al or Si, for example with pyrophyllite, via O to the d(x-y) (e_g) orbital of Ni(II). Ideally, since Ni(II) is octahedrally bound, it should bond to Al(III) since it is also octahedrally bound in most mineral lattices.

While sorption of Ni is one reaction option in the environment, desorption or mobility is another option. Metals, such as Ni(II), rely on ligands to aid in its their movement within aquatic and soil environments. One mode of this transport many cause the Ni(II) atom to bond to a chelating ligand that will keep it in solution and not available for sorption. If one compares $Ni(NH_3)_6^{2+}$ and a Ni-EDTA complex, the $Ni(NH_3)_6^{2+}$ molecule is more susceptible to dissociation than the Ni-EDTA complex due to the chelate effect as a result of increased entropy. In comparison to other first row transition metal complexes, the Irwing-William ordered series applies as Mn(II)<Fe(II)<Co(II)<Ni(II)<Cu(II)>Zn(II), meaning that similar metal complexes to the right of Ni are more stable than those to the left. Therefore ligand exchange rates are important to understand. Ligand exchange reactions can follow a series of events such as when Ni is complexed with NH_3 for example. $Ni(H_2O)_6^{2+}$ will allow one NH_3 ligand to replace one water ligand in successive steps, however, each step increases

the stability of the new complex. One can then assume that $Mn(d^5)(NH_3)_6$ << $Ni(d^8)(NH_3)_6$ in terms of complex stability which can also be explained by LFSE of 4 vs. 12, respectively.

Nickel, the 28th element on the periodic table, has an atomic weight of 58.7 and an electron configuration of $t_{2g}^6 - e_g^2$ (when octahedrally bound) which indicates that it possesses high spin characteristics. Since Ni(II) is found in the first row of the transition metals, it tends to be in a high spin state which means it could have octahedral ($t_{2g}^6 - e_g^2$) (CFSE = 12 and MOSE = 6) or tetrahedral ($t_{2g}^4 - e_g^4$) (CFSE = 4/9(Oct) = 5.3) coordination geometries. Another geometry available for Ni(II) is square planar ($t_{2g}^6 - e_g^2$) in which the only ligand that comes to mind that will permit this geometry is CN^- to have $Ni(CN)_4^{2-}$. Ni(II) in its octahedral form tends to be bound to ligands such as H_2O or NO_3^- while in its tetrahedral geometry it can be bound to a halide such as Br^- or Cl^-. In terms of lability of the three complexes, the tetrahedral geometry would be most labile followed by the octahedral complex and lastly the square planar complex. Therefore in a kinetic sorption study, one would expect tetrahedral Ni complexes to sorb most rapidly followed by octahedral and finally square planar complexes.

The desorptive/dissolution agents that were employed in the research were HNO_3 (pH = 4 and 6), 1 mM EDTA (pH = 4 and 7.5), 3 mM oxalate (pH = 4), and 3 mM acetylacetone (2,4-pentanedione) (pH = 6), a simple β-diketone). Nitric acid, HNO_3, is usually produced by the catalytic oxidation of ammonia. Nitric acid was used to represent proton-promoted dissolution. EDTA has long been known for its chelating abilities. EDTA reacts well with most divalent and trivalent metallic ions to form soluble metal chelates. Ligand-promoted dissolution was observed with EDTA. Oxalate, or oxalic acid, is present in many plants and vegetables, notably in those of the *Oxalis* and *Rumex* families, where it occurs in the cell sap of the plant as the potassium or calcium salt. It is also a metabolic by-product of many fungi. Oxalate is industrially produced by passing carbon monoxide (CO) into concentrated NaOH or by heating sodium formate in the presence of NaOH or Na_2CO_3. Oxalate illustrated ligand-catalyzed dissolution that naturally occurs in the soil environment. Acetylacetone (2,4-pentanedione) is the simpliest of the β-diketones. Acetylacetone forms organometallic complexes which are industrially used in gasoline additives, lubricant additives, driers for varnishes and inks, and pesticides. Nickel acetylacetonate is readily formed from acetylacetone and $Ni(OH)_{2\,(S)}$ (Budavari et al, 1989).

Chapter 2

SORPTION OF NI(II) ON CLAY MINERALS AND OXIDES

2.1 Abstract

The kinetics of mixed Ni-Al layered double hydroxide (LDH) and α-$Ni(OH)_2$ precipitate formation on clay minerals and oxides was monitored using X-ray absorption fine structure (XAFS) spectroscopy, diffuse reflectance spectroscopy (DRS), high-resolution thermogravimetric analysis (HRTGA), atomic force microscopy (AFM), and high-resolution transmission electron microscopy (HRTEM). The kinetic behavior showed that as pH increased the rate of Ni uptake increased. Initial Ni sorption kinetics were rapid at all pH values but differed at each pH for longer reaction times. The spectroscopic, microscopic, and thermogravimetric sorption studies conducted at pH 7.5 showed the formation of Ni-Al LDH on pyrophyllite and gibbsite while α-$Ni(OH)_2$ formed on talc, silica, and a gibbsite/silica mixture. The Al source for the Ni-Al LDH precipitates was believed to be derived from the sorbent (pyrophyllite and gibbsite). XAFS studies revealed that the Ni-Ni

interatomic bond distances for Ni-Al LDH and α-$Ni(OH)_2$ were 3.06 Å and 3.08 Å, respectively. This finding was supported by evidence from DRS investigations that showed v2 band positions of 15,300 cm^{-1} for Ni-Al LDH and 14,900 cm^{-1} for α-$Ni(OH)_2$. DRS and HRTGA results show that as aging time progressed up to 1 year, the formation of a Ni-phyllosilicate precursor may be occurring on the Si-containing sorbents. Kinetic AFM experiments showed that cone-shaped clusters formed on the surfaces of pyrophyllite, talc, and silica, however, with this technique one cannot ascertain any chemical information. HRTEM studies coupled with energy dispersive X-ray spectroscopy (EDS) revealed 1-year aged Ni precipitates on pyrophyllite and talc possessed well-defined lattice fringes at spacings of approximately 0.2 nm, which is consistent with the lattice spacings of Ni-hydrotalcite. The results of this study reveal important information on Ni sorption and precipitate formation behavior on clay mineral and oxide surfaces monitored by an array of spectroscopic, microscopic, and thermogravimetric techniques. These findings should be incorporated into sorption models to better predict the fate of metals in subsurface environments.

2.2 Introduction

Many kinetic studies have shown that sorption of metal cations onto soil, clay mineral and metal oxide surfaces is described by a two step process comprising a rapid

stage and a slow stage (Burns, 1976; Kinniburgh and Jackson, 1981; Kou, 1986; Brümmer et al., 1988; Ainsworth et al., 1994). The rapid initial stage, occurring on time scales of seconds, minutes or hours, has been interpreted as an adsorption phenomenon (Kinniburgh and Jackson, 1981; Sparks, 1995). However, the slow reaction stage, associated with time scales on the order of days, weeks or months is not clearly understood. Three possible mechanisms have been attributed to the slow sorption stage: 1) adsorption onto sites of lower reactivity (Benjamin and Leckie, 1981; Dzombak and Morel, 1986), 2) diffusion of the adsorbate into the adsorbent via micropores and/or directly in the solid material (absorption) (Ogwada and Sparks, 1986b; Steinberg et al., 1987; Brümmer et al., 1988; Comans and Hockley, 1992; Pignatello and Xing, 1995), and 3) surface precipitation formation (Sposito, 1984; Farley et al., 1985; Davis et al., 1987; Chisholm-Brause et al., 1990; Charlet and Manceau, 1992; Fendorf et al., 1994; O'Day et al., 1994; Fendorf et al., 1996; Scheidegger et al., 1996a,b; 1997; 1998; Scheidegger and Sparks, 1996; O'Day et al., 1996; Towle et al., 1997; Xia et al., 1997; Thompson, 1998; Scheinost et al., 1999; Scheckel and Sparks, 2000a). However, until recently, the proposed mechanisms for slow metal sorption were based strictly on macroscopic measurements through sorption isotherms and kinetic studies. To definitively prove the suggested mechanisms one must employ molecular approaches such as X-ray absorption fine structure (XAFS) spectroscopy. With the advent of in-situ spectroscopic and

microscopic techniques, it is possible to identify the cause of slow sorption mechanisms.

While adsorption has been characterized as a two-dimensional surface feature, surface precipitation has been depicted as three-dimensional growth. According to Sposito (1986), precipitation is the formation of a solid mixture either by inclusion or by coprecipitation or on the surface of a pre-existing solid phase (surface precipitate). Precipitation is initiated by either homogeneous or heterogeneous nucleation. Surface precipitation follows a process which involves 1) adsorption of the metal onto the surface, 2) surface nucleation, and 3) crystalline growth outward from the surface (Stumm, 1992). Site saturation is manifested in pH edges by a plateauing of the curve at some level below 100 percent sorption. However, it is difficult to detect site saturation for metal cations because of the formation of hydroxide precipitates either in solution or on the surface, occurring at both high- and low-affinity binding sites, prior to bulk solution precipitation (James and Healy, 1972; Farley et al., 1985). Contribution of surface precipitates to overall sorption increases as sorbate/sorbent ratios increase and may become the dominant sorption mechanism at very high ratios (Harvey and Linton, 1984; Farley et al., 1985). However, recent studies on the formation of surface precipitates indicate that high sorbate/sorbent ratios are not necessary and that site saturation is not achieved (Chisholm-Brause et al., 1990;

Charlet and Manceau, 1992; Fendorf et al., 1994; O'Day et al., 1994; Fendorf et al., 1996; Scheidegger et al., 1996a,b; 1997a,b; Scheidegger and Sparks, 1996; O'Day et al., 1996; Towle et al., 1997; Xia et al., 1997; Thompson, 1998; Scheinost et al., 1999; Scheinost and Sparks, 1999; Thompson et al., 1999a and b).

Pioneering work by Scheidegger et al. (1996a,b; 1997; 1998) and Scheidegger and Sparks (1996) explains the kinetic reactions of Ni(II) sorption on the surfaces of pyrophyllite and metal oxides to form a mixed cation (Ni-Al) hydroxide phase. They demonstrated that surface precipitation can occur at: 1) low sorbate concentrations, much less than monolayer coverage, 2) short time scales, within 15 minutes, and 3) pH values lower than where one would expect the precipitation of a metal's hydroxide phase according to its thermodynamic solubility product. This is contrary to the previous equilibrium equations for a mononuclear surface hydroxide precipitate. Surface clusters began growth within 15 minutes, an extremely short time in comparison to traditional thinking (Scheidegger et al., 1998). Scheidegger et al. (1998) noted that the bond distances for Ni-Ni were distinctly shorter in the polynuclear precipitates than in $Ni(OH)_{2\,(S)}$, indicating that the complexes are not $Ni(OH)_{2\,(S)}$. The nucleation of the heterogeneous solid at the surface interface has not been positively identified but the structure of the precipitate is similar to takovite ($Ni_6Al_2(OH)_{16}CO_3 \bullet H_2O$), based on XAFS data analysis and comparison to the

reference takovite sample. It appears that Al plays an important role in the formation of these surface precipitates but its contribution is not fully understood nor have the roles of other trivalent cations been studied as to their importance in precipitation. In fact, O'Day et al. (1994), observing Co (II) reactions on kaolinite, Charlet and Manceau (1992), studying Cr (III) interactions with hydrous ferric oxides, Roe et al. (1991) examining Pb(II) reactions on goethite. and Chisholm-Brause et al. (1990), working with Pb on γ-Al_2O_3, also determined that the respective metal that they were studying formed multinuclear complexes on the surface of clay minerals and metal oxides. However, additional XAFS Pb studies on γ-Al_2O_3 by Strawn et al. (1998) and on α-Al_2O_3 by Bargar et al. (1997) demonstrated that surface precipitation did not occur. The previous research clearly shows that surface precipitates form on clay mineral and metal oxide surfaces and can form over short reaction times.

However, other XAFS spectroscopic studies examining surfaces that do not contain Al or other trivalent cations have concluded that the sorbing trivalent or divalent cation employed in the studies formed $Me^{(+3)+2}$-(oxy)hydroxide phases and not the multinuclear complexes noted above. Fendorf et al. (1994) observed the formation of γ-CrOOH due to interactions of Cr(III) with silica. The Cr-Cr bond distances of 2.99 Å are indicative of edge-sharing Cr octrahedra. Research by O'Day

et al. (1996), using XAFS spectroscopy, examined the sorption complexes of Co(II) on amorphous silica (α-SiO_2) and rutile (TiO_2). The complexes that formed on the surface of amorphous silica were the same, $Cr(OH)_{2\,(S)}$, regardless of the surface coverage and incubation time. The rutile sorption products varied depending on surface coverage. At low Co(II) coverages, Co apparently sorbed directly to the rutile surface to form monodentate or small mononuclear complexes occupying Ti-equivalent sites at the rutile surface. Higher coverages yielded an increase in Co second-neighbor backscattering, indicating larger multinuclear complexes believed to be similar to anatase, a TiO_2 polymorph, and not $Cr(OH)_{2\,(S)}$, possibly due to the comparable bond distances of Cr-Cr to Ti-Ti. Scheinost et al. (1999) and Scheinost and Sparks (1999) employed XAFS and DRS to study the role of Al in the formation of secondary Ni precipitates on pyrophyllite, gibbsite, talc, and amorphous silica. Scheinost and coworkers found similar results to that of Scheidegger and coworkers for the Ni-pyrophyllite and -gibbsite sorption systems in which mixed Ni-Al LDH (layered double hydroxide) precipitates formed. However, using XAFS, Scheinost and Sparks (1999) determined that Ni sorption on Al-free talc and silica resulted in the formation of α-$Ni(OH)_2$ precipitates with a Ni-Ni bond distance of 3.08 Å, which is distinctly different than the 3.06 Å bond distance for Ni-Al LDH. These findings coincided with DRS work by Scheinost et al. (1999) that found v2 band positions of 15,300 cm^{-1} and 14,900 cm^{-1} for Ni-Al LDH and α-$Ni(OH)_2$, respectively.

The objective of this study was to observe Ni(II) sorption and possible surface precipitation formation on pyrophyllite ($Al_2Si_4O_{10}(OH)_2$), talc ($Mg_3Si_4O_{10}(OH)_2$), gibbsite ($Al(OH)_3$), amorphous silica (SiO_2), and a mixture of gibbsite and amorphous silica over various times, pHs, and temperatures employing spectroscopic (XAFS and DRS), microscopic (AFM and HRTEM), and thermogravimetric (HRTGA) techniques.

2.3 Materials and Methods

2.3.1 Materials

The pyrophyllite (Robbins, NC, USA; Ward's), talc (Cherokee Co., NC, USA; Excalibur) and gibbsite (Arkansas, USA; Ward's) samples from natural clay deposits were prepared by grinding the clay in a ceramic ball mill for approximately 14 days, centrifuging to collect the < 2 μm fraction in the supernatant, Na^+ saturating the < 2 μm fraction, and then removing excess salts by dialysis followed by freeze drying of the clay. X-ray diffraction (XRD) showed minor impurities of kaolinite and quartz in pyrophyllite, and about 10 % bayerite in the gibbsite. Although the talc sample had about 20 % chlorite according to XRD, acid digestion resulted in an Al/Mg ratio of

only 0.01. This small Al-content was not sufficient in former experiments to induce the formation of detectable amounts of Ni-Al LDH (Scheinost et al., 1999). In addition, amorphous silica (SiO_2) (Zeofree® 5112) from the Huber Corporation was employed. The mixture of gibbsite and amorphous silica consisted of 40% gibbsite and 60% silica by weight. A mixture was used to more closely mimic heterogeneous systems in the natural environment. The N_2-BET surface areas of the sorbent phases were 95 $m^2 g^{-1}$ for pyrophyllite, 75 $m^2 g^{-1}$ for talc, 25 $m^2 g^{-1}$ for gibbsite, 90 $m^2 g^{-1}$ for amorphous silica, and 64 $m^2 g^{-1}$ for the gibbsite/silica mixture.

2.3.2 Ni Sorption Kinetics

Nickel sorption on the clay mineral and oxide surfaces was examined macroscopically by employing a pH-stat batch technique at 25 °C. Temperature was controlled through the use of a thermostatted stir plate equipped with a temperature probe to monitor and correct temperature changes in the batch experiments. The suspensions were stirred so that a small vortex was formed to eliminate film diffusion (approximately 350 rpm). The majority of nickel sorption experiments were examined by reacting a 3 mM $Ni(NO_3)_2$ solution with a 10 g/L suspension of the sorbent in 0.1 M $NaNO_3$ at pH 7.5. Ni sorption on pyrophyllite was also conducted at pH values of 7.0, 6.5, 6.0 and 5.5 using the same $[Ni]_o$, solid:solution ratio, and I as above. The

sorption experiments were undersaturated with respect to the thermodynamic solubility product of β-$Ni(OH)_2$ (Scheidegger and Sparks, 1996; Scheidegger et al., 1998). The systems were purged with N_2 to eliminate CO_2, and the pH was maintained through addition of freshly prepared 0.1 M NaOH via a Radiometer pH-stat titrator. Periodic 10 mL aliquots were removed from the batch reactor and filtered via a syringe equipped membrane filter apparatus. The filtered solution was then analyzed by ICP for Ni and Si, if applicable.

2.4 Spectroscopic, Microscopic, and Thermogravimetric Characterization of Surface Precipitates

Changes in Ni speciation of the sorbed phase at 25 °C and pH 7.5 were periodically assessed via spectroscopic, microscopic, and thermoanalytical techniques. For XAFS, DRS, and AFM analyses, samples were examined in-situ by centrifuging the suspensions and using the wet clay paste. For HRTGA and HRTEM analyses, the clay pastes were washed three times with D.I. water and freeze-dried before examination.

2.4.1 X-Ray Absorption Fine Structure (XAFS) Spectroscopy

XAFS was applied to determine information on the nearest-neighbor chemical environment of Ni such as coordination numbers and atomic distances. Experiments were conducted at the National Synchrotron Light Source (NSLS), Brookhaven National Laboratory (BNL), Upton, New York, on beamline X-11A. The electron storage ring was operated at 2.528 GeV with beam currents in the 180 - 310 mA range. A 0.5 mm premonochromator slit width and a Si(111) double-crystal monochromator detuned by 25% to reject higher-order harmonics was used. The beam energy was calibrated by assigning the first inflection of the K_{α}-absorption edge of nickel metal to 8333 eV. The XAFS spectra were collected in fluorescence mode using a Lytle detector. The ionization chamber of the Lytle detector was filled with Ar and the chamber of I_o was filled with N_2 gas. Samples were positioned at a 45° angle relative to the incident beam and the ionization chamber was situated at 45° off the sample (90° off the incident beam). A Co-3 filter and Soller slits were arranged between the sample and the Lytle detector to reduce scattered X-rays reaching the fluorescence detector. Spectra were collected at 77 K to reduce thermal disorder. Previous studies in our laboratory indicate that Ni speciation does not change by cooling to 77 K versus room temperature (Roberts et al., 1999). Triplicate scans were collected for each sample.

MacXAFS 4.0 (Bouldin et al., 1995) was employed for background subtraction and Fourier filtering. The χ function was extracted from the raw data by using a linear preedge background and a spline postedge background, and by normalizing the edge to unity. The data were next converted from energy to k space and weighted by k^3 to compensate for the dampening of the XAFS amplitude with increasing k. Structural parameters were extracted with fits to the standard XAFS equation. Using the FEFF6 and ATOMS codes (Zabinsky et al., 1995), *ab initio* amplitude and phase functions for single shells were calculated. A natural takovite ($Ni_6Al_2(OH)_{16}CO_3 \bullet H_2O$) (Kambalda W.A., Australia) and a synthetic β-$Ni(OH)_2$ (Johnson Mattey Co.) were used as reference compounds. Multishell fitting was done in R space over the range $1.104<R<3.129$ Å with $3.2<k<13.6$ $Å^{-1}$ for pyrophyllite and gibbsite samples and $1.104<R<3.191$ Å with $3.2<k<13.6$ $Å^{-1}$ for talc, amorphous silica, and gibbsite/silica mixture samples. The number of free floating parameters was reduced by one by allowing only equal values for the Debye-Waller factors of the Ni-Ni and Ni-Al shells for pyrophyllite and gibbsite. The R_{Ni-O} and R_{Ni-Ni} values are estimated to be accurate to ±0.02 Å, and the N_{Ni-O} and N_{Ni-Ni} are estimated to be accurate to ±20%. The estimated accuracies for N_{Ni-Al} and R_{Ni-Al} are ±60% and ±0.06 Å, respectively. The accuracy estimates are based on the results of theoretical fits to spectra of the reference compounds of known structure (O'Day et al., 1994b).

2.4.2 Diffuse Reflectance Spectroscopy (DRS)

Although the information provided by DRS is restricted to local symmetry of the first coordination shell, it is more sensitive to changes in the coordination distance of Ni-O (R_{Ni-O}) than XAFS. Therefore, this method proved to be very sensitive in distinguishing between Ni-Al LDH (smaller R_{Ni-O}) and α-Ni hydroxide (larger R_{Ni-O}) by using the energy position of the ν2 band which corresponds to the ${}^3A_{2g} \rightarrow {}^3T_{1g}$ transition (Scheinost et al., 1999). A Perkin Elmer Lambda 9 diffuse reflectance spectrophotometer fitted with a 5 cm Spectralon-coated integrating sphere was employed to collect spectra in the UV-VIS-NIR range. Extraction of the band position was as in Scheinost et al. (1999).

2.4.3 High Resolution Thermogravimetric Analysis (HRTGA)

HRTGA was employed to characterize thermal decomposition reactions attributed to the Ni precipitate phases in the reacted clay mineral samples. Changes in the quantity and temperature of decomposition are indicative of compositional changes in the precipitate. The studies employed a TA Instruments 2950 High-

Resolution Thermogravimetric analyzer to examine approximately 15-20 mg samples from sorption studies that were previously freeze-dried. The analysis was run under a N_2 atmosphere over a temperature range of 30 to 800 °C. The following high-resolution settings were used: (1) maximum heating rate = 20° C min^{-1}, (2) resolution = 5.0, and (3) sensitivity = 1.0 (Ford and Bertsch, 1999). Data are presented as the derivative of the weight loss curve versus temperature.

2.4.4 Atomic Force Microscopy (AFM)

While AFM is a useful in-situ technique to view reactions at the mineral-water interface, its biggest disadvantage is that it does not provide chemical data and must be utilized in conjunction with spectroscopic and thermogravimetric instruments. AFM was employed to observe the distribution and topographical changes of unreacted and Ni-reacted pyrophyllite, talc, and silica. Given the size and rough features of gibbsite, AFM could not be used to examine the growth of Ni precipitates on gibbsite and the gibbsite/silica mixture. Experiments were conducted in TappingMode™ on a MultiMode Nanoscope IIIa AFM from Digital Instruments (Santa Barbara, CA). TappingMode™ imaging overcomes the limitations of the conventional contact scanning modes by alternately placing the tip in contact with the surface to provide high resolution and then lifting the tip off the surface to avoid dragging the tip across

the surface. TappingMode™ imaging was implemented in ambient air by oscillating the cantilever assembly at or near the cantilever's resonant frequency using a piezoelectric crystal. The oscillating tip was then moved towards the surface until it began to lightly touch, or "tap" the surface. During scanning, the tip was generally oscillating at a frequency of 50,000 to 500,000 cycles per second. As the cantilever began to intermittently contact the surface, the cantilever oscillation was necessarily reduced due to energy loss caused by the tip contacting the surface. The reduction in oscillation amplitude was used to identify and measure surface features.

Samples were taken from batch reaction vessels for the unreacted and reacted time periods. Samples were prepared by removing 2 mL of suspension from the batch reactor and depositing the suspension into a 15 mL test tube containing 8 mL of deionized H_2O. The test tube was shaken by hand and the suspension was added to a 10 mL syringe equipped with a membrane filter apparatus. The filter was removed from the apparatus and allowed to air dry before examination with TappingMode™ AFM. The collected unaltered scans were 1 μm by 1 μm with Z ranges of 60 nm (pyrophyllite) and 40 nm (talc and silica) at the maximum resolution of 512 lines and an initial set point of 2 volts. Multiple scans were collected and each scan was collected with a fresh tip.

2.4.5 High Resolution Transmission Electron Microscopy (HRTEM)

HRTEM was employed to observe the distribution of 1-year aged Ni precipitates on pyrophyllite and talc surfaces. Studies were conducted under the supervision of Ken Livi at the Earth and Planetary Sciences Department of the Johns Hopkins University in Baltimore, MD. A Philips CM300FEG/ST (300 kV) was used, a HRTEM with a field-emission electron source and a super-twin objective lens with low spherical aberration (Cs = 2.0 mm) and a line resolution of 1.0Å. Images were recorded digitally with a CCD (charge-coupled device) camera or on plates. The TEM was equipped with an energy dispersive X-ray spectroscopy (EDS) unit to identify and gain gross approximations of the quantity of elements present in the system such as Ni, Si, Al, or Mg.

Samples were prepared from batch sorption studies that were previously freezed-dried. A small amount of the dried sample was placed in approximately 5 mL of deionized water and sonicated for 2 minutes. Next, using a tweezers with a locking mechanism, a Cu grid with lacy carbon support film was dipped into the suspension to deposit the Ni-clay particles and allowed to air dry. The sample grid was then placed in a sample holder for HRTEM examination.

2.5 Results

2.5.1 Macroscopic Sorption Kinetic Data

Figure 2.1 illustrates the kinetics of Ni sorption on and Si release (except gibbsite) from pyrophyllite, talc, gibbsite, silica, and the gibbsite/silica mixture from a 3 mM Ni solution at pH = 7.5, I = 0.1 M, and 25 °C. It shows that relative Ni removal from solution within the first 24 hours was 46, 20, 4, 8, and 57 %, respectively. Ni sorption on these sorbents exhibits a fast initial step and, thereafter, relative Ni removal from solution slows down. The release of Si into solution shows a similar kinetic behavior as Ni sorption on pyrophyllite, talc, silica, and the mixture. Scheidegger et al. (1997) demonstrated this trend for Ni sorption on pyrophyllite but also noted that the Si release rate compared to the dissolution rate of the clay alone was much greater indicating that Ni may be promoting dissolution of the pyrophyllite surface during sorption. The dominant Si species in solution at pH 7.5 is $Si(OH)_4$ and is available in solution to exchange for nitrate in the interlayer of the Ni precipitate as aging time progresses (Ford et al., 1999). The Si-for-NO_3 substitution will be examined in more detail later in this chapter and in Chapter 4.

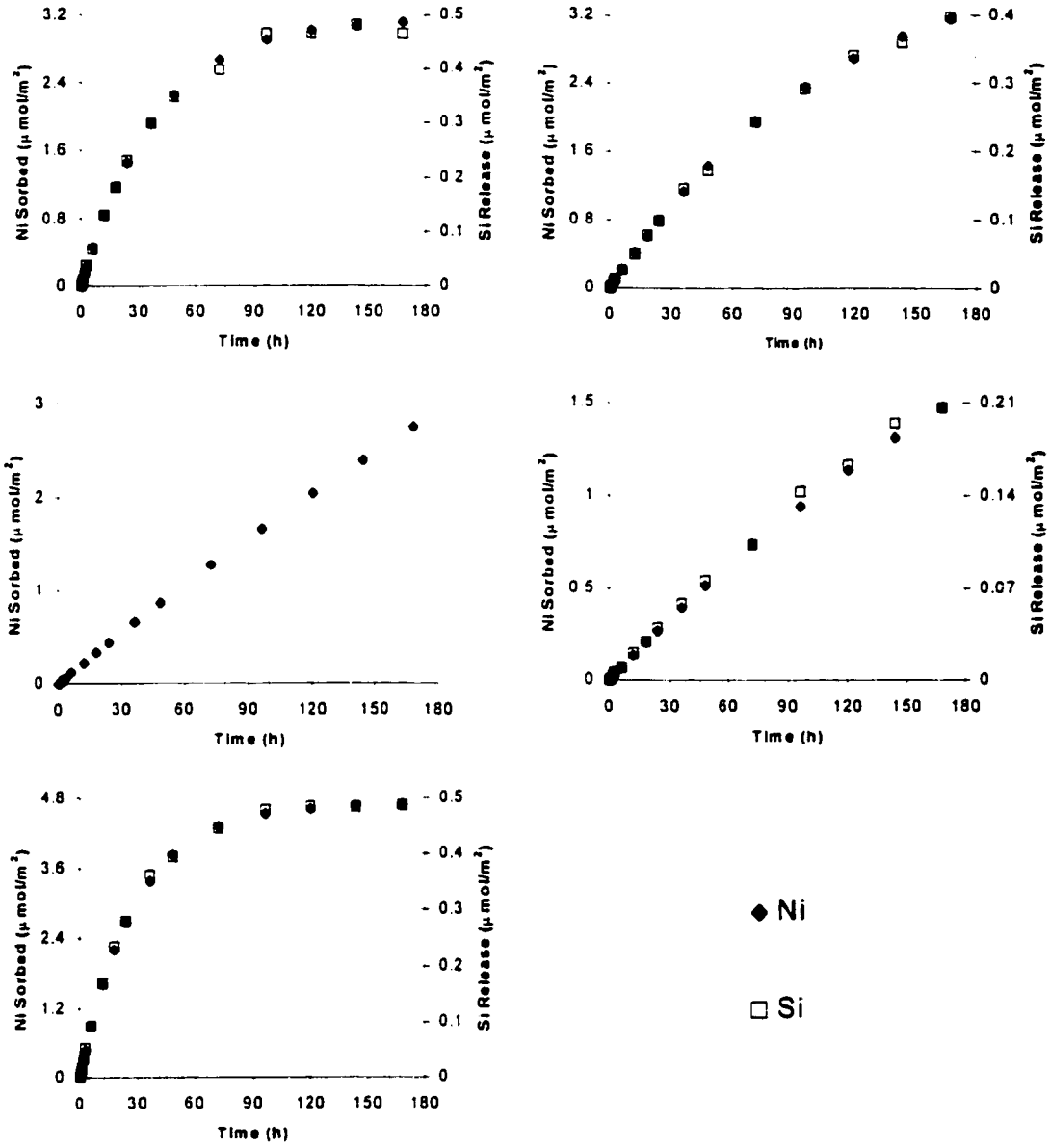

Figure 2.1. Ni sorption and Si release kinetics on (a) pyrophyllite, (b) talc, (c) gibbsite, (d) silica, and (e) gibbsite/amorphous silica mixture at pH 7.5, $I = 0.1$ M $NaNO_3$, $[Ni]_o = 3$ mM, solid:solution = 10 g/L.

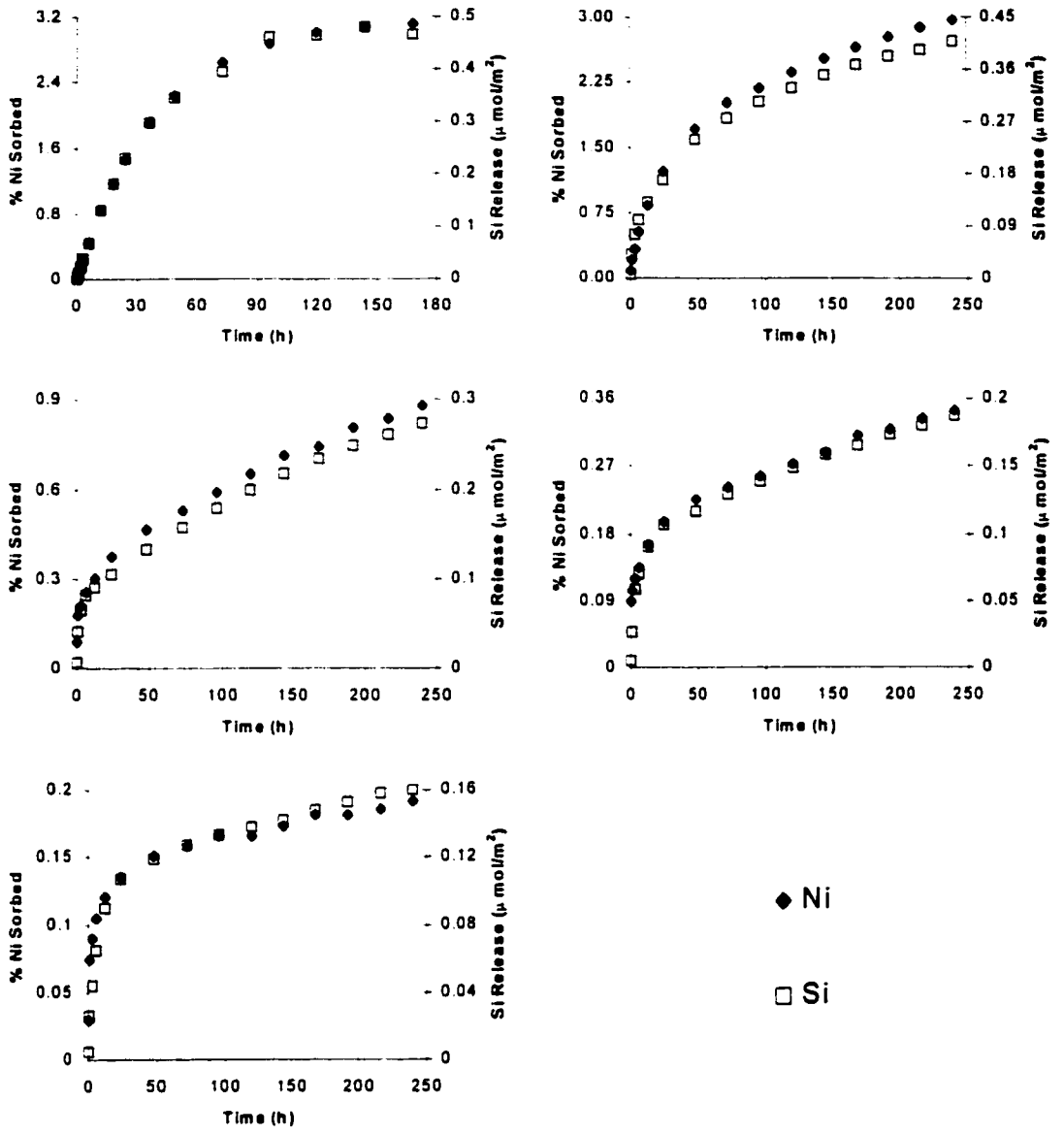

Figure 2.2. Ni sorption and Si release kinetics on pyrophyllite at (a) pH 7.5, (b) pH 7.0, (c) pH 6.5, (d) pH 6.0, and (e) pH 5.5. $I = 0.1$ M $NaNO_3$, $[Ni]_o = 3$ mM, solid:solution = 10 g/L.

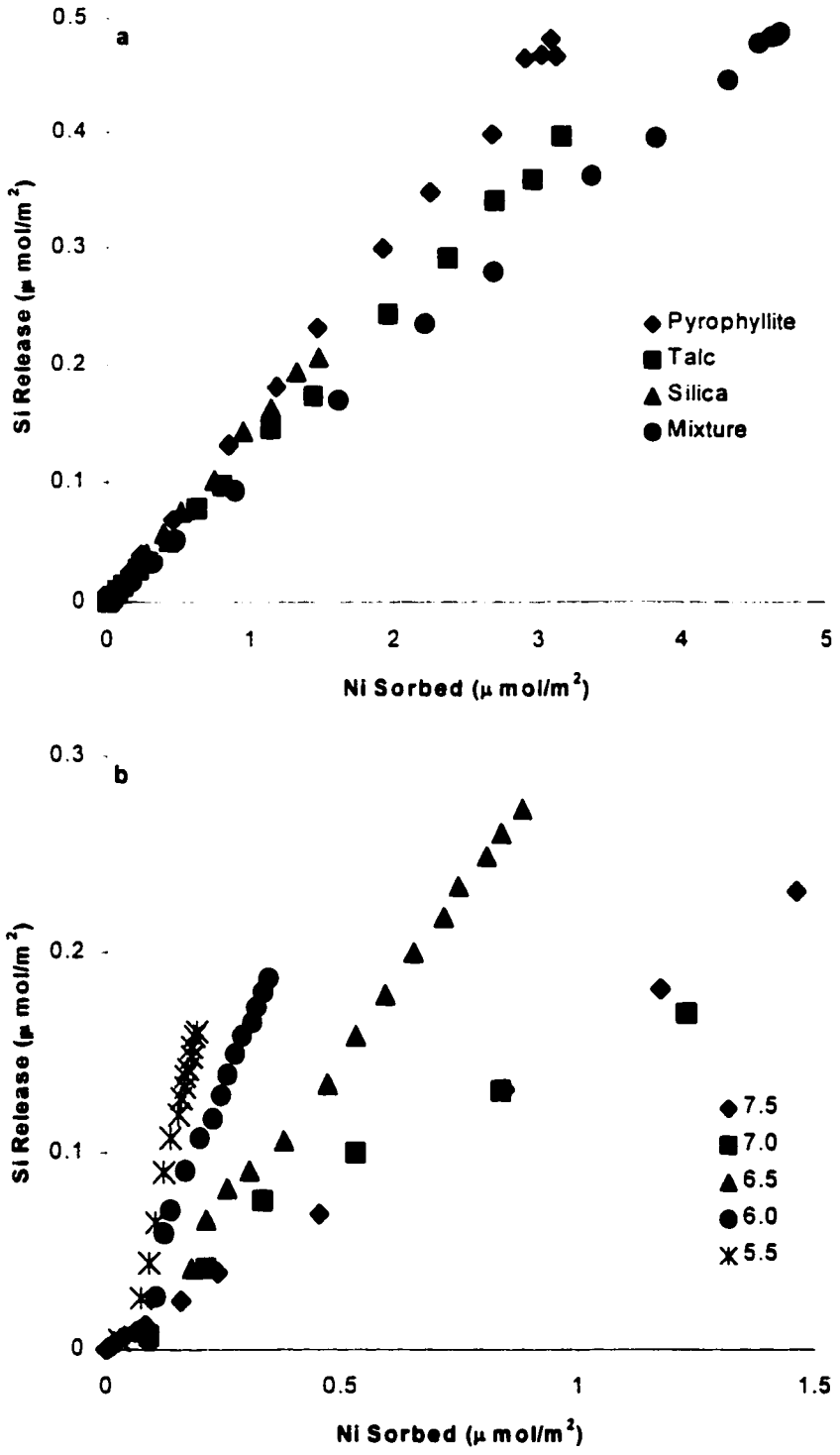

Figure 2.3. Relationship between Si release and Ni sorption on (a) the various sorbents and (b) pyrophyllite at various solution pH values. Data extracted from Figures 2.1 and 2.2.

In Figure 2.2, one sees the influence of pH (5.5 - 7.5) on Si release and Ni sorption onto pyrophyllite from a 3 mM Ni solution at I = 0.1 M and 25 °C. Typically with metals such as Ni, as pH increases, metal sorption increases and this is seen in Figure 2.2. After 24 hours of sorption at pH values of 5.5, 6.0, 6.5, 7.0, and 7.5, Ni removal from solution is 4, 6, 12, 39, and 46 %, respectively. As mentioned earlier, the release of Si into solution shows a similar kinetic behavior as Ni sorption on pyrophyllite indicating that Ni sorption may be enhancing the release of Si. Roberts et al. (1999) found that Ni precipitates do not form on the clay fraction of a Matapeake soil at a pH of 6.0 but formed slowly at pH 6.8. From the results in Figure 2.2, it is expected that adsorption was the dominant sorption mechanism at pH 5.5 – 6.5 and precipitation predominated at pH 7.0 and 7.5.

Figure 2.3 shows the relationship of Si release during Ni sorption. In Figure 2.3a, one sees a direct relationship for Ni sorption at pH 7.5 (data extracted from Figure 2.1) on the sorbents examined in this study and shows that Si release during Ni sorption is not sorbent dependent but influenced by the surface area of the sorbent. This trend shows that approximately 10 times more Ni is sorbed than Si released at pH 7.5. The increase in Ni:Si main be explained by clustering of Ni in precipitates thus not allowing Ni to attack the surface to release Si. Additionally, the low Si concentrations may be attributed to an exchange mechanism in which silicate is

substituted into the interlayer of the surface precipitates for nitrate even at early reaction times. Evidence for the formation of Ni precipitates on these sorbents and silication of the interlayer space will be provided later in this chapter.

Figure 2.3b shows Si release versus Ni sorption on pyrophyllite for solution pH values of 5.5, 6.0, 6.5, 7.0, and 7.5 (extracted from Figure 2.2). As pH decreases, the concentration of Si release per concentration of Ni sorbed increases. This may suggest that at lower pH, Ni sorption is limited due to competition from protons, which increase in concentration at pH decreases. The increased proton concentration may induce proton-promoted dissolution of the sorbent surface thus increasing the amount of Si released per amount of Ni sorbed. Note that the curves for sorption at pH 7.0 and 7.5 are nearly identical for which precipitation is the known mechanism.

2.5.2 XAFS Analysis of Sorption Samples

Figures 2.5 – 2.8 show normalized, background subtracted, k-weighted, and Fourier transformed XAFS radial structure functions (RSFs) of Ni sorbed on pyrophyllite, talc, gibbsite, silica, and the gibbsite/silica mixture at pH 7.5, respectively. The spectra are uncorrected for phase shift. The XAFS samples were collected at various aging times ranging from 15 minutes to 2 years during the Ni

Table 2.1. Percent Ni removed from solution during kinetic studies prior to XAFS analysis for each surface.

Sorption Time	Pyrophyllite	Talc	Gibbsite	Silica	Mixture
15 minutes	1				
1 hour	3	1		1	3
12 hours	27	11		4	34
1 day	46	20	4	8	57
3 days	84	49		22	92
7 days	99	78	23	44	99
1 month	99	99	73	80	100
3 months	99	99	81	85	100
6 months	100	100	90	91	100
1 year	100	100	100	99	100
2 years	100				

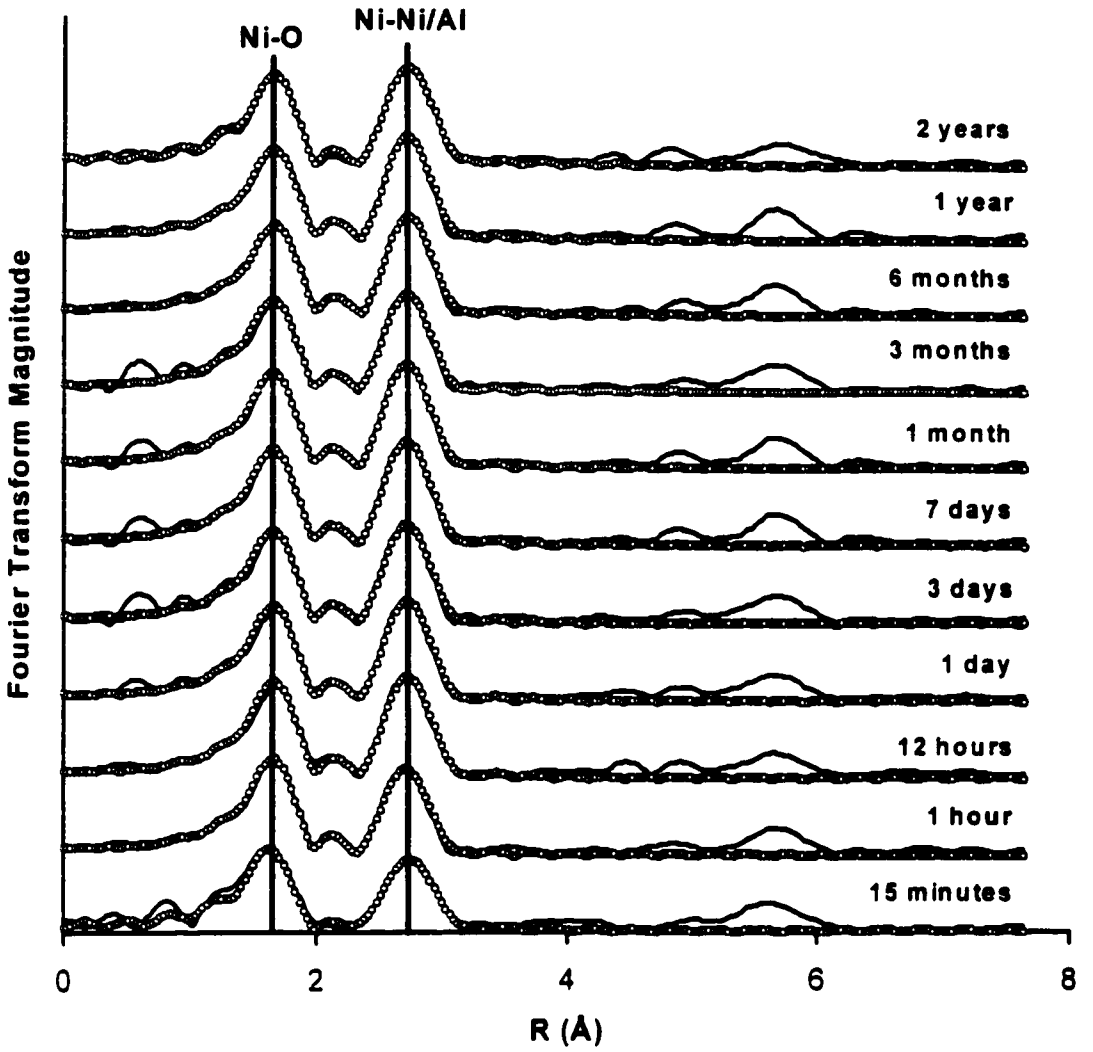

Figure 2.4. Measured (solid lines) and fitted (dotted lines) radial structure functions (RSFs) produced by forward Fourier transforms of Ni sorbed on pyrophyllite with time. The spectra are uncorrected for phase shift.

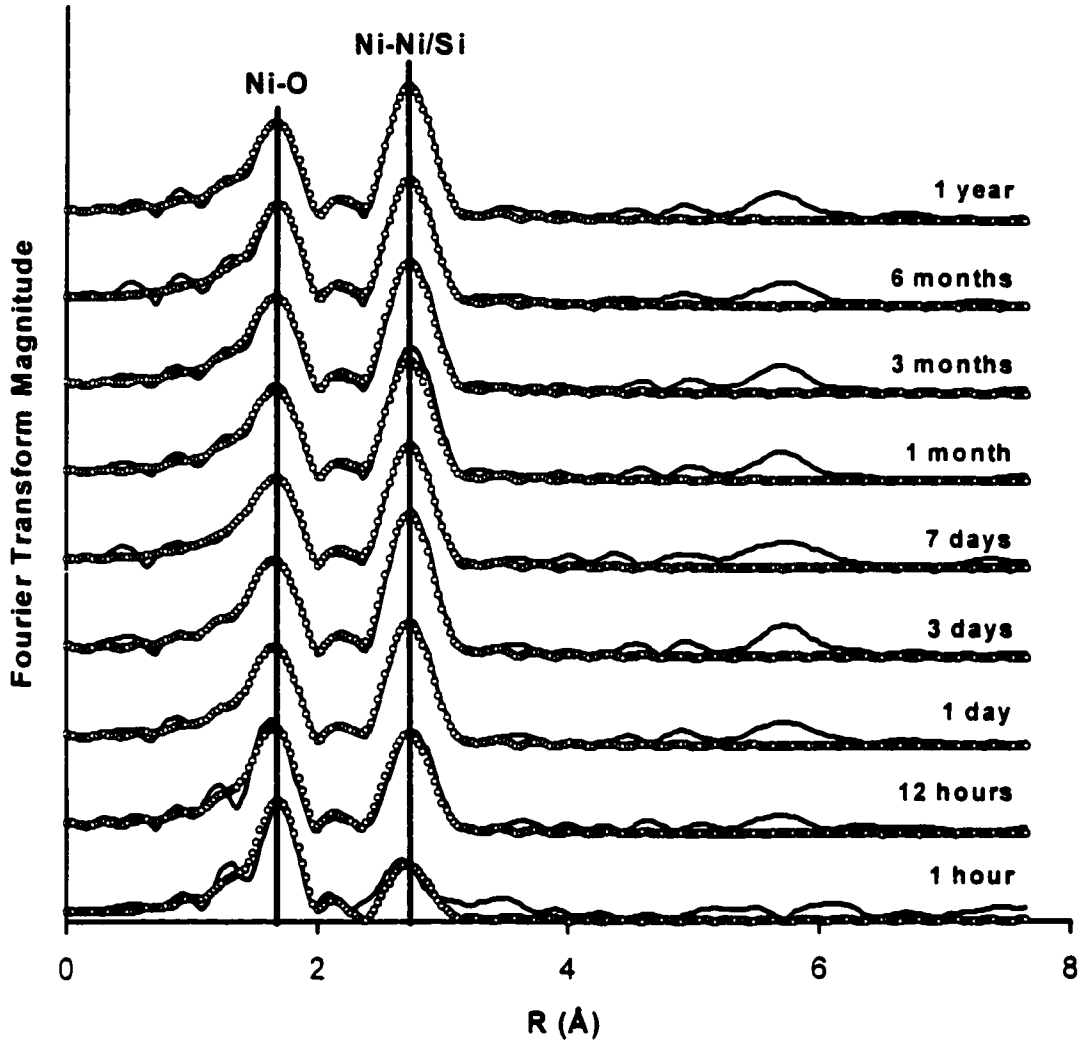

Figure 2.5. Measured (solid lines) and fitted (dotted lines) radial structure functions (RSFs) produced by forward Fourier transforms of Ni sorbed on talc with time. The spectra are uncorrected for phase shift.

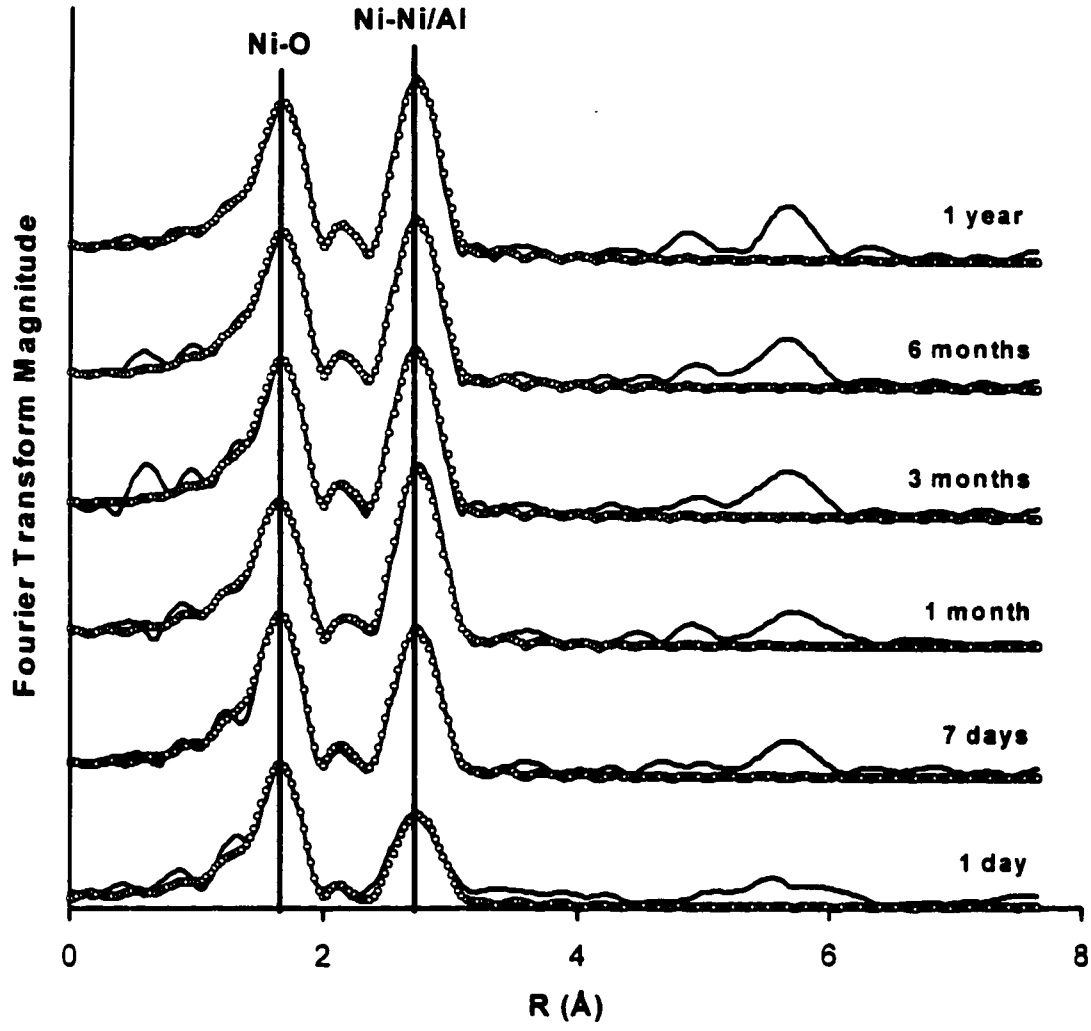

Figure 2.6. Measured (solid lines) and fitted (dotted lines) radial structure functions (RSFs) produced by forward Fourier transforms of Ni sorbed on gibbsite with time. The spectra are uncorrected for phase shift.

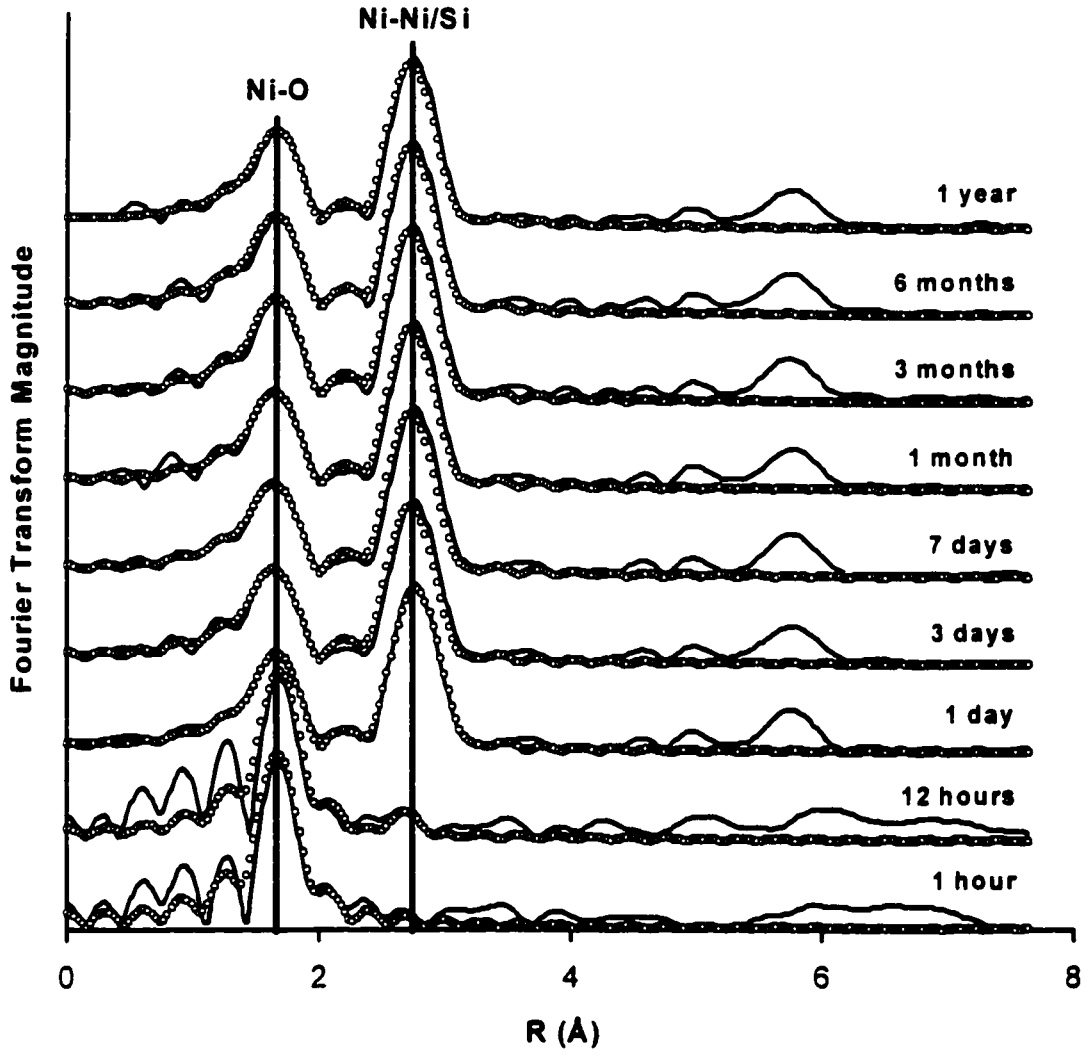

Figure 2.7. Measured (solid lines) and fitted (dotted lines) radial structure functions (RSFs) produced by forward Fourier transforms of Ni sorbed on silica with time. The spectra are uncorrected for phase shift.

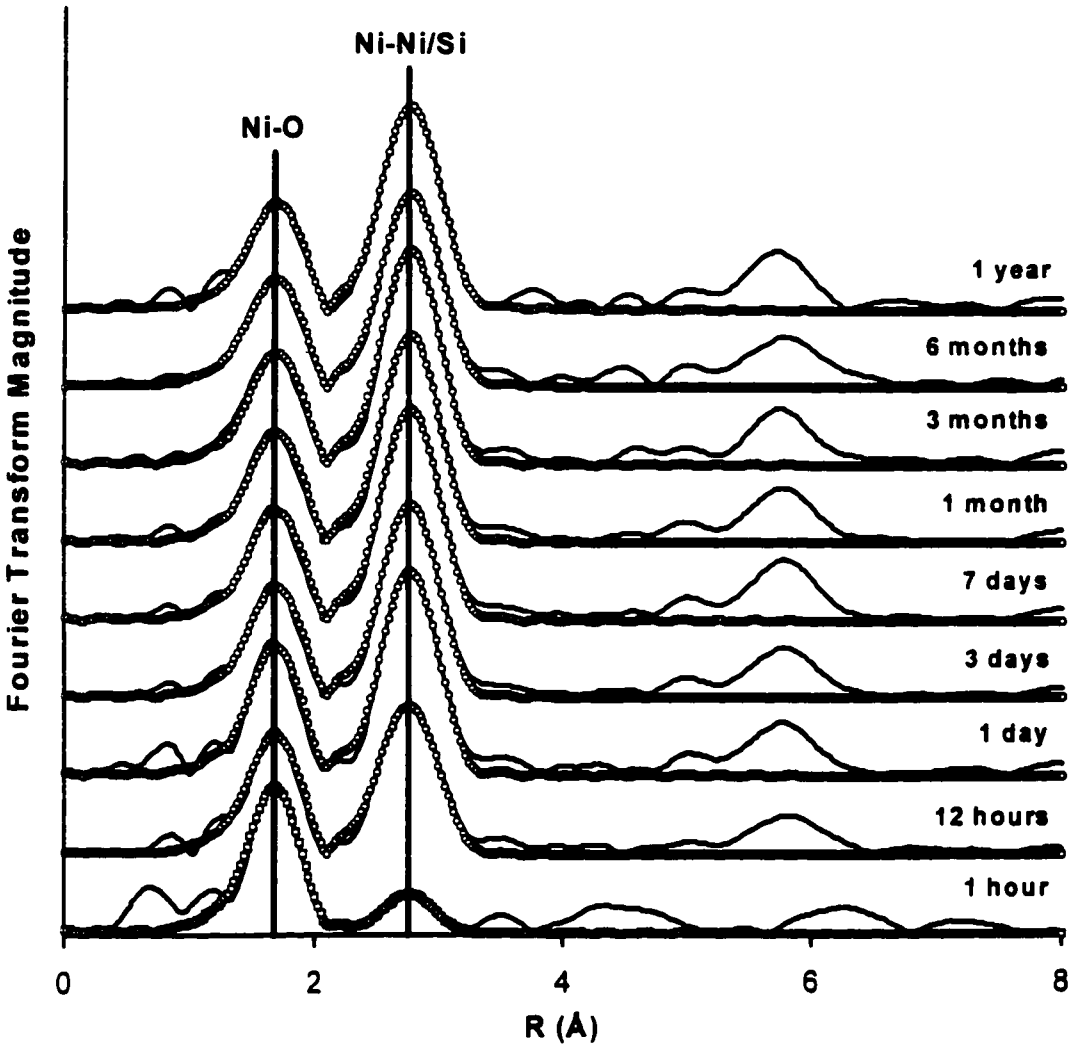

Figure 2.8. Measured (solid lines) and fitted (dotted lines) radial structure functions (RSFs) produced by forward Fourier transforms of Ni sorbed on gibbsite/silica mixture with time. The spectra are uncorrected for phase shift.

sorption experiments. In most cases, the growth of the second shell increased in intensity with increased Ni uptake from solution. The percent Ni sorbed from solution at the kinetic aging times for each surface is presented in Table 2.1. The first shell (R ≈ 1.8 Å) in Figures 2.5 – 2.8 is indicative of a Ni-O bond and the presence of a second shell (R ≈ 2.8 Å) signifies a Ni-Ni interatomic shell suggesting the formation of a Ni precipitate. The figures also show peaks beyond the second shell at R ≈ 6 Å that results from multi-scattering among Ni atoms, however, these were not included in the fitting procedure.

The structural parameters derived from XAFS analysis are summarized in Tables 2.2 – 2.6. In all cases, fits of the first RSF shell reveal that Ni is coordinated with 6 O atoms with a bond distance of 2.05 Å. This bonding environment indicates that Ni is octahedrally coordinated. For the second shell, fits were obtained by including Ni and Al (pyrophyllite and gibbsite) or Si (talc, silica, and mixture). Inclusion of a Si shell for talc, silica, and the mixture was excluded in the early aging times but was particularly useful in the long-term aged samples as Si substituted for nitrate in the interlayer of the precipitate thus leading to the formation of a Ni-phyllosilicate precursor. Since Si and Al are similar in atomic number, it is difficult to distinguish between their backscattering behavior and it was therefore impossible to include a Si shell with the pyrophyllite analysis. However, Ford et al. (1999) using

HRTGA investigations clearly demonstrated that as residence time increased Si was indeed in the interlayer of the pyrophyllite precipitates.

Using takovite, a mixed Ni-Al layered double hydroxide (LDH) mineral, and β- $Ni(OH)_2$ as reference compounds, Ni-Ni interatomic bond distances of 3.06 and 3.08 Å were determined (Tables 2.2 – 2.6). The Ni-Ni interatomic bond distance for the second shell of pyrophyllite and gibbsite was 3.06 Å while for talc, silica, and the mixture the Ni-Ni interatomic bond distances were 3.08 Å. These analyses suggest a LDH phase formed on pyrophyllite and gibbsite while a α-$Ni(OH)_2$ phase formed on talc, silica, and the gibbsite/silica mixture. The identity of the Ni precipitates on the sorbents can, in part, be determined from the normalized, background subtracted and k-weighted XAFS χ functions. Shown in Figure 2.9 are the χ functions of one-month aged Ni-sorbent samples. At approximately 8 $Å^{-1}$ in Figure 2.9, there is a characteristic beat pattern (indicated by the dashed circle) that is indicative of the presence or absence of Al backscattering associated with these Ni precipitates (Scheinost et al., 1999). In the case of talc, silica, and the mixture, the peak is predominant suggesting no dampening from Al backscattering. However, one does see the influence of Al backscattering and dampening of the peak at 8 $Å^{-1}$ for pyrophyllite and gibbsite when compared to talc, silica, and the mixture. Therefore, Figure 2.9 further confirms that Ni-Al LDH was

Table 2.2. EXAFS structural parameters of Ni sorbed on pyrophyllite.

Aging Time	ΔE_o (eV)	Ni - O			Ni - Ni			Ni - Al		
		R (Å)[a]	N[b]	σ^2 (Å^2)[c]	R (Å)[a]	N[b]	σ^2 (Å^2)[c]	R (Å)[a]	N[b]	σ^2 (Å^2)[c]
2 Years	3.3	2.05	6.0	0.004	3.07	4.6	0.003	3.12	1.9	0.003
1 Year	3.5	2.05	6.0	0.003	3.06	4.5	0.003	3.11	1.1	0.003
6 Months	2.7	2.05	6.0	0.003	3.06	4.8	0.003	3.11	1.6	0.003
3 Months	4.4	2.06	6.0	0.003	3.06	5.0	0.004	3.10	1.5	0.004
1 Month	4.8	2.05	6.0	0.003	3.06	4.9	0.003	3.11	1.4	0.003
7 Days	4.1	2.05	6.0	0.004	3.06	4.9	0.003	3.10	1.3	0.003
3 Days	3.2	2.05	6.0	0.003	3.06	5.5	0.003	3.11	1.2	0.003
1 Day	3.6	2.05	6.0	0.003	3.06	5.7	0.003	3.11	1.3	0.003
12 Hours	3.9	2.05	6.0	0.003	3.07	5.2	0.004	3.11	1.1	0.004
1 Hour	4.7	2.05	6.0	0.003	3.06	4.5	0.004	3.09	1.6	0.004
15 Minutes	3.7	2.05	6.0	0.004	3.08	5.0	0.005	3.15	2.2	0.005
Ni-Al LDH[d]		2.05	6.5		3.06	4.8		3.06	1.4	

[a] Interatomic Distance; [b] Coordination Number; [c] Debye-Waller factor; [d] d'Esponose de la Caillerie et al. (1995)

Table 2.3. EXAFS structural parameters of Ni sorbed on talc.

Aging Time	ΔE_o (eV)	Ni - O			Ni - Ni			Ni - Si		
		R (Å)[a]	N[b]	σ^2 (Å^2)[c]	R (Å)[a]	N[b]	σ^2 (Å^2)[c]	R (Å)[a]	N[b]	σ^2 (Å^2)[c]
1 Year	3.1	2.05	6.0	0.004	3.08	5.4	0.004	3.28	2.0	0.004
6 Months	2.9	2.05	6.0	0.003	3.08	5.5	0.004	3.29	2.0	0.004
3 Months	3.2	2.06	6.0	0.003	3.08	5.7	0.004			
1 Month	3.4	2.05	6.0	0.004	3.08	5.8	0.004			
7 Days	3.7	2.05	6.0	0.005	3.08	5.2	0.004			
3 Days	4.2	2.05	6.0	0.004	3.08	5.4	0.004			
1 Day	4.4	2.05	6.0	0.004	3.08	5.1	0.004			
12 Hours	4.5	2.05	6.0	0.003	3.08	3.9	0.004			
1 Hour	3.1	2.06	6.0	0.002	3.08	2.9	0.006			
α-Ni(OH)$_2$[d]		2.04	5.8		3.07	5.7				
Lizardite[e]		2.06	6.0		3.08	6.0		3.29	2.0	

[a] Interatomic Distance; [b] Coordination Number; [c] Debye-Waller factor; [d] Pandya et al. (1990), [e] Mellini (1982)

Table 2.4. EXAFS structural parameters of Ni sorbed on gibbsite.

Aging Time	ΔE_o (eV)	Ni - O			Ni - Ni			Ni - Al		
		R (Å)[a]	N[b]	σ^2 (Å^2)[c]	R (Å)[a]	N[b]	σ^2 (Å^2)[c]	R (Å)[a]	N[b]	σ^2 (Å^2)[c]
1 Year	3.7	2.05	6.0	0.003	3.06	4.9	0.003	3.11	1.2	0.003
6 Months	3.1	2.05	6.0	0.004	3.06	4.8	0.004	3.12	1.5	0.004
3 Months	4.3	2.05	6.0	0.003	3.06	5.1	0.004	3.10	1.4	0.004
1 Month	3.8	2.05	6.0	0.003	3.06	4.7	0.003	3.11	1.6	0.003
7 Days	3.1	2.05	6.0	0.004	3.08	4.9	0.003			
1 Day	3.6	2.06	6.0	0.003	3.09	3.6	0.005			
Ni-Al LDH[d]		2.05	6.5		3.06	4.8		3.06	1.4	

[a] Interatomic Distance; [b] Coordination Number; [c] Debye-Waller factor; [d] d'Esponose de la Caillerie et al. (1995)

Table 2.5. EXAFS structural parameters of Ni sorbed on silica.

Aging Time	ΔE_o (eV)	Ni - O			Ni - Ni			Ni - Si		
		R (Å)[a]	N[b]	σ^2 (Å^2)[c]	R (Å)[a]	N[b]	σ^2 (Å^2)[c]	R (Å)[a]	N[b]	σ^2 (Å^2)[c]
1 Year	0.5	2.06	6.0	0.004	3.08	6.2	0.005	3.27	2.0	0.005
6 Months	5.1	2.05	6.0	0.003	3.08	6.3	0.004	3.28	2.0	0.004
3 Months	4.5	2.05	6.0	0.004	3.08	6.7	0.004			
1 Month	4.9	2.05	6.0	0.004	3.08	6.4	0.004			
7 Days	5.4	2.05	6.0	0.004	3.08	6.5	0.003			
3 Days	5.4	2.05	6.0	0.003	3.08	6.5	0.004			
1 Day	3.7	2.05	6.0	0.004	3.08	5.1	0.005			
12 Hours	5.3	2.05	6.0	0.001	3.08	1.7	0.003			
1 Hour	3.7	2.05	6.0	0.001	3.08	1.1	0.006			
α-Ni(OH)$_2$[d]		2.04	5.8		3.07	5.7				
Lizardite[e]		2.06	6.0		3.08	6.0		3.29	2.0	

[a] Interatomic Distance; [b] Coordination Number; [c] Debye-Waller factor; [d] Pandya et al. (1990), [e] Mellini (1982)

Table 2.6. EXAFS structural parameters of Ni sorbed on gibbsite/silica mixture.

Aging Time		Ni - O			Ni - Ni			Ni - Si		
	ΔE_o (eV)	R (Å)[a]	N[b]	σ^2 (Å^2)[c]	R (Å)[a]	N[b]	σ^2 (Å^2)[c]	R (Å)[a]	N[b]	σ^2 (Å^2)[c]
1 Year	0.5	2.06	6.0	0.004	3.08	6.2	0.004	3.28	2.0	0.004
6 Months	0.5	2.05	6.0	0.004	3.09	6.2	0.004	3.28	2.0	0.004
3 Months	0.3	2.06	6.0	0.004	3.08	6.6	0.004			
1 Month	0.1	2.05	6.0	0.004	3.08	6.9	0.004			
7 Days	0.1	2.05	6.0	0.004	3.08	6.9	0.003			
3 Days	0.2	2.05	6.0	0.003	3.08	6.5	0.003			
1 Day	0.6	2.05	6.0	0.003	3.08	5.7	0.003			
12 Hours	0.8	2.05	6.0	0.004	3.08	5.3	0.004			
1 Hour	1.6	2.05	6.0	0.003	3.08	0.8	0.001			
α-Ni(OH)$_2$[d]		2.04	5.8		3.07	5.7				
Lizardite[e]		2.06	6.0		3.08	6.0		3.29	2.0	

[a] Interatomic Distance; [b] Coordination Number; [c] Debye-Waller factor; [d] Pandya et al. (1990), [e] Mellini (1982)

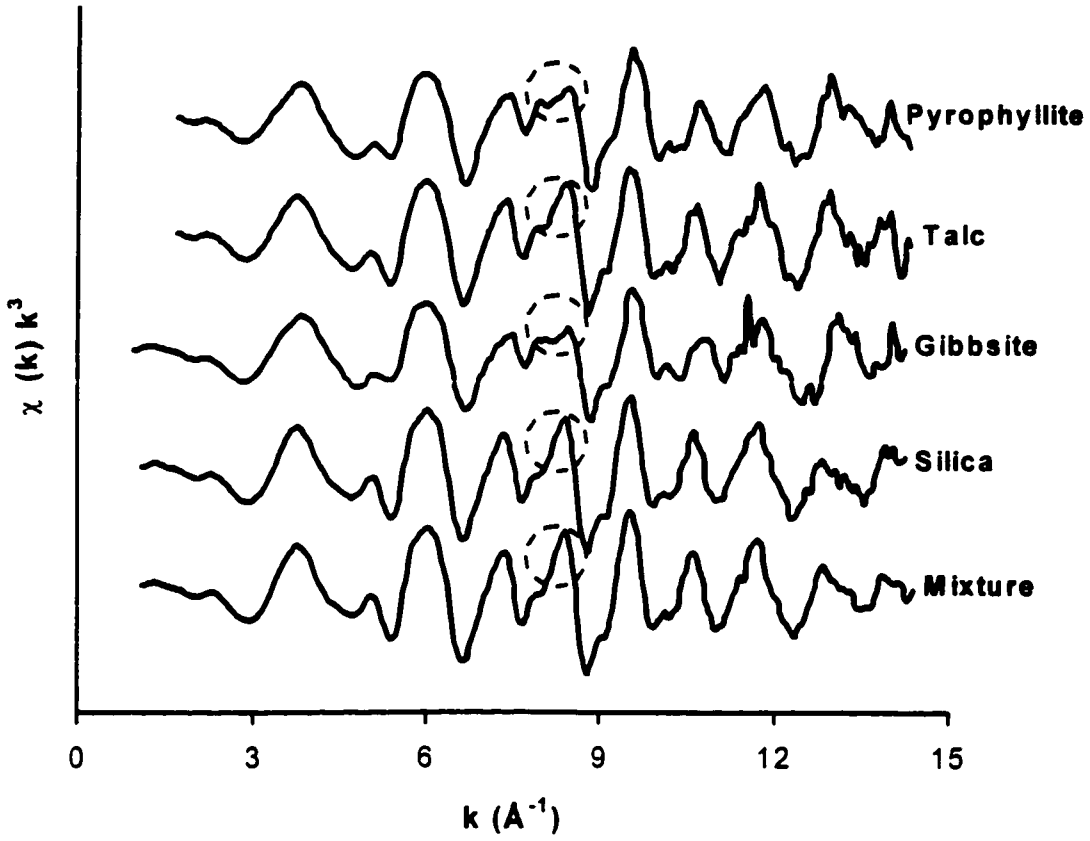

Figure 2.9. The k^3 weighted χ functions of one month aged Ni reacted pyrophyllite, talc, gibbsite, silica, and gibbsite/silica mixture samples. The circles show key identification for Ni-Al LDH versus α-Ni hydroxide (Scheinost and Sparks, 1999).

formed on pyrophyllite and gibbsite while α-$Ni(OH)_2$ was present on talc, silica, and the mixture surfaces.

The coordination numbers (N) are also presented in Tables 2.2 – 2.6. The second shell increased in intensity with increased Ni uptake from solution (Table 2.1). As mentioned earlier regarding the Ni-O shell, Ni is octahedrally coordinated to O resulting in a coordination number of 6 for all samples. For the Ni-Al LDH precipitates on pyrophyllite (Table 2.2), one sees N_{Ni-Ni} is approximately 5 (4.5 – 5.7) and N_{Ni-Al} is about 1.5 (1.1 – 2.2) with an average interatomic bond distance of 3.11 Å. Similarly for gibbsite (Table 2.3), N_{Ni-Ni} is approximately 5 (3.6 – 5.1) and N_{Ni-Al} is about 1.5 (1.2 – 1.6) with an average interatomic bond distance of 3.11 Å. These results are consistent with a takovite ($Ni_6Al_2(OH)_{16}CO_3 \bullet H_2O$) structure. The α-$Ni(OH)_2$ precipitates on talc (Table 2.4) show N_{Ni-Ni} to range from 2.10 – 5.8 with an average of 5.5. For the Ni-Si shell for talc at longer aging times, N_{Ni-Si} is 2 with a interatomic bond distance of 3.28 Å, which is indicative of a Ni-phyllosilicate. Similar results were seen for silica (Table 2.5) and the gibbsite/silica mixture (Table 2.6) with N_{Ni-Ni} slightly above 6 and N_{Ni-Si} equal to 2 at 3.28 Å.

2.5.3 DRS Analysis of Sorption Samples

A very complete DRS study of Ni sorption on pyrophyllite, gibbsite, talc, and amorphous silica under the same reaction conditions in this study was conducted by Scheinost et al. (1999) in our lab at the University of Delaware. A summary of the work by Scheinost et al. (1999) will be presented along with DRS studies for the gibbsite/silica mixture.

Scheinost et al. (1999) examined the $^3A_{2g} \rightarrow {}^3T_{1g}$ band (ν2) of octahedrally coordinated Ni(II) sorbed on pyrophyllite, gibbsite, talc, and amorphous silica. By comparison with model Ni compounds, they determined a unique fingerprint for α-$Ni(OH)_2$ and Ni-Al LDH for the ν2 band at approximately 14,900 and 15,300 cm^{-1}, respectively. The authors also noted the transformation of α-$Ni(OH)_2$ to a Ni-phyllosilicate causes a contraction of the octahedral Ni hydroxide sheets and resulted in a ν2 band between those of α-$Ni(OH)_2$ and Ni-Al LDH at about 15,100 cm^{-1}. Although the longest aging time observed in the study by Scheinost et al. (1999) was only 4 months, the shift of α-$Ni(OH)_2$ to a Ni-phyllosilicate was not fully observed. Scheinost et al. (1999) examined Ni sorption kinetically on these sorbents and observed an increase in ν2 band heights with increasing sorption time. Because the

absorption coefficient of aqueous Ni^{2+} complexes is 2 orders of magnitude lower than that of Ni^{2+} in a three-dimensional, polynuclear structure, band heights are indicative of the amount of Ni present in a precipitate phase. Therefore, the increase of band heights with increasing Ni sorption is clear evidence that the sorbed Ni is predominantly due to precipitation and not due to adsorption of Ni.

The time-resolved $\nu 2$ bands of α-$Ni(OH)_2$ precipitates on the gibbsite/silica mixture at pH 7.5 are shown in Figure 2.10 for sorption times of 1 day to 1 year. Note that the early sorption times in Figure 2.10a are not very pronounced suggesting that adsorption is the primary sorption mechanism although XAFS (Figure 2.8) indicates the formation of precipitates at these times. Figure 2.10b shows an expanded y-axis to view the early sorption times in more detail, illustrating that there is substantial precipitate growth between 3 and 7 days. The position of the 14,800 cm^{-1} marker is for α-$Ni(OH)_2$ precipitates with a nitrate interlayer and the 15,060 cm^{-1} marker is for a silicate substituted interlayer of α-$Ni(OH)_2$. For the earlier reaction times up to 1 month, the precipitate is primarily α-$Ni(OH)_2$. However, at aging times of 6 months and 1 year, there was a shift of the $\nu 2$ band from 14,800 cm^{-1} to 15,060 cm^{-1}, indicating a transformation of the α-$Ni(OH)_2$ phase to a Ni-phyllosilicate at these later aging times.

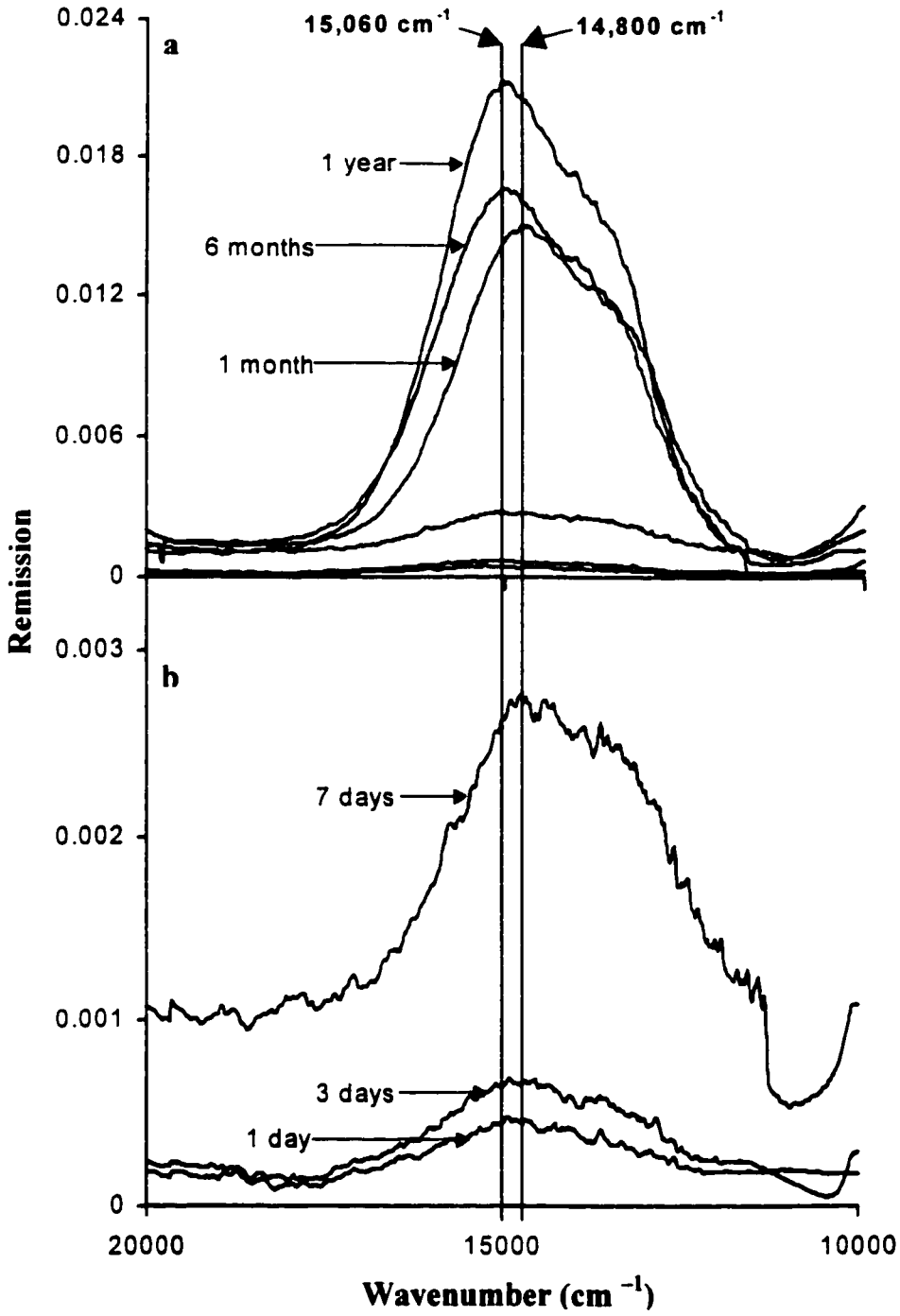

Figure 2.10. The DRS ν2 bands for the Ni surface precipitates on the gibbsite/amorphous silica mixture for various aging times. (a) All spectra collected; note that the three smaller curves for the early reaction times are unmarked. (b) Spectra were collected for reaction times of 1 to 7 days with an expanded y-axis.

2.5.4 HRTGA Investigation of Sorption Samples

Due to large weight loss events associated with the talc and gibbsite surfaces, it was difficult to examine by HRTGA sorption samples for these minerals. This study investigated the changes in the thermal stability of Ni-Al LDH precipitates on pyrophyllite with aging (Figure 2.11a) (Ford et al., 1999). There were four weight loss events associated with the Ni-pyrophyllite system: (1) expulsion of water and nitrate from the LDH interlayer at about 223 °C, (2) dehydroxylation of nitrate-bearing LDH at about 284 °C, (3) decomposition of the Ni-Al phyllosilicate precursor at approximately 462 °C, and (4) dehydroxylation of the pyrophyllite surface at about 550 °C. There was not a detectable weight loss event for a silicate-bearing LDH phase because of the complexity of the system. These weight loss events were compared to derivative curves of known reference compounds (Figure 2.11b). These curves show that less stable α-$Ni(OH)_2$ decomposes at about 275 °C when mixed with pyrophyllite. In Figure 2.11b, the decomposition temperature shifts to 304, 357, and about 450 °C for Ni-Al LDH, Si-exchanged Ni-Al LDH, and Ni-Al phyllosilicate, respectively. These results show the silication of the precipitate interlayer and further conversion to a phyllosilicate precursor significantly enhances the stability of the precipitate.

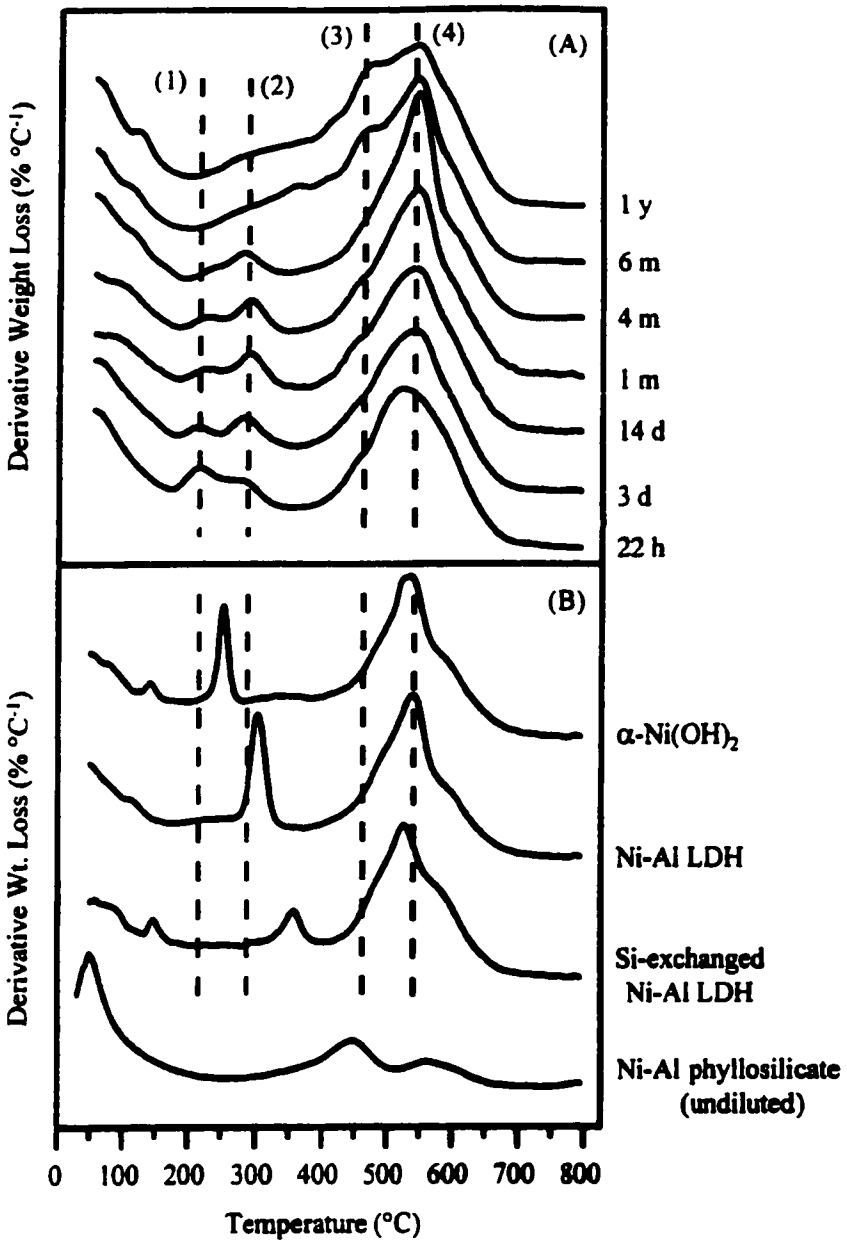

Figure 2.11. Changes in the thermal stability of Ni-Al LDH precipitates on pyrophyllite with aging. The derivative of the weight loss curve is shown for (A) aged Ni-pyrophyllite samples and (B) reference precipitates physically diluted with pyrophyllite to match surface loading in sorption samples. Weight loss events: (1) expulsion of H_2O and nitrate from LDH interlayer, (2) dehydroxylation of nitrate-bearing LDH, (3) decomposition of the precursor Ni-Al phyllosilicate, and (4) dehydroxylation of pyrophyllite. Adapted from Ford et al. (1999).

High-resolution thermogravimetric analysis (HRTGA) was successfully employed to show that α-$Ni(OH)_2$ precipitates on the gibbsite/silica mixture transform into a Ni phyllosilicate precursor within one year at ambient reaction conditions (Figure 2.12) (Scheckel et al., 2000a). This transformation progressed by silicate-for-nitrate exchange in the interlayer, and the subsequent polymerization of single silicate units which may then become connected with the octahedral hydroxide layers (Depège et al., 1996). This transformation was slightly detectable by DRS and EXAFS for the later aging times (Figures 2.8 and 2.10). Since there is a major weight loss occurrence at about 230 °C for the gibbsite surface, no weight loss at 220 °C is detectable which would occur due to water and nitrate expulsion for the interlayer (Bellotto et al., 1996; Ford et al., 1999). To observe only weight loss events associated with the Ni precipitates on the mixture, the curve for the unreacted mixture surface was subtracted from the curves for the sorption samples (Figure 2.12). Synthesis of reference compounds for comparison in the HRTGA studies was similar to methods in Ford et al. (1999). The synthetic references were mixed with a dry gibbsite/silica mixture sample at a 1:100 weight ratio prior to HRTGA analysis. Significant weight loss events for α-$Ni(OH)_2$ (NO_3^- interlayer), Si-exchanged α-$Ni(OH)_2$ (partial silication of the interlayer), and Ni phyllosilicate reference compounds when combined with the gibbsite/silica mixture occurred at approximately 332, 438, and 533 °C, respectively.

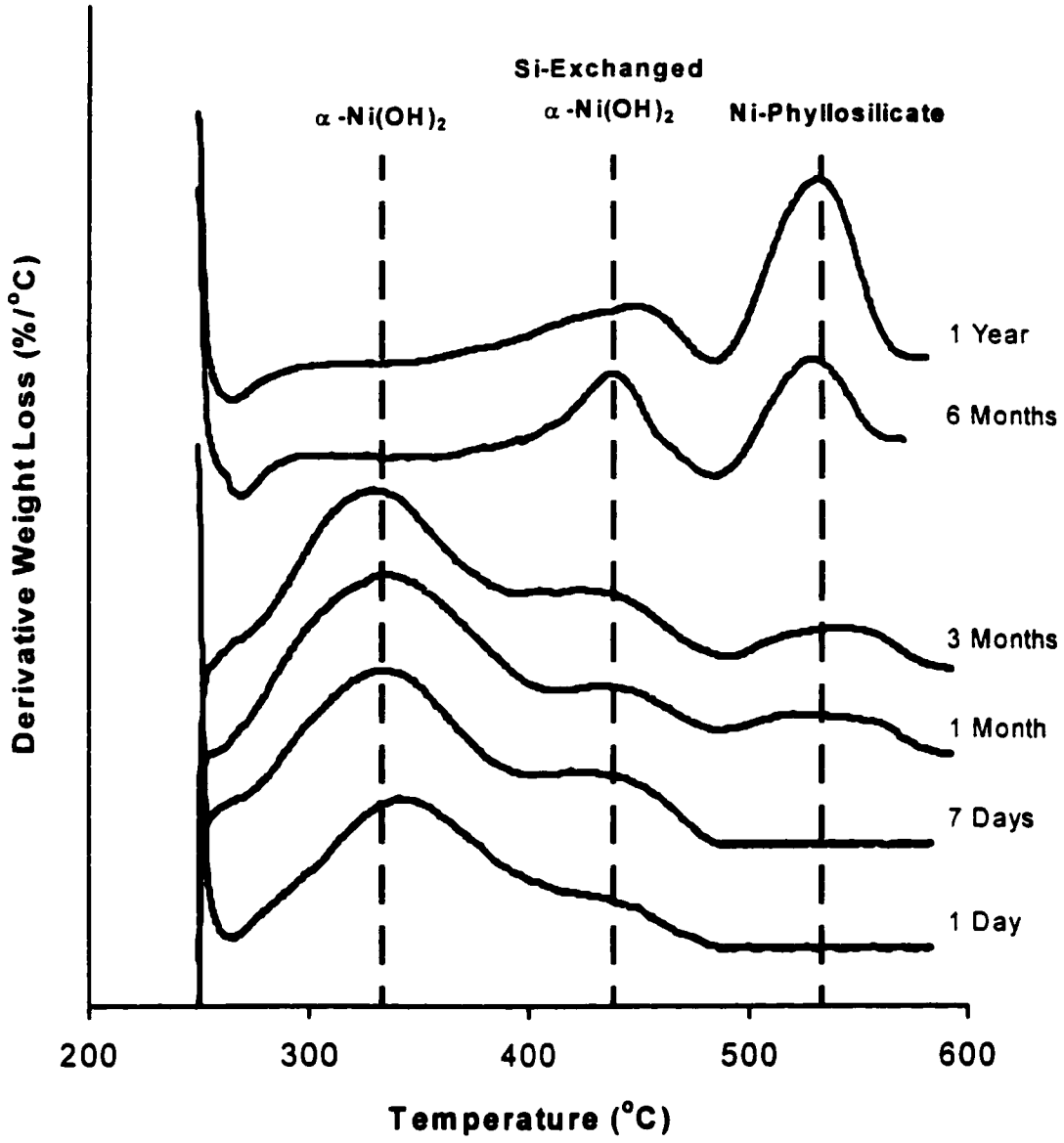

Figure 2.12. Changes in the thermal stability of the Ni surface precipitates on the mixture showing the conversion from α-$Ni(OH)_2$ to a Ni phyllosilicate with aging. The derivative weight loss curves are background subtracted from an unreacted sample to show only weight loss events associated with the precipitate phases. The identification markers are derived from reference compounds.

One sees for the 1 and 7 day samples a substantial α-$Ni(OH)_2$ peak with a small shoulder in the Si-exchanged interlayer α-$Ni(OH)_2$ region and no indication of Ni phyllosilicate. The 1 month and 3 months curves have evidence of α-$Ni(OH)_2$ and Si-exchanged α-$Ni(OH)_2$ precipitates with a small peak arising at the Ni phyllosilicate marker. For the long-term aging times of 6 months and 1 year, one notices very little α-$Ni(OH)_2$ but well defined peaks comparable with the Si-exchanged α-$Ni(OH)_2$ and Ni phyllosilicate reference precipitates. The data from the HRTGA experiments demonstrate that Ni sorption on the gibbsite/silica mixture results initially in the formation of α-$Ni(OH)_2$ precipitates followed by a Si-exchanged α-$Ni(OH)_2$ and with time the subsequent conversion to a Ni phyllosilicate.

The generalized weight loss (decomposition) events may be explained by the following equations:

<u>α-$Ni(OH)_2$</u>

$$Ni(OH)_2A^-_{interlayer}\bullet H_2O \rightarrow NiO + 2\,H_2O + A^-_{interlayer}$$

<u>Ni-Al LDH (Takovite)</u>

$$Ni_6Al_2(OH)_{18}\,A^-_{interlayer}\bullet H_2O \rightarrow 6\,NiO + Al_2O_3 + 10\,H_2O + A^-_{interlayer}$$

where $A^-_{interlayer}$ is the interlayer anion (H_2O, NO_3^- or silica).

2.5.5 AFM Analysis of Sorption Samples

TappingMode™ AFM was employed to observe the growth of Ni precipitates on pyrophyllite, talc, and amorphous silica (Figures 2.13 – 2.15). For comparison, an unreacted surface scan for each of the sorbents was examined. The unaltered micrographs are shown in height mode. Figure 2.13 shows the growth of Ni-Al LDH precipitates on pyrophyllite for sorption times of 0 hours (unreacted), 3 hours, 1 day, and 1 month. As reaction time progresses, one sees the formation of precipitates as mountainous growths on the pyrophyllite surface. This is also seen for Ni sorption on talc (Figure 2.14) and silica (Figure 2.15) for reaction times of 0 hours (unreacted), 1 day, 3 days, and 1 month resulting in the formation of α-$Ni(OH)_2$ precipitates on the sorbent interface. As one can see from Figures 2.13 – 2.15, there is an even distribution of precipitates and, after 1 month of reaction, the precipitates are relatively equal in size.

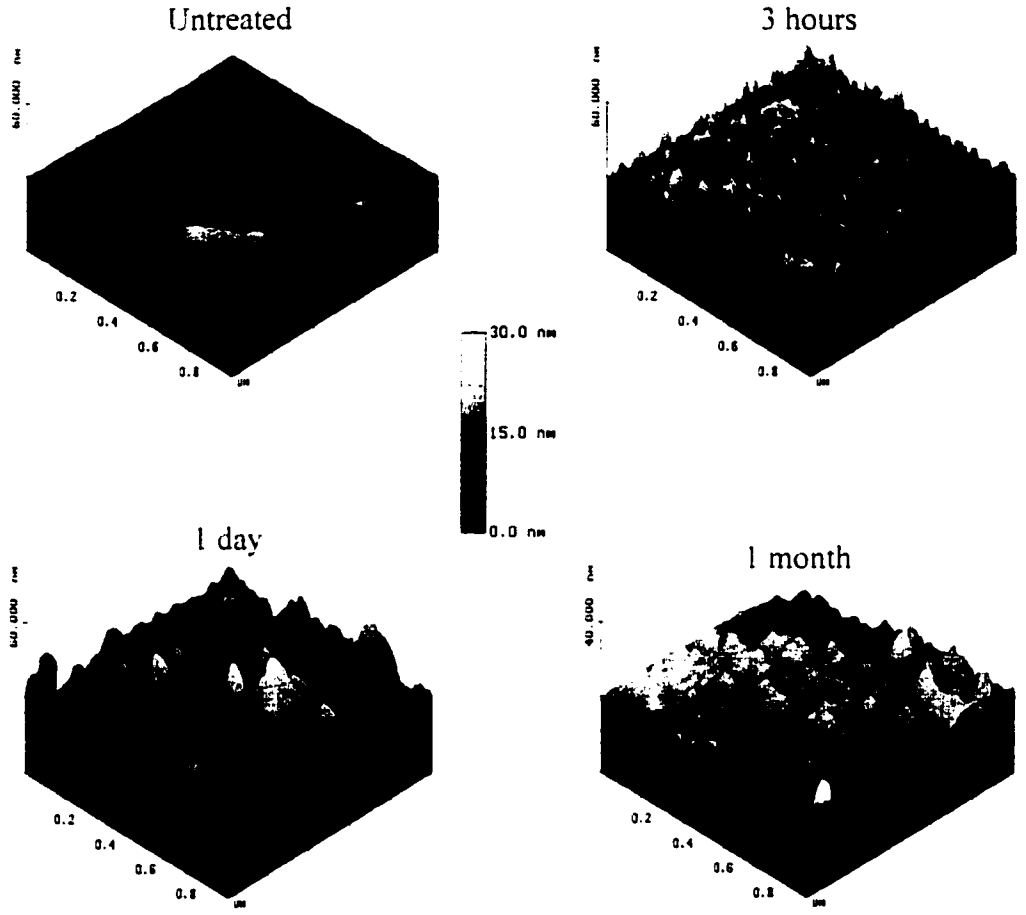

Figure 2.13. Atomic force micrographs (AFM) of pyrophyllite unreacted and reacted with Ni (pH 7.5, $[Ni]_o$ = 3 mM) for times of 3 hours, 1 day, and 1 month. The scan size was 1 μm by 1 μm with a maximum Z-range of 60 nm. The scans were collected in TappingMode™ AFM.

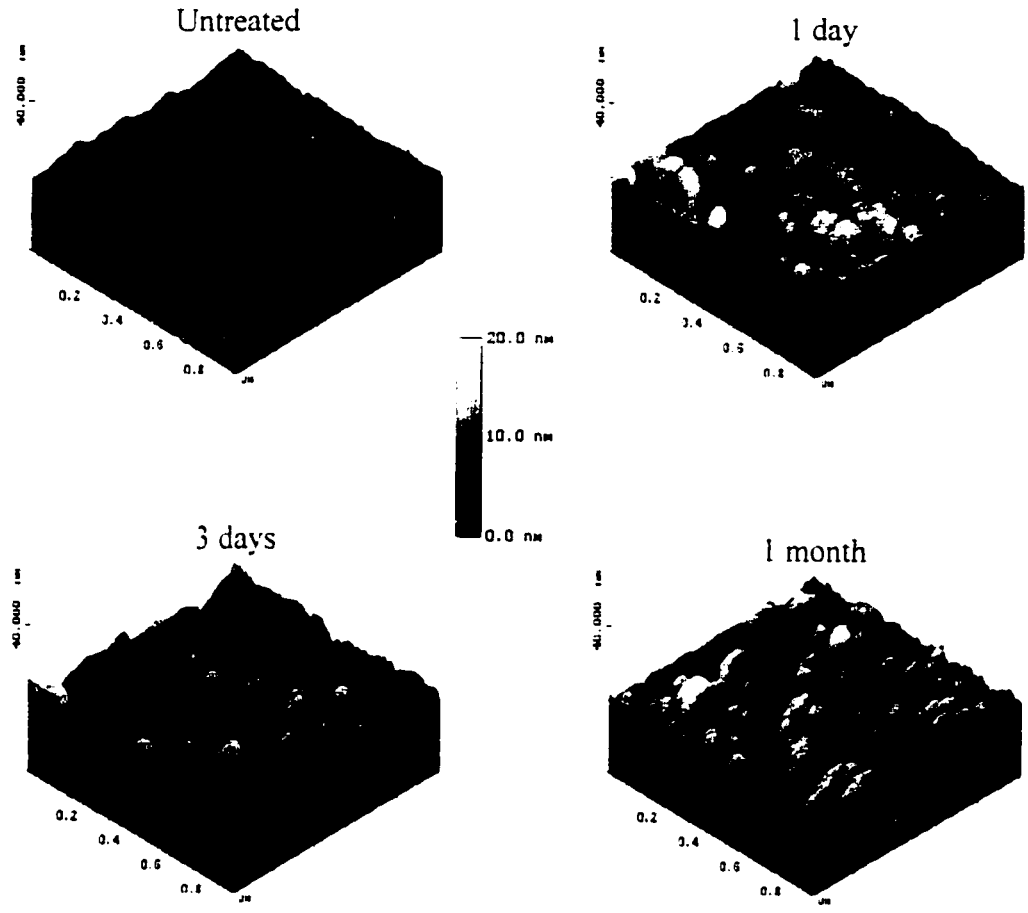

Figure 2.14. Atomic force micrographs (AFM) of talc unreacted and reacted with Ni (pH 7.5, $[Ni]_o$ = 3 mM) for times of 1 day, 3 days, and 1 month. The scan size was 1 μm by 1 μm with a maximum Z-range of 40 nm. The scans were collected in TappingMode™ AFM.

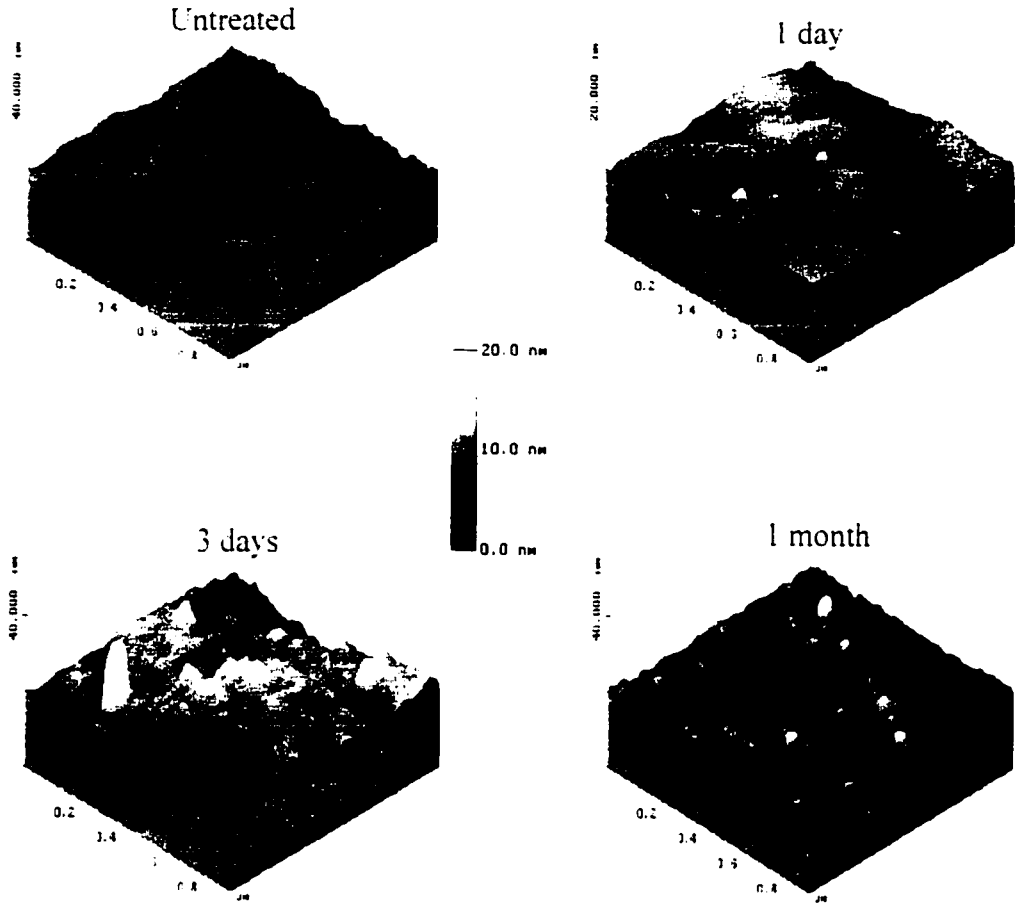

Figure 2.15. Atomic force micrographs (AFM) of silica unreacted and reacted with Ni (pH 7.5, $[Ni]_0$ = 3 mM) for times of 1 day, 3 days, and 1 month. The scan size was 1 μm by 1 μm with a maximum Z-range of 40 nm. The scans were collected in TappingMode™ AFM.

2.5.6 HRTEM Analysis of Sorption Samples

HRTEM analyses of 1-year aged Ni reacted pyrophyllite (Figure 2.16a) and talc (Figure 2.17a) show nanometer-sized crystalline precipitates across the mineral surfaces at edge and basal plane sites. The Ni precipitates, noted by arrows, were evident from their lattice fringes in the HRTEM images. The grainy, light-colored material around the precipitates is the mineral surface. Lattice fringes occupying a single orientation extended over areas of 2 to 15 nm in diameter. Lattice fringe orientation of the Ni precipitates in regard to the pyrophyllite and talc surfaces varied from one set of fringes to the next but Fourier transformation of the images indicate a coordinated arrangement of the precipitates with respect to the mineral surfaces. Lattice fringe spacings of approximately 0.20 nm were measured from the images and are consistent with the primary lattice spacings for Ni hydrotalcite precipitates.

The EDS spectra collected near the edges of 1-year aged Ni reacted pyrophyllite (Figure 2.16b) and talc (Figure 2.17b) particles show the identity and approximate quantities of the dominant elements. The large Cu peaks in these spectra

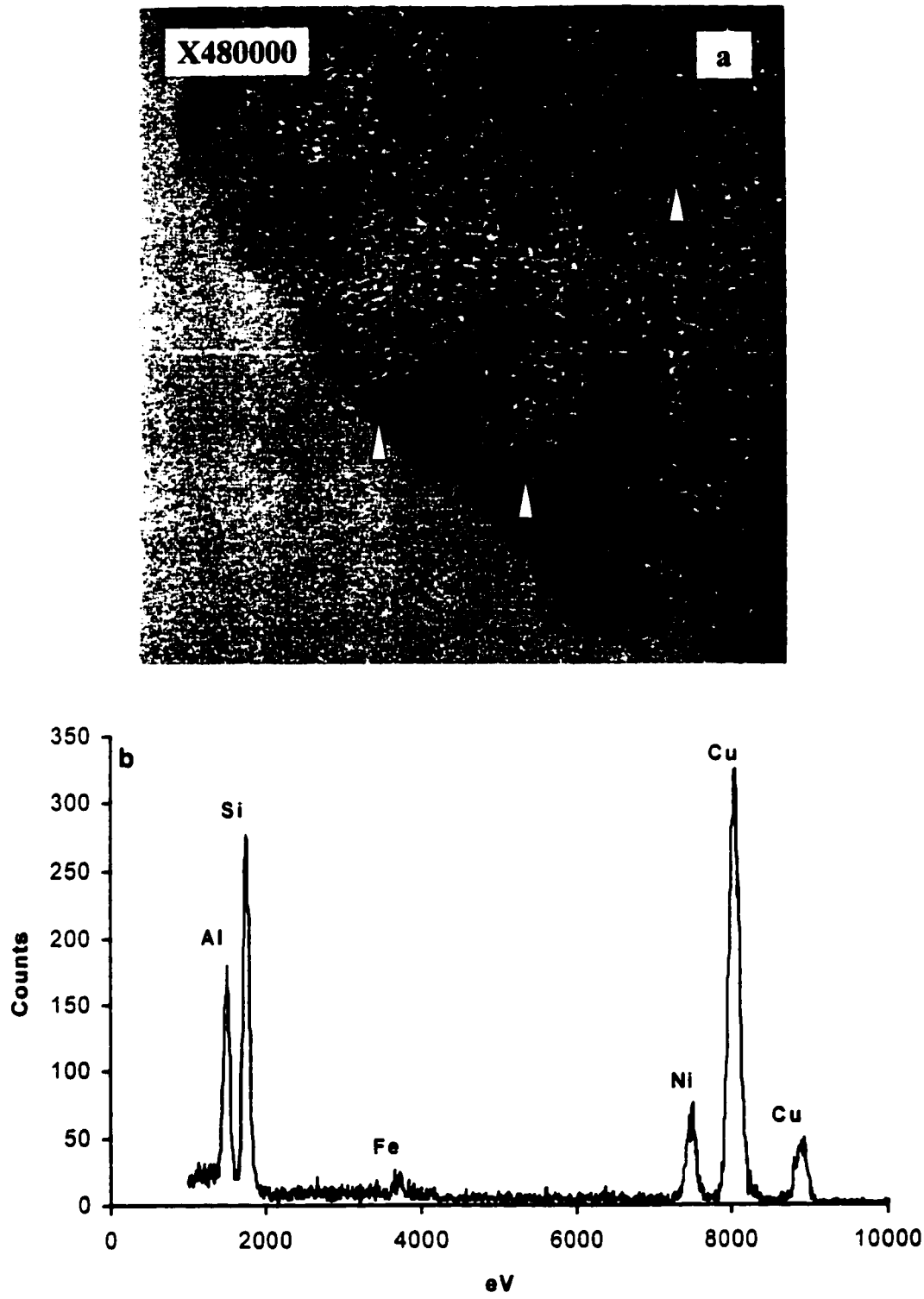

Figure 2.16. High magnification HRTEM (a) and EDS (b) of 1-year aged Ni-pyrophyllite. Ni precipitates are noted with arrows.

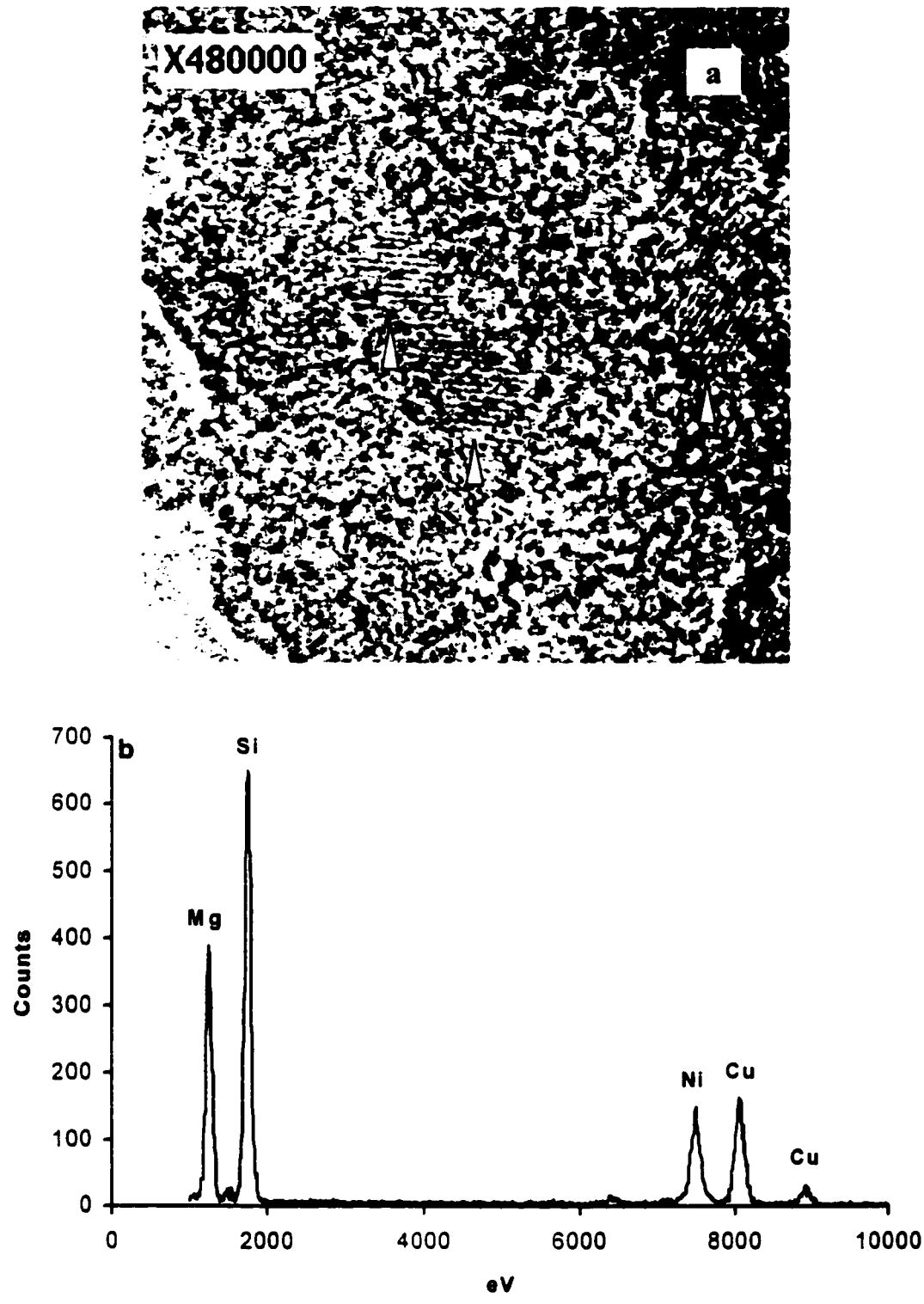

Figure 2.17. High magnification HRTEM (a) and EDS (b) of 1-year aged Ni-talc. Ni precipitates are noted with arrows.

are from the Cu sample grid. For the pyrophyllite sample (Figure 2.16b), one sees about a 2:1 peak size for Si and Al with some Fe associated with the pyrophyllite surface and a substantial peak for Ni. In Figure 2.17b, one sees a Si:Mg peak ratio consistent with talc and a dominant peak for Ni. The quantity of Ni in these spectra is estimated to be in line with the amount of Ni sorbed.

2.6 Conclusions

Macroscopic sorption of Ni on pyrophyllite, talc, gibbsite, amorphous silica, and a mixture of gibbsite and silica exhibit typical metal sorption behavior for the reaction conditions employed in this study. Nickel sorption increased on the variably charged pyrophyllite as solution pH increased. Ni sorption exhibited a rapid initial uptake of the metal followed by a slower, second phase of sorption.

This study revealed that Ni sorption at pH 7.5 resulted in the formation of Ni-Al LDH or α-$Ni(OH)_2$ precipitates depending on whether the sorbent contained available Al (pyrophyllite and gibbsite) or not (talc, silica, and mixture), respectively. The formation of these precipitates occurred on mineral and oxide surfaces from solutions which were undersaturated with respect to the thermodynamic solubility product of $Ni(OH)_2(s)$.

XAFS analyses showed that Ni-Ni bond distances were distinctly different between the Ni-Al LDH phases (3.06 Å) on pyrophyllite and gibbsite and the α-$Ni(OH)_2$ precipitates (3.08 Å) on talc, silica, and the mixture. The k^3 weighted χ functions for each of the sorbents also revealed that the two Ni phases (Ni-Al LDH and α-$Ni(OH)_2$) were present and that dampening due to Al backscattering could be used to identify them. The incorporation of a Si shell for some of the long-term aged samples suggested that a Ni-phyllosilicate might have formed. This was confirmed from the DRS and HRTGA investigations.

The position of the $^3A_{2g} \rightarrow {}^3T_{1g}$ electronic transition (ν2) showed that α-$Ni(OH)_2$ formed on the gibbsite/silica mixture (Figure 2.10). The Si-for-NO_3^- substitution in the hydroxide interlayer caused a band shift from 14, 800 to 15,060 cm^{-1}. These results were in line with XAFS analysis of Ni sorption on the mixture. Previous DRS work demonstrated that Ni-Al LDH formed in the presence of pyrophyllite and gibbsite, and α-$Ni(OH)_2$ formed in the presence of talc and silica based on ν2 band positions of 15,300 and 14,900 cm^{-1}, respectively (Scheinost et al., 1999). However, in this study, aging times were not long enough to see the transition

of the nitrate-containing interlayer precipitates to a Si-containing interlayer species or a Ni(-Al) phyllosilicate.

HRTGA was employed to further verify that α-$Ni(OH)_2$ precipitates on the gibbsite/silica mixture transformed into a Ni-phyllosilicate precursor within 1 year of aging. This study also demonstrated a Ni-Al LDH to Ni-phyllosilicate transformation in Ni-pyrophyllite samples aged up to 1 year (Ford et al., 1999). Under the same experimental design as Ford et al. (1999), HRTGA investigation of the gibbsite/silica mixture over various aging times showed that nitrate-bearing α-$Ni(OH)_2$ was prevalent at early sorption times followed by Si-bearing α-$Ni(OH)_2$ at intermediate aging times and finally Ni-phyllosilicate dominated at long-term residence times. These transitions were not sharp or distinct, meaning that substitution of Si-for-nitrate or conversion to a phyllosilicate was gradual as seen by multiple phases.

The microscopic studies were useful in allowing one to see the relative size and distribution of the Ni precipitates on the mineral and oxide surfaces. AFM analysis of the short-term aged Ni precipitates on pyrophyllite, talc, and silica showed that cone-shaped clusters formed evenly over the sorbent surface. Examination of 1-year aged Ni-pyrophyllite and Ni-talc samples by HRTEM observed precipitates

randomly distributed on the surfaces but primarily near edge sites. The lattice spacings of the Ni precipitates were in line with those of Ni hydrotalcite.

By employing spectroscopic, microscopic, and thermogravimetric techniques, this study demonstrated that Ni surface precipitates form on clay mineral and oxide surfaces at circumneutral pH. This research coincides with that of a number of other researchers and establishes the need to incorporate metal precipitation reactions into sorption models. The predominance of Al- and Si- containing minerals and oxides in soils and sediments makes the initial formation of metal LDH phases and conversion to a metal phyllosilicate quite possible under natural environmental conditions. The next step in this area of soil chemistry must be to address metal reaction mechanisms on more complex sorbents such as mixed model components and soils.

Chapter 3

INFLUENCE OF TEMPERATURE ON NI(II) SORPTION

3.1 Abstract

In recent years, innovative studies have shown that sorption of metals onto natural materials results in the formation of new mineral-like precipitate phases that increase in stability with aging time. While these findings have demonstrated the usefulness of current state-of-the-art molecular scale methods for confirming macroscopic data and elucidating mechanisms, basic kinetic and thermodynamic parameters for the formation of the metal precipitates have not been examined. Such information would be useful in developing sorption models to better predict the mobility and fate of metal contaminants in natural environments and understanding the influence of temperature on the sorption kinetics.

This study examined Ni sorption kinetics on pyrophyllite, talc, gibbsite, amorphous silica, and a mixture of gibbsite and amorphous over a temperature range

of 9 °C to 35 °C. Using the Arrhenius and Eyring equations, we were able to derive thermodynamic information, such as energy of activation (E_a) and enthalpy ($\Delta H^{\ddagger}$), entropy ($\Delta S^{\ddagger}$), and free energy of activation ($\Delta G^{\ddagger}$), related to the formation of the Ni precipitates. Based on values of E_a (93.05 to 123.71 kJ mol^{-1}) and $\Delta S^{\ddagger}$ (-27.51 to -38.70 J mol^{-1}), Ni sorption on these sorbents was surface-controlled (associative mechanism). The $\Delta H^{\ddagger}$ values (90.60 to 121.26 kJ mol^{-1}) suggest, as indicated by E_a values, that an energy barrier was present for the system to overcome in order for the reaction to occur. Additionally, the large, positive $\Delta G^{\ddagger}$ values suggest there is an energy barrier for product formation. This was the first study to examine metal surface precipitation as a function of temperature. Although metal precipitation can occur in the natural environment, this study shows that temperature plays a significant role on the rate of metal sorption.

3.2 Introduction

Recently there have been several studies that point to the formation of metal hydroxide precipitates upon reaction of clay minerals and metal oxides with metals such as Ni(II), Co(II), Cu(II) and Cr(III) (Chisholm-Brause et al., 1989; Charlet and Manceau, 1992; Fendorf et al., 1994; O'Day et al., 1994; Fendorf et al., 1996; O'Day

et al., 1996; Scheidegger et al., 1996a,b; 1997, 1998; Scheidegger and Sparks, 1996; Towle et al., 1997; Xia et al., 1997; Ford et al, 1999; Thompson et al., 1999; Scheinost et al., 1999; Scheinost and Sparks, 1999; Scheckel et al., 2000). In cases where the sorbent contained Al within its lattice structure, the resulting precipitate was a mixed metal-Al layered double hydroxide that was distinctly different from the pure metal hydroxide phase (Scheidegger et al., 1996a,b; 1997, 1998; Scheidegger and Sparks, 1996; Towle et al., 1997; Scheinost et al., 1999; Scheinost and Sparks, 1999; Thompson et al., 1999). Likewise, metal sorption onto Al-free sorbents has been examined and the subsequent precipitate was described as metal hydroxide-like (O'Day et al., 1994; Fendorf et al., 1996; Scheinost et al., 1999; Scheinost and Sparks, 1999). Sorption of Ni onto Al containing pyrophyllite and gibbsite, (Scheidegger et al., 1996a,b; 1997, 1998; Scheidegger and Sparks, 1996, Scheinost et al., 1999; Scheinost and Sparks, 1999) resulted in the formation of Ni/Al layered double hydroxide (LDH) precipitates while on Al-free talc, amorphous silica, and a mixture of gibbsite and amorphous silica (Scheinost et al., 1999; Scheinost and Sparks, 1999; Scheckel and Sparks, 2000) α-$Ni(OH)_2$-like precipitates resulted.

While the formation of surface precipitates is well established, determinations of basic thermodynamic and kinetic parameters for the formation of these precipitates such as energy of activation and enthalpy, entropy, and free energies of activation are

nonexistent. In view of the common formation of metal precipitates on natural materials, such information is vital if one is to better predict the fate of metals in the subsurface environment through reaction models.

The effect of temperature on reaction rates is well known and important in understanding reaction mechanisms. Svante Arrhenius, a Swedish physical chemist, who received the 1903 Nobel Prize for chemistry, noted that, for most reactions, the increase in rate with increasing temperature is nonlinear. Drawing upon work by van't Hoff (1884) for the decomposition of chloracetic acid in an aqueous solution, Arrhenius (1889) published his famous paper "Ober die Reacktionsgeschwindigkait bei der Inversion von Rohrzucker durch Säuren" in which he derived an expression for the kinetic temperature dependence of reactions. He concluded that most reaction-rate data obeyed the equation

$$k = Ae^{-Ea/RT} \qquad [1]$$

where k is the rate constant, E_a is the activation energy, R is the gas constant (8.31451 J/mol-K), T is the absolute temperature in Kelvin and A is the frequency or pre-exponential factor. The frequency factor is related to the frequency of collisions and the probability that the collisions are favorably oriented for reaction. As the

magnitude of E_a increases, k becomes smaller. Thus, reaction rates decrease as the energy barrier increases (Brown et al., 1994).

Taking the natural log of both sides of Eq. [1] one obtains

$$\ln k = - E_a /RT + \ln A \qquad [2]$$

By plotting ln k vs. $1/T$ a linear relationship is obtained and one can determine E_a from the slope (- E_a /R) and A from the y-intercept. This equation assumes that E_a and A are constant or nearly constant and vary slightly with temperature.

Energies of activation below 42 kJ mol^{-1} generally indicate diffusion-controlled processes and higher values represent chemical reaction processes (Sparks, 1985, 1986, 1989, 1995). Several studies investigating the effect of temperature on metal adsorption have been examined. Elkhatib et al. (1993) examined Pb sorption on three soils and found that E_a ranged from 1.5 to 27.7 kJ mol^{-1}. Ma and Liu (1997), employing a miscible displacement procedure, studied zinc sorption in a calcareous soil over a wide pH scale. They found that E_a ranged from 5.0 to 17 kJ mol^{-1}. The removal of Ba^{2+}, Cd^{2+}, UO^{2+} and Zn^{2+} from aqueous solutions by Ca-alginate beads resulted in a range of E_a from 0 to 11.3 kJ mol^{-1}, indicating diffusion-controlled

biosorption (Apel and Torma, 1993). Ogwada and Sparks (1986) compared thermodynamic parameters for K-Ca exchange, using equilibrium and kinetic approaches, of two Delaware soils. They determined energies of activation for adsorption (E_{aa}) for the two soils which ranged from 7.42 kJ mol^{-1}, using a miscible displacement method, to 32.96 kJ mol^{-1} with a vigorously mixed batch technique. Energies of activation for desorption (E_{ad}) ranged from 11.87 to 42.1 kJ mol^{-1} for the two methods, respectively. However, we could not find E_a, $\Delta H^{\ddagger}$, $\Delta S^{\ddagger}$ or $\Delta G^{\ddagger}$ data in literature for Ni sorption or other metal sorption on mineral surfaces where it has been definitely proven that metal surface precipitates form. The best possible analogy to metal precipitation is mineral formation reactions. E_a for several minerals are summarized in Table 3.1. The range in E_a values is relatively large ($12.09 < E_a < 198.3$).

In addition to determining E_a values, one can calculate the enthalpy, entropy, and free energy of activation for metal sorption by applying the Eyring equation (Eq. 3). The Eyring equation, also referred to as activated complex theory (ACT), transition-state theory (TST), or absolute reaction rate theory, is commonly employed to describe theoretical environments for elementary solution and interfacial reactions based on statistical mechanics (Stumm and Morgan, 1996). Eyring (1935) formulated his theory of absolute reaction rate with the following characteristics: 1) k is based on

Table 3.1. Summary of energy of activation values for the formation of various surfaces and their formulas.

Surface	Formula	Ea (kJ / mol)	Reference
Calcite	$Ca(CO)_3$	12.09	Stumm and Morgan (1996)[1]
Dolomite	$CaMg(CO)_3$	41.96	Stumm and Morgan (1996)[1]
Apatite	$Ca_5(PO_4)_3OH$	47.30	Tanahashi et al. (1996)
Green Rust	$Fe(II)_4Fe(III)_2(OH)_{12}SO_4\ yH_2O$	90.50	Hansen and Koch (1998)
Gibbsite	$Al(OH)_3$	97.87	Stumm and Morgan (1996)[1]
Cadmium Sulfate	CdS	100.4	Dutt et al. (1998)
Ferrous Carbonate	$Fe(CO)_3$	108.3	Greenberg and Tomson (1992)
Amorphous $Al(OH)_3$	$Al(OH)_3$	113.4	Stumm and Morgan (1996)[1]
Brucite	$Mg(OH)_2$	115.9	Stumm and Morgan (1996)[1]
Cu - In Alloy	Not Determined	127.0	Das et al. (1999)
Potlandite	$Ca(OH)_2$	132.2	Stumm and Morgan (1996)[1]
Kaolinite	$Al_2Si_2O_5(OH)_4$	150.2	Stumm and Morgan (1996)[1]
Chrysotile	$Mg_3Si_2O_5(OH)_4$	198.3	Stumm and Morgan (1996)[1]

[1] Values determined from $E_a = \Delta H_r + RT$ (T = 25 °C)

intermediate states or "activated complexes" situated at the saddle point of the potential energy surface, 2) the activated complexes are in quasi-equilibrium with the reactants which govern the energetics of the reaction rate and 3) the reactive system moves along a reaction coordinate, thus acting as a pure translational motion. In the Arrhenius equation form, the Eyring equation in its thermodynamic version becomes

$$k = (k_b T / h)\, e^{-\Delta G^{\ddagger} / RT} = (k_b T / h)\, e^{-\Delta S^{\ddagger} / R}\, e^{-\Delta H^{\ddagger} / RT} \qquad [3]$$

where k is the rate constant, $\Delta G^{\ddagger}$ is the standard Gibbs free energy of activation, $\Delta H^{\ddagger}$ is the standard enthalpy of activation, $\Delta S^{\ddagger}$ is the standard entropy of activation, k_b is

the Boltzmann constant (1.380658 X 10^{-23} J K^{-1}), h is Planck's constant (6.6260755 X 10^{-34} J s), R is the gas constant (8.31451 J mol-K^{-1}), and T is the absolute temperature in Kelvin.

Taking the natural log of both sides of Eq. [3] one obtains

$$\ln (k/T) = [\ln (k_b / h) + (\Delta S^{\ddagger} / R)] - \Delta H^{\ddagger} / RT \qquad [4]$$

By plotting ln (k/T) vs. $1/T$ a linear relationship is obtained and one can determine $\Delta H^{\ddagger}$ from the slope ($-\Delta H^{\ddagger}/R$) and $\Delta S^{\ddagger}$ from the y-intercept [ln (k_b / h) + ($\Delta S^{\ddagger} / R$)]. The Gibbs free energy of activation can be determined by

$$\Delta G^{\ddagger} = \Delta H^{\ddagger} - T\Delta S^{\ddagger} \qquad [5]$$

Furthermore, a relationship between E_a and $\Delta H^{\ddagger}$ has been noted (Noggle, 1996) for reactions in solution by the following equation:

$$E_a = \Delta H^{\ddagger} - RT \ (T = 25\ ^{\circ}C) \qquad [6]$$

Since the majority of laboratory experiments are conducted at room temperature (T = 20 – 25 °C), data gathered from such experiments are limited in understanding reactions in natural settings that often undergo seasonal temperature changes. Accordingly, the objective of this study was to observe the influence of temperature upon the kinetics of Ni sorption on clay minerals and oxides and to determine E_a, A, $\Delta G^{\ddagger}$, $\Delta H^{\ddagger}$ and $\Delta S^{\ddagger}$ through the application of the Arrhenius and Eyring models.

3.3 Materials and Methods

3.3.1 Materials

The pyrophyllite (Robbins, NC, USA; Ward's), talc (Cherokee Co., NC, USA; Excalibur) and gibbsite (Arkansas, USA; Ward's) samples from natural clay deposits were prepared by grinding the clay in a ceramic ball mill for approximately 14 days, centrifuging to collect the < 2 μm fraction in the supernatant, Na^+ saturating the < 2 μm fraction, and then removing excess salts by dialysis followed by freeze drying of the clay. X-ray diffraction (XRD) showed minor impurities of kaolinite and quartz in pyrophyllite, and about 10 % bayerite in the gibbsite. Although the talc sample had about 20 % chlorite according to XRD, acid digestion resulted in an Al/Mg ratio of

only 0.01. This small Al-content was not sufficient in former experiments to induce the formation of detectable amounts of Ni-Al LDH (Scheinost et al., 1999). In addition, amorphous silica (SiO_2) (Zeofree® 5112) from the Huber Corporation was employed. A mixture of gibbsite and amorphous silica consisted of 40% gibbsite and 60% silica by weight. A mixture was used to more closely mimic heterogeneous systems in the natural environment. The N_2-BET surface areas of the sorbent phases were 95 $m^2 g^{-1}$ for pyrophyllite, 75 $m^2 g^{-1}$ for talc, 25 $m^2 g^{-1}$ for gibbsite, 90 $m^2 g^{-1}$ for amorphous silica, and 64 $m^2 g^{-1}$ for the gibbsite/silica mixture.

3.3.2 Temperature and Kinetic Studies

Nickel sorption on the clay mineral and oxide surfaces was examined macroscopically by employing a pH-stat batch technique at reaction temperatures of 9, 25, and 35 °C. Temperature was controlled through the use of a thermostatted stir plate equipped with a temperature probe to monitor and correct temperature changes in the batch experiments. The suspensions were stirred so that a small vortex was formed to eliminate film diffusion (approximately 350 rpm) (Ogwada and Sparks, 1986). Nickel sorption was examined by reacting a 3 mM $Ni(NO_3)_2$ solution with a 10 g/L suspension of the sorbent in 0.1 M $NaNO_3$ at pH 7.5. The sorption experiments were undersaturated with respect to the thermodynamic solubility product of β-

$Ni(OH)_2$ (Scheidegger and Sparks, 1996; Scheidegger et al., 1998). The systems were purged with N_2 to eliminate CO_2, and the pH was maintained through addition of freshly prepared 0.1 M NaOH via a Radiometer pH-stat titrator. Periodic 10 mL aliquots were removed at reaction times ranging from one minute to 180 hours (at or nearing equilibrium) from the batch reactor and filtered via a syringe equipped membrane filter apparatus. The filtered solution was then analyzed for Ni by ICP in order to calculate the amount of sorption. The sorption data were applied to an array of kinetic models (zero – third-Order models, parabolic diffusion, Elovich, and power function). The first-order kinetic model provided, in terms of R^2 and standard error, the best fits of the data and apparent rate constants, k_a', were calculated. The data were also applied to the Arrhenius and Eyring equations to determine E_a, A, $\Delta G^{\ddagger}$, $\Delta H^{\ddagger}$ and $\Delta S^{\ddagger}$.

3.4 Results and Discussion

Ni sorption on the clay mineral and oxide surfaces in this study exhibited typical metal sorption behavior. Previous studies at 25 °C, have shown that Ni surface precipitates formed on pyrophyllite, talc, gibbsite, silica, and the mixture within 15 minutes, 1 hour, 24 hours, 12 hours, and 1 hour, respectively (Scheidegger et al., 1996; Scheidegger et al., 1997; Scheidegger and Sparks, 1996; Scheidegger et al., 1998;

Scheinost et al. 1999; Scheinost and Sparks, 1999; Scheckel and Sparks, 2000). Figure 3.1 shows percent Ni sorbed on the sorbents with time for the three temperatures used in this study. As the temperature of the reaction increases from 9 °C to 35 °C, with all other reaction conditions remaining constant, the rate of Ni sorption increases on all sorbents. The Ni sorption rate on the sorbents, from greatest to least, at all three temperatures was as follows: gibbsite/silica mixture > pyrophyllite > talc > silica > gibbsite. Ni sorption on pyrophyllite, for example, at 9, 25, and 35 °C for 6 and 24 hours of reaction resulted in 2, 15, and 46 % versus 8, 46, and 92 % removal of Ni from solution, respectively. Comparable tendencies were observed with the other sorbing materials demonstrating the influence of increasing temperature on increasing sorption rates.

This work shows that at a low temperature (9 °C), metal uptake is relatively slow when compared to research commonly examined around 25 °C in the laboratory. Often times soil temperatures can fall below the 9 °C temperature mark examined in this study indicating that sorption rates can be even slower than reported here and thus allowing for easy and rapid transport of metals through the soil profile. Likewise, if the soil temperature is elevated, we have observed rapid sorption kinetics at higher temperatures that may lead to the formation of stable metal precipitates at

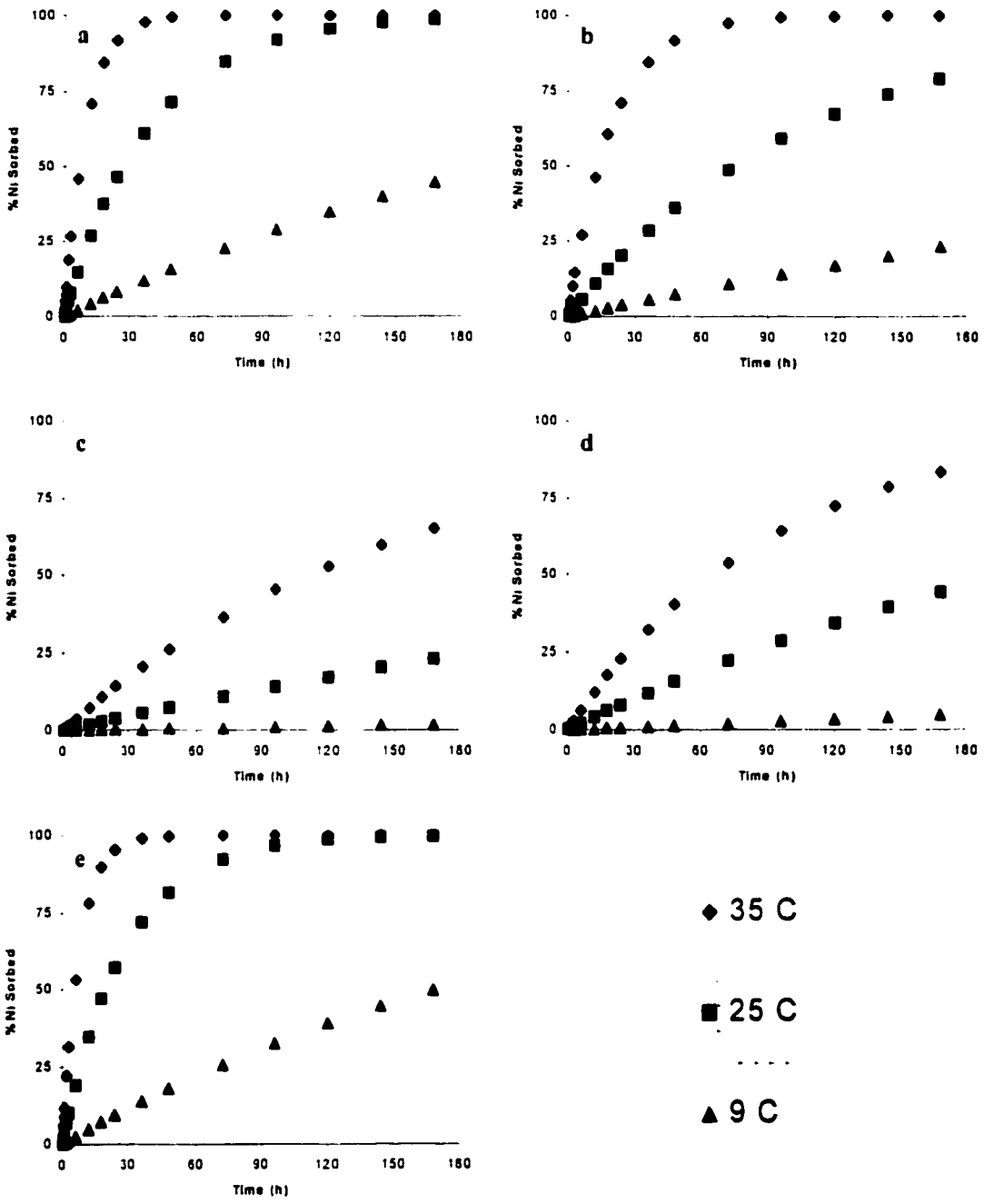

Figure 3.1. Macroscopic sorption of percent Ni sorbed on (a) pyrophyllite, (b) talc, (c) gibbsite, (d) silica, and (e) gibbsite/silica mixture at three different temperatures versus time.

circumneutral pH. Higher surface loading levels at higher temperature at a particular time could enhance the formation of metal surface precipitates. Formation of metal precipitates may be an important mode of sequestering metals in the soil environment (Ford et al, 1999; Scheckel et al., 2000; Scheckel and Sparks, 2000) and may be aided by increasing temperatures. However, this has not been shown spectroscopically or microscopically. Temperature studies such as this are quite necessary in order to construct full functioning models that will enable researchers to better predict mobility and bioavailability of metals in soils.

The sorption rate for all surfaces followed first-order kinetics ($\ln C = \ln C_o - k_a t$) where k_a is the apparent rate constant and t is time. C is defined as the concentration in solution and C_o is the initial concentration so that at $t = 0$, $C = C_o$. In Figure 3.2, one sees the first-order kinetic plots of the data presented in Figure 3.1 for Ni sorption on the clay minerals and oxides. Kinetic sorption data were collected up to a point on the sorption curves before a steady-state equilibrium was reached to determine the apparent forward rate constants (k_a'). The apparent rate constants are summarized in Table 3.2 for each surface at the three temperatures examined in this study. The magnitude of the k_a''s is consistent with the time-dependent data shown in Figure 3.1. For example, when comparing the apparent rate constants for the minerals at 25 °C, k_a''s were 9.78×10^{-6}. 7.18×10^{-6}, 2.58×10^{-6}, 1.93×10^{-8}, and 8.61×10^{-11}

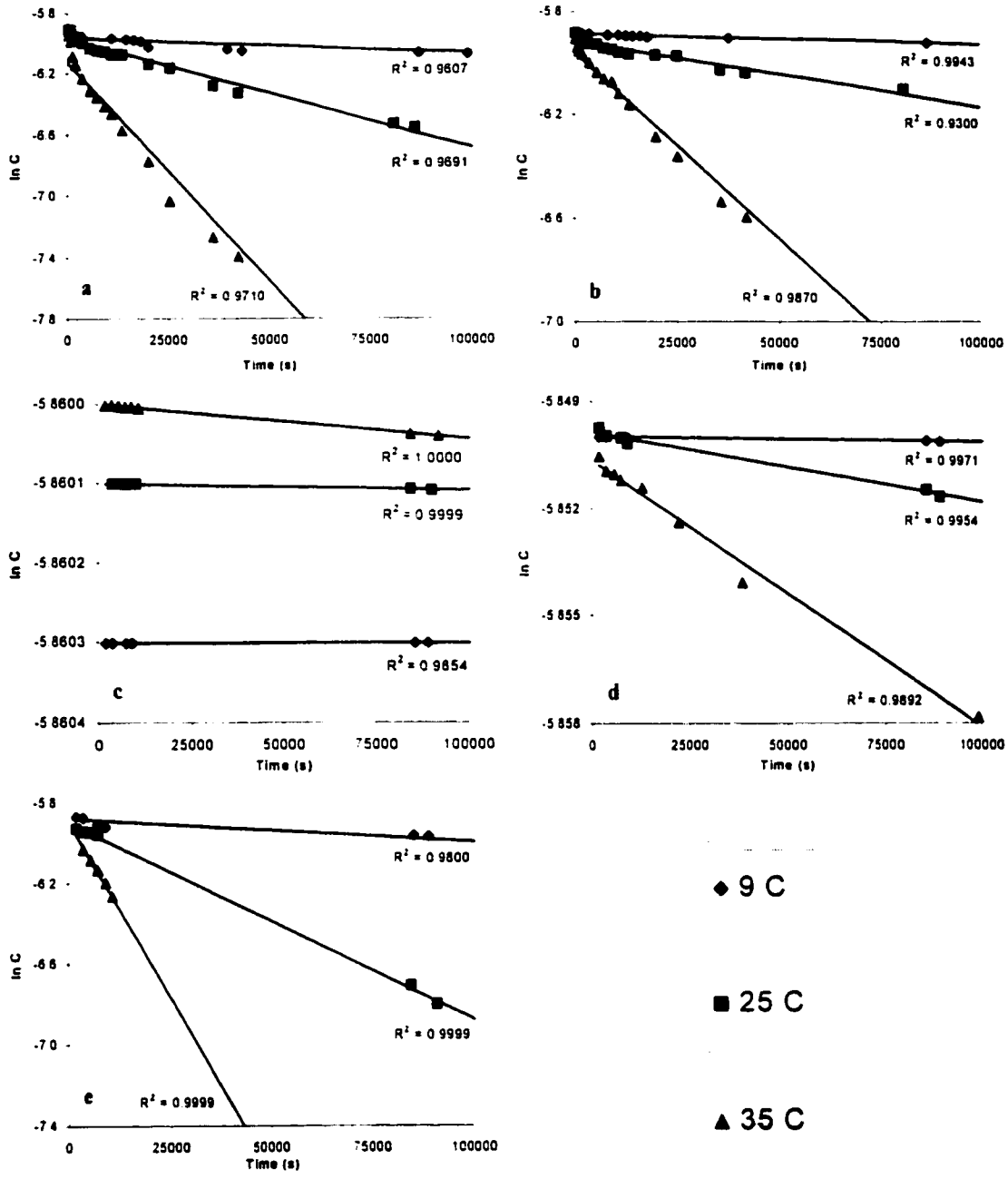

Figure 3.2. Apparent first-order kinetic plots of Ni sorption on (a) pyrophyllite, (b) talc, (c) gibbsite, (d) silica, and (e) gibbsite/silica mixture at three different temperatures.

Table 3.2. Apparent first-order forward sorption rate coefficients (k_a') for Ni sorption at three temperatures on clay mineral and oxide surfaces.

	k (s^{-1})		
SURFACE	**9 ° C**	**25 ° C**	**35 ° C**
Pyrophyllite	9.77×10^{-7}	7.18×10^{-6}	2.85×10^{-5}
Talc	4.33×10^{-7}	2.58×10^{-6}	1.44×10^{-5}
Silica	1.37×10^{-9}	1.93×10^{-8}	7.44×10^{-8}
Gibbsite	5.09×10^{-12}	8.61×10^{-11}	4.36×10^{-10}
Gibbsite/Silica	1.14×10^{-6}	9.78×10^{-6}	3.49×10^{-5}

s^{-1} for Ni sorption on the gibbsite/silica mixture, pyrophyllite, talc, silica, and gibbsite, respectively, reflecting the highest rate of Ni sorption on the gibbsite/silica mixture and the lowest rate on gibbsite. The k_a''s were used with the Arrhenius [2] and Eyring [4] equations to obtain linear relationships shown in Figures 3.3 – 3.5. From these plots, kinetic parameters were calculated as described earlier. In Figure 3.3, one observes the parallel relationship of the Arrhenius and Eyring equations when applied to data collected from Ni sorption on pyrophyllite (Figures 3.1a and 3.2a). Similar trends were observed for the other sorbents (Figures 3.4 – 3.5).

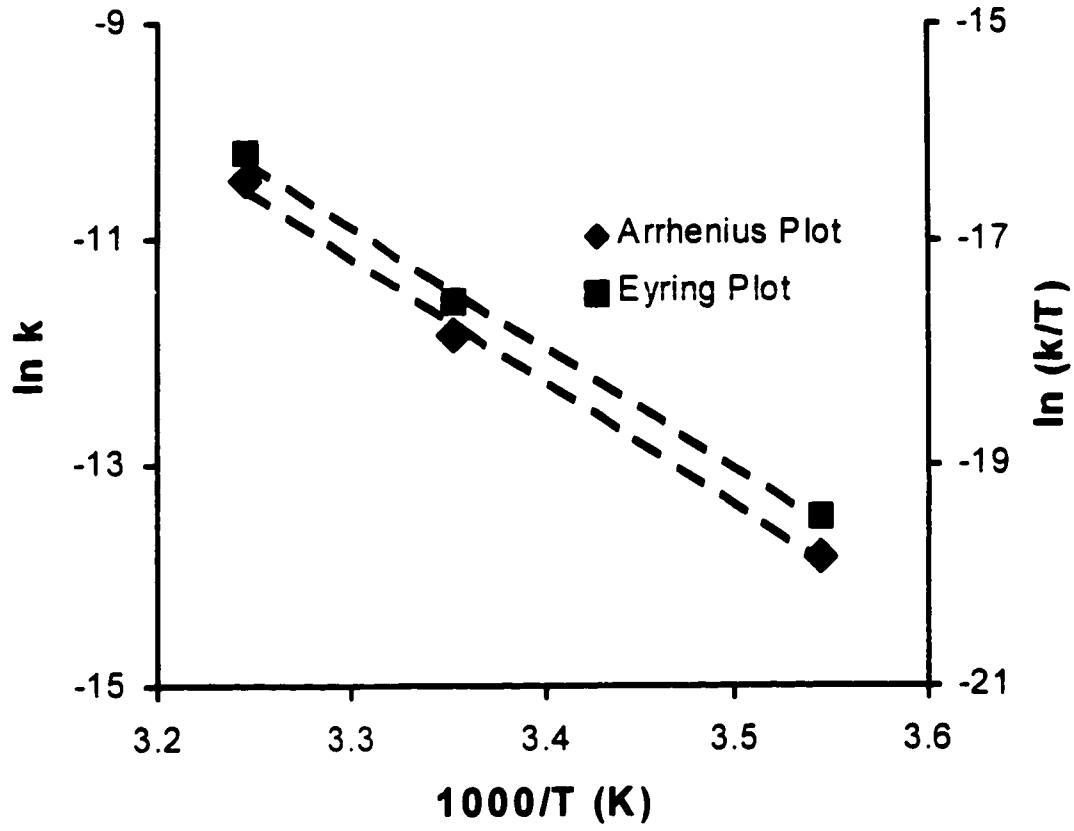

Figure 3.3. Comparison showing the near parallel relationship of Arrhenius and Eyring plots for data collected for Ni sorption on pyrophyllite at three various temperatures.

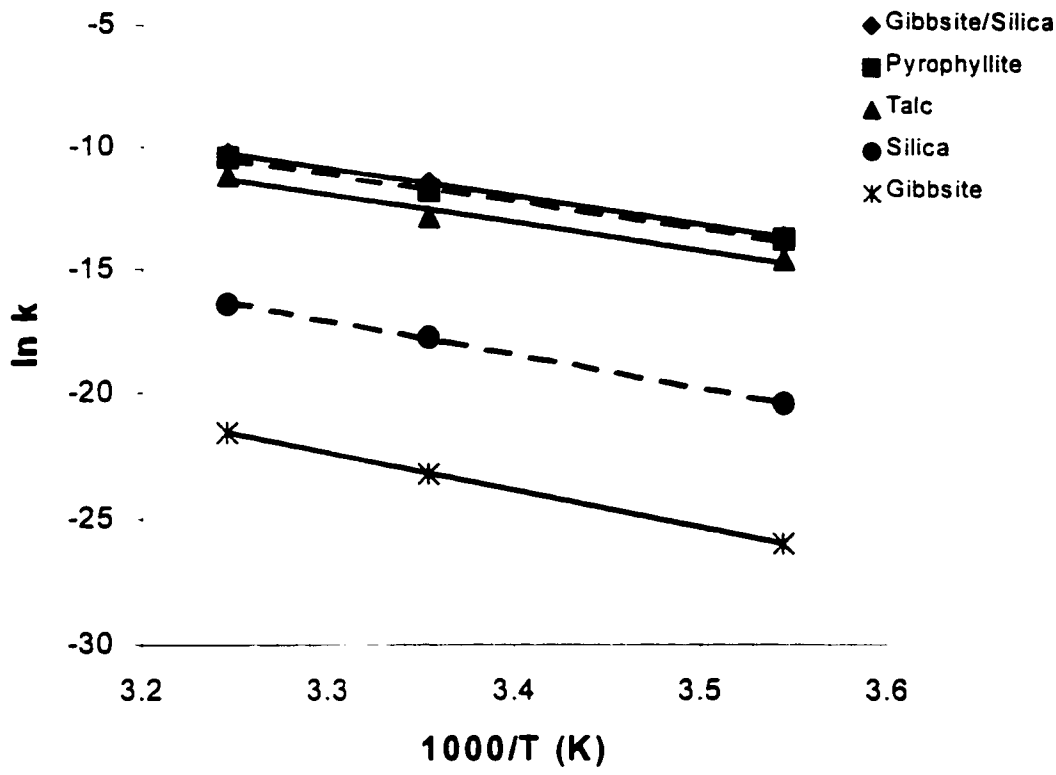

Figure 3.4. Compiled Arrhenius plots of Ni sorption on clay mineral and oxide surfaces at three different temperatures.

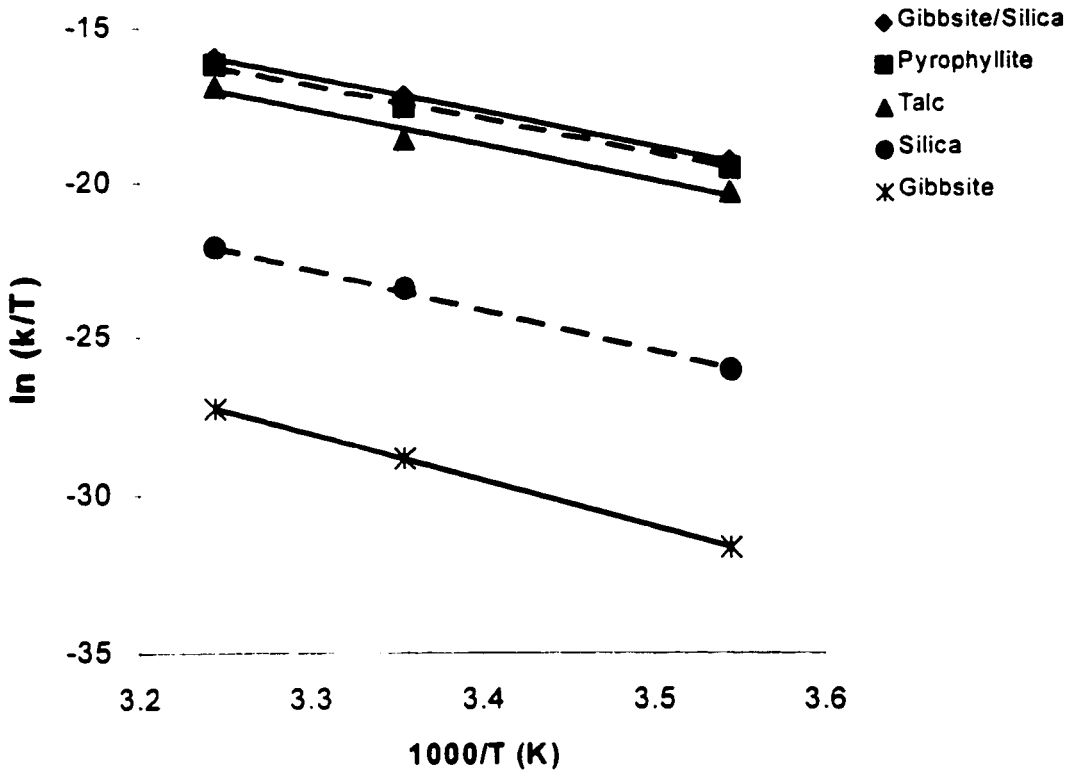

Figure 3.5. Compiled Eyring plots of Ni sorption on clay mineral and oxide surfaces at three different temperatures.

Table 3.3. Summary of reaction parameters derived from the Arrhenius and Eyring equations for Ni sorption on clay mineral and oxide surfaces.

SURFACE	E_a (kJ mol^{-1})	A (s^{-1})	$\Delta H^{\ddagger}$ (kJ mol^{-1})	$\Delta S^{\ddagger}$ (J mol^{-1})	$\Delta G^{\ddagger}$ (kJ mol^{-1}) 25°C
Pyrophyllite	93.05	1.6E+11	90.60	-38.70	102.23
Talc	95.35	1.8E+11	92.90	-37.91	104.20
Silica	111.47	6.1E+11	109.02	-27.51	117.22
Gibbsite	123.71	4.1E+11	121.26	-30.90	130.47
Gibbsite/Silica	95.09	4.5E+11	92.64	-29.96	101.57

One sees a range in E_a values from 93.05 to 123.71 kJ mol^{-1} (Table 3.3). E_a values for the phyllosilicates (pyrophyllite and talc, 93.05 and 95.35 kJ mol^{-1}, respectively) were lower than the oxide surfaces (gibbsite and silica, 123.71 and 111.47 kJ mol^{-1}, respectively) but comparable to the gibbsite/silica mixture (95.09 kJ mol^{-1}). These results fall within the mid-range of the E_a values for many mineral formation reactions (Table 3.1). Our data fit between the E_a values for green rust (a mixed Fe(II) and Fe(III) mineral) and a mixed Cu-In alloy (Table 3.1), and included in the list of minerals between these two extremes are several metal hydroxides and a metal carbonate. As noted earlier, E_a values above 42 kJ mol^{-1} indicate surface-controlled reactions (Sparks, 1989, 1995). We can, therefore, conclude that the E_a parameters calculated from our data suggest a surface-controlled reaction, which seems consistent with previous studies showing that Ni sorption on the minerals and at

the environmental conditions employed in this study (pH 7.5, $[Ni]_o$ = 3 mM) resulted in the formation of Ni surface precipitates.

The enthalpy ($\Delta H^{\ddagger}$). entropy ($\Delta S^{\ddagger}$), and Gibbs free energy ($\Delta G^{\ddagger}$) of activation values are also presented in Table 3.3. The $\Delta H^{\ddagger}$ values are a measure of the energy barrier which must be overcome by reacting molecules (Jencks, 1969). The values for $\Delta H^{\ddagger}$ (90.60 – 121.26 kJ mol^{-1}) suggest that these reactions are endothermic meaning they consume energy (Jardine and Sparks, 1981). The relationship between $\Delta H^{\ddagger}$ and E_a is noted in Eq. [6]. This relationship is observed in Figure 3.6 for the data collected in this study for the five mineral systems. Note the extremely good fit of the data and excellent agreement of the y-intercept (actual -RT = - 2.477 kJ mol^{-1}, T = 25 °C) to our experimental data (2.450 kJ mol^{-1}). The value of $\Delta S^{\ddagger}$ is also an indication whether or not a reaction is an associative or dissociative mechanism (Atwood, 1997). The entropy of activation ($\Delta S^{\ddagger}$) parameter is often regarded as a measure of the width of the saddle point of the potential energy surface over which reactant molecules must pass as activated complexes (Jencks, 1969). Entropy values greater than negative 10 J mol^{-1} generally imply a dissociative mechanism (Atwood, 1997). However, in Table 3.3, one sees large negative values for $\Delta S^{\ddagger}$ which suggests that Ni sorption on these clay mineral and oxide surfaces

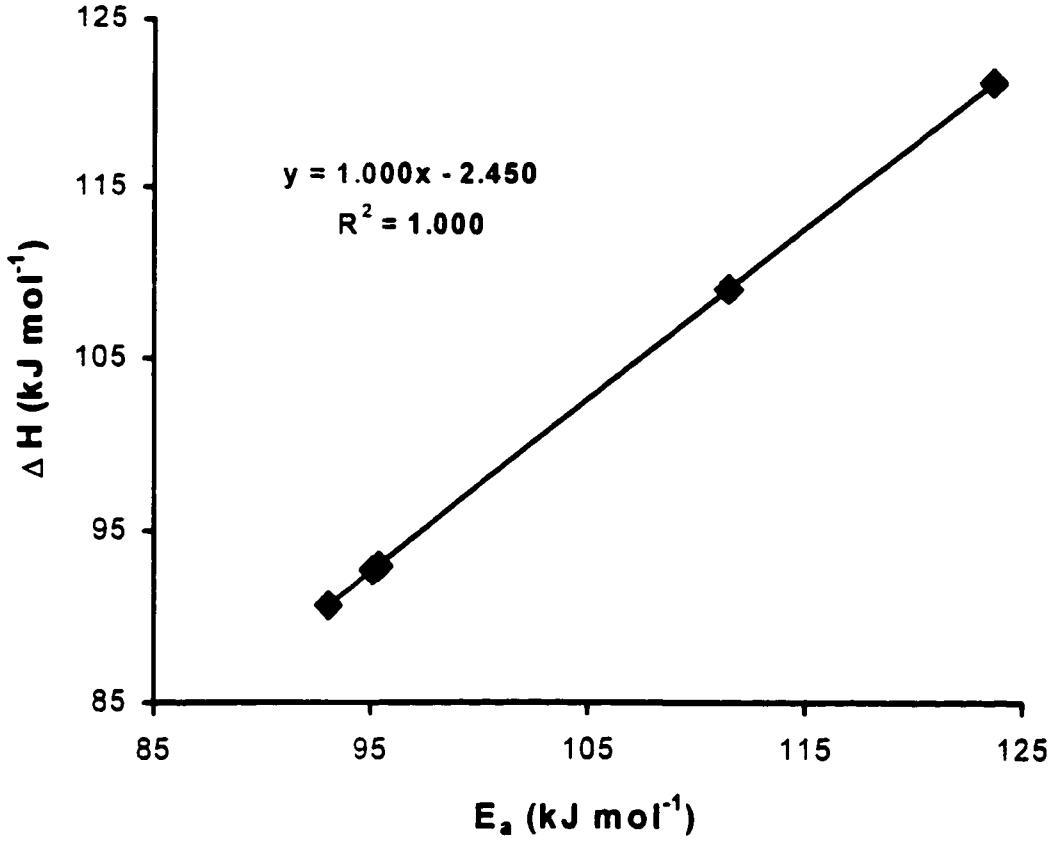

Figure 3.6. Relationship of energy of activation (E_a) and enthalpy of activation ($\Delta H^{\ddagger}$) by $\Delta H^{\ddagger} = E_a - RT$.

is an associative mechanism. Free energies of activation are considered to be the difference in free energy between the activated complex and the reactants from which it was formed (Laidler, 1965). Additionally, the large, positive $\Delta G^{\ddagger}$ values suggest that these reactions require energy to convert reactants into products. Typically, the $\Delta G^{\ddagger}$ value determines the rate of the reaction (rate increases as $\Delta G^{\ddagger}$ decreases) and once the energy requirement is fulfilled, the reaction proceeds. This is seen when comparing the data from Table 3.2 and 3.3. In Table 3.2, one sees that the gibbsite/silica mixture has the highest k_a' (9.78×10^{-6} s^{-1} at 25 °C) and gibbsite has the lowest sorption rate coefficient (8.61×10^{-11} s^{-1} at 25 °C) for the sorbents examined in this study. Table 3.3 illustrates this trend for $\Delta G^{\ddagger}$ in which the gibbsite/silica mixture has the lowest $\Delta G^{\ddagger}$ value (101.57 kJ mol^{-1}) compared to the largest $\Delta G^{\ddagger}$ value for gibbsite (130.47 kJ mol^{-1}) showing that the higher k_a' yields a lower $\Delta G^{\ddagger}$ for the gibbsite/silica mixture than for gibbsite.

3.5 Conclusions

Ni sorption was examined on pyrophyllite, talc, gibbsite, amorphous silica, and a mixture of gibbsite and amorphous silica at temperatures of 9, 25, and 35 °C to determine kinetic parameters. Based on these parameters, it was concluded that Ni sorption on these sorbents was surface-controlled which corroborates previous

molecular scale investigations suggesting the formation of surface precipitates (Scheidegger et al., 1996; Scheidegger et al., 1997; Scheidegger and Sparks, 1996; Scheidegger et al., 1998; Scheinost et al. 1999; Scheinost and Sparks, 1999; Scheckel and Sparks, 2000). The values of E_a in this study for the formation of Ni precipitates, which are mineral-like, coincide well with E_a values for the formation of various minerals listed in Table 3.1. The $\Delta H^{\ddagger}$ values suggest, as indicated by E_a values, that an energy barrier was present for the system to overcome in order for the reaction to occur. It was noted earlier from data in Tables 3.2 and 3.3 that reaction rates increase (gibbsite/silica mixture > pyrophyllite > talc > silica > gibbsite), as free energies of activation ($\Delta G^{\ddagger}$) decrease (gibbsite/silica mixture < pyrophyllite < talc < silica < gibbsite) signifying less energy requirements for the reaction system.

The information is this study will be helpful to scientists seeking to develop inclusive models that describe all possible sorption conditions and reactions within the soil environment. First of all. since most sorption models dismiss precipitation as a means of metal uptake in natural environments, many are missing an important aspect that has been reported increasingly in the geochemistry literature. The most likely explanation of this oversight is that until recently molecular scale information on metal precipitation has been lacking, and macroscopic studies cannot differentiate adsorption from precipitation. Secondly, and more related to this study, temperature plays an important, and often overlooked, role in the fate of contaminants in the environment. Temperature studies such as this are quite necessary in order to

construct full functioning models that will enable researchers to better predict mobility and bioavailability of metals in soils.

Chapter 4

DISSOLUTION OF NI(II) PRECIPITATES ON CLAY MINERALS AND OXIDES

4.1 Abstract

In recent years, studies have shown that sorption of metals onto natural materials results in the formation of new mineral-like precipitate phases. However, the stability of the precipitates and the potential long-term release of the metal back into the soil solution are poorly understood. Therefore, this study investigated the influence of residence time and dissolution agent on the release of nickel from five sorbents; pyrophyllite, talc, gibbsite, amorphous silica, and a gibbsite/silica mixture. Complementing the macroscopic, kinetic studies, X-ray absorption fine structure (XAFS) and diffuse reflectance spectroscopies (DRS), and high-resolution thermogravimetric analysis (HRTGA) were employed to elucidate dissolution mechanisms. Dissolution of the surface precipitates was compared to dissolution of reference Ni compounds.

In the sorption experiments conducted at pH 7.5, Ni-Al layered double hydroxide (LDH) formed in the presence of pyrophyllite and gibbsite, and α-Ni hydroxide formed with talc, amorphous silica, and the gibbsite/silica mixture, in line with former published studies. The stability of the precipitate phases decreased in the order Ni-Al LDH on pyrophyllite > α-Ni hydroxide on the gibbsite/silica mixture > α-Ni hydroxide on talc > α-Ni hydroxide on amorphous silica > Ni-Al LDH on gibbsite. This sequence can be explained by the greater stability of precipitates with Al-for-Ni substituted hydroxide layers compared to pure Ni hydroxide layers, and by the greater stability of precipitates with silicate-for-nitrate exchanged in the interlayer space. With increasing residence time, all precipitate phases drastically increased in stability, as was documented by decreasing amounts of Ni released by ethylenediaminetetraacetic acid (EDTA), oxalate, acetylacetone, and nitric acid (HNO_3) treatments. This aging effect may be partly explained by the silicate-for-nitrate exchange during the first days of reaction, and subsequently by silicate polymerization and partial grafting onto the hydroxide layers (Ford et al., 1999). However, even Si-free, Ni-reacted gibbsite showed a substantial aging effect, suggesting that factors other than interlayer silication may be equally important. Such a factor may be crystal growth due to Ostwald ripening. Based on XAFS, DRS, and HRTGA investigations, the Ni precipitates which remained at the end of the dissolution experiments were similar to the precipitates at the beginning of the

dissolution, indicating that no preferential dissolution of a structurally less stable phase occurred. Therefore, the precipitate phases seem to be structurally very homogeneous.

4.2 Introduction

Dissolution of metal surface precipitates is analogous to mineral dissolution and involves several key steps which are either rate-limiting or not depending on whether the dissolution is transport (diffusion)- or surface-controlled. A transport-controlled rate-determining step involves the movement of a reactant or a weathering product through a layer of the surface of the mineral. Likewise, surface-controlled processes are generally slower than transport-controlled reactions so that concentrations adjacent to the surface build up to values essentially identical to those in the surrounding bulk solution. The possible rate-limiting steps are: 1) mass transfer of the reactants in the bulk solution to the surface, 2) adsorption of the reactants, 3) interlattice transfer of reacting species, 4) chemical reactions at the surface, 5) movement of the reactants away from the surface, and 6) mass transfer of products and excess reactants into the bulk solution. Under normal system conditions, Steps 1 and 6 (transport-controlled) are not usually rate-limiting while Steps 3, 4, and 5 (surface-controlled) are often rate-limiting (Stumm and Wollast, 1990).

Mineral dissolution is one of the major processes influencing the overall cycle of elements within the subsurface environment. Dissolution is known to occur by interactions of surfaces with ligands, protons, deprotonation of surfaces, water, and recent studies indicate that metals may play a part in surface dissolution. The surface protonation of O and OH lattice sites is the mechanism of dissolution of silicates and accelerates with decreasing pH (Stumm and Morgan, 1996). The points of attack of the protons in layered silicates are the O atoms that interlink the Al-oxide groups with the Si-oxide structures for layer silicates. The protonation slowly releases Al from the silicate surface followed by the subsequent detachment of $Si(OH)_4$ species. Ligands, including environmentally important low molecular weight organic acids of biological decomposition and root exudates, are known to promote the dissolution of Al silicates (Brady and Walther, 1992). Dissolution of silicates and other minerals have been widely studied on a macroscopic scale: kaolinite and muscovite as a function of pH (Stumm and Wieland, 1990), δ-Al_2O_3 as influenced by pH (Furrer and Stumm, 1986), orthosilicates by divalent metal-oxygen bonds (Casey and Westrich, 1992), α-FeOOH as a function of pH (Zinder et al., 1986), Fe (III) (hydr)oxides via reductive dissolution (Biber et al.,1994), albite promoted by temperature and pressure (Chou and Wollast, 1984), and biotite with acids (Grandstaff, 1986) to name a few.

The influence of ligands and oxyanions in dissolution was studied by Bondietti et al. (1993) who examined the effects of EDTA, phosphate, arsenate and selenite on the reactivity of Fe(III) (hydr)oxides. Dissolution was severely inhibited by phosphate, arsenate and selenite at near neutral pH values. At pH < 5, dissolution was accelerated by the presence of phosphate, arsenate and selenite.

A metal-promoted dissolution mechanism has also been proposed which suggests that sorbing cations may induce the dissolution of cations held within the sorbent and that these released cations then become incorporated in precipitates to form multinuclear surface precipitates with the sorbing cation in the bulk solution (Scheidegger et al., 1997; Sparks et al., 1998; Scheidegger et al., 1998).

Sorption reactions at the mineral/water interface largely determine the mobility and bioavailability of metals in soils and sediments. Spectroscopic and microscopic studies in the last decade showed the importance of metal hydroxide precipitate formation upon reacting a variety of clay mineral and oxide surfaces with Ni or Co (Chisholm-Brause et al., 1990; O'Day et al., 1994a; Scheidegger et al., 1996; Towle et al., 1997; Thompson, 1998; Thompson et al., 1999a). In spite of the difficulties in studying trace amounts of low-crystalline surface precipitates, substantial advances have been achieved in characterizing their chemical composition and structure. In the

case where the sorbent phase released Al during reaction with the metal solutions, the precipitates were predominantly Al-containing layered double hydroxide (LDH) phases (d'Espinose de la Caillerie et al., 1995; Scheidegger et al., 1996; Scheidegger et al., 1997; Scheidegger and Sparks, 1996; Scheidegger et al., 1998; Scheinost et al., 1999; Towle et al., 1997; Thompson, 1998; Thompson et al., 1999a). In the case of Al-free or inert sorbents, however, metal sorption resulted in α-type metal hydroxide precipitates (O'Day et al., 1994a; Scheinost et al., 1999; Scheinost and Sparks, 1999). Both types of precipitates consist of brucite-like metal hydroxide layers. In contrast to the well-crystalline hydroxide minerals, however, the layers are separated from each other by water and anions, leading to a turbostratic structure, and metal-metal distances within the layer are significantly reduced with respect to the well-crystalline metal hydroxides (Bish, 1980; d'Espinose de la Caillerie et al., 1995; Génin et al., 1991; Kamath and Therese, 1997; Pandya et al., 1990; Taylor and McKenzie, 1980).

Formation of these precipitate phases drastically reduces metal concentration in soil and sediment solutions, and effectively competes with adsorption on soil minerals (Elzinga and Sparks, 1999). While it is evident from the literature that studies on the formation of surface precipitates often occur, investigations on the dissolution of surface precipitates are not common. To date, only a few papers have appeared in the literature on the dissolution of surface precipitates (Scheidegger and

Sparks, 1996; Fendorf et al., 1996; Ford et al., 1999; Thompson et al., 1999b, Scheckel et al., 2000). Accordingly, is a veritable need, in view of the common formation of polynuclear metal complexes on natural materials, to better understand the degree and mechanism(s) of metal dissolution from surface precipitates. Such information is vital if one is to better assimilate the fate of metals in the subsurface environment.

Fendorf et al. (1996) examined the ligand-promoted dissolution of Cr(III) precipitates from silica and goethite surfaces with oxalate, a common plant root exudate. Ligand-promoted dissolution involves the formation of a surface complex with a ligand (e.g., oxalate, EDTA, PO_4^{3-}, etc.) via a ligand exchange mechanism. In this mechanism, a surface hydroxyl exchanges with the organic or inorganic ligand which adds a negative charge to the Lewis acid center coordination sphere and lowers the Lewis acid acidity. This reaction polarizes the metal-oxygen bonds and the metal is released from the surface into the solution (Sparks, 1995). Fendorf et al. (1996) noted from AFM studies that the morphologies of the hydrous chromium oxides on the two surfaces were very different. The silica surface exhibited small cone-shaped clusters while the goethite material revealed a "smoothing" effect from the precipitates. Therefore, one can conclude that the surface area of the precipitates on silica is greater than those on goethite; thus, the metal is more likely released at a

higher rate. In fact, after one hour of reaction, 17% of the sorbed Cr(III) on silica was released while < 1% of the Cr(III) from the goethite was dissolved. A solution of a pure hydrous chromium oxide solid resulted in the most rapid dissolution with 20% dissolved within one hour. After 29 hours, Cr (III) dissolution was 35%, 22.4% and 6.6% for pure hydrous chromium oxide, silica, and goethite, respectfully. Overall, Cr(III) detachment from goethite was approximately 70% less than that from silica.

Scheidegger and Sparks (1996) examined the dissolution of polynuclear Ni(II) surface complexes from pyrophyllite via proton-promoted dissolution with HNO_3 at pH = 4 and pH = 6. Proton-promoted dissolution occurs when protons bind to surface oxide ions, which causes the bonds to weaken. Thereafter, the metal is detached into the solution phase (Sparks, 1995). This study (Scheidegger and Sparks, 1996) was unique in that it examined the kinetics of precipitation and dissolution of the mixed Ni-Al hydroxide phases from the surface. Nickel detachment from surface complexes was rapid initially at both pH values (with < 10% of total Ni released) and was attributable to desorption of specifically adsorbed, mononuclear bound Ni. Dissolution then slowed tremendously primarily due to the gradual dissolution of the multinuclear surface precipitates. A reference compound, crystalline $Ni(OH)_2$, was also examined for its dissolution potential. The replenishment method was employed to simulate steady-state flow and a conventional batch method was also used to

compare the influence of reaction products present in solution on dissolution. The replenishment method was more effective in removing Ni from the surface precipitates (~ 12% at pH = 6 and ~ 48 % at pH = 4). Compared to the dissolution of crystalline $Ni(OH)_2$ (~ 96% dissolved), Ni release from pyrophyllite was extremely slow.

Thompson et al. (1999b) established solubility constants for Co-Al LDH and found also that the Al-containing phase is less soluble than Co hydroxide and Co carbonate at circum-neutral pH. Ford et al. (1999) investigated the dissolution of Ni-Al LDH surface precipitates on pyrophyllite using an EDTA solution at pH 7.5. Detachable Ni drastically decreased when the age of the precipitate increased from one hour to one year. By employing high-resolution thermogravimetric analysis which is sensitive to changes in the interlayer composition of LDH, and by comparing the results of the surface precipitates with those of reference compounds, the authors could show that a substantial part of the aging effect was due to replacement of interlayer nitrate by silicate which transformed the initial Ni-Al LDH into a Ni-Al phyllosilicate precursor. The source of the silicate was the dissolving surface of the pyrophyllite. The studies in this chapter also investigated the dissolution of Ni-Al LDH phases on pyrophyllite and gibbsite and α-$Ni(OH)_2$ precipitates on talc and a mixture of gibbsite/amorphous silica employing EDTA (pH 7.5) and nitric acid (pH 4.0) for sorption aging times ranging from one hour to one year. In these studies, an

array of analytical techniques was applied to examine the dissolution of Ni surface precipitates formed on pyrophyllite, talc, gibbsite, and the mixture. The differences in stability due to aging of the surface precipitates could be explained by a combination of Al-for-Ni substitution in the hydroxide layers (for pyrophyllite and gibbsite) and silicate-for-nitrate substitution in the interlayer (for pyrophyllite, talc, and mixture). The macroscopic dissolution studies demonstrated increased stability in Ni surface precipitates with aging. The aging effect may be attributed partially to the solid-state transformation of the precipitate phases (silication of Ni-Al LDH and α-Ni hydroxide), and to crystal growth due to Ostwald ripening.

These investigations reveal a substantial influence of the sorbent phase on the composition of the precipitate phases and, in turn, on their resistance against dissolution. The objective of this study was to systematically investigate the influence of Al-for-Ni substitution and of silicate-for-nitrate substitution on the kinetics of Ni release. Therefore, this study used (Al- and Si-containing) pyrophyllite and a mixture of gibbsite and amorphous silica as a sorbent phases, but also Si-free gibbsite and Al-free talc and amorphous silica to be able to study the influence of Al and Si separately. The precipitates were subjected to variable residence time periods up to two years before conducting the dissolution experiments in order to study the influence of aging. For comparison, this study examined the dissolution of synthetic reference phases to

reproduce the effect of Al in the hydroxide layer and of exchanged silicate in the interlayer. In this study six different dissolution agents were used, EDTA (pH 4.0), EDTA (pH 7.5), oxalate, acetylacetone, HNO_3 (pH 4.0), and HNO_3 (pH 6.0), to compare Ni release by complexation versus release by Ni protolysis (Bryce and Clark, 1996; Stumm, 1997). In addition to describing the dissolution rates macroscopically, the experiments monitored the structure and composition of the remaining Ni phase of the 1-month aged samples using XAFS, DRS, and HRTGA.

4.3 Materials and Methods

4.3.1 Materials

The pyrophyllite (Robbins, NC, USA; Ward's), talc (Cherokee Co., NC, USA; Excalibur) and gibbsite (Arkansas, USA; Ward's) samples from natural clay deposits were prepared by grinding the clay in a ceramic ball mill for approximately 14 days, centrifuging to collect the < 2 μm fraction in the supernatant, Na^+ saturating the < 2 μm fraction, and then removing excess salts by dialysis followed by freeze drying of the clay. X-ray diffraction (XRD) showed minor impurities of kaolinite and quartz in pyrophyllite, and about 10 % bayerite in the gibbsite. Although the talc sample had about 20 % chlorite according to XRD, acid digestion resulted in an Al/Mg ratio of

only 0.01. This small Al-content was not sufficient in former experiments to induce the formation of detectable amounts of Ni-Al LDH (Scheinost et al., 1999). The precipitated amorphous silica (SiO_2) (Zeofree® 5112) was obtained from the Huber Corporation. The mixture of gibbsite and amorphous silica consisted of 40% gibbsite and 60% silica by weight. The mixture was used to more closely mimic heterogeneous systems that are found in natural environments. The N_2-BET surface areas of the sorbent phases were 95 $m^2 g^{-1}$ for pyrophyllite, 75 $m^2 g^{-1}$ for talc, 25 $m^2 g^{-1}$ for gibbsite, 90 $m^2 g^{-1}$ for amorphous silica, and 64 $m^2 g^{-1}$ for the gibbsite/amorphous silica mixture.

The six dissolution agents employed in this study were nitric acid (HNO_3) at pH 4 and 6 to induce proton promoted dissolution and 1 mM ethylenediaminetetraacetic acid (EDTA) at pH 4 and 7.5, 3 mM oxalate at pH 4, and 3 mM acetylacetone at pH 6 to induce ligand-promoted dissolution. EDTA forms a stable Ni solution complex, and previous studies have shown that EDTA promotes desorption of Ni sorbed to oxide surfaces and the dissolution of poorly crystalline oxide phases (Borggaard, 1992; Bryce and Clark, 1996). Oxalate, a common root exudate, illustrates ligand-catalyzed dissolution that naturally occurs in the soil environment. Nickel acetylacetonate is readily formed from acetylacetone and

$Ni(OH)_{2\,(s)}$, and acetylacetone is commonly used commercially to clean surfaces that have been in contact with metals.

4.3.2 Ni Sorption and Kinetics of Dissolution

To investigate the influence of aging on the stability of the precipitate phases, pyrophyllite, talc, gibbsite, amorphous silica and gibbsite/silica mixture were reacted with Ni for periods of one hour to two years. Experimental conditions were as described in Scheidegger and Sparks (1996) using an initial concentration of 3 mM Ni as $Ni(NO_3)_2$, 10 g/L sorbents and a background electrolyte of 0.1 M $NaNO_3$ at pH 7.5. The systems were purged with N_2 to eliminate CO_2, and the pH was maintained through addition of 0.1 M NaOH via a Radiometer pH-stat titrator. After one week, the batch reaction vessel was removed from the pH-stat and placed in a 25° C incubation chamber. The pH was subsequently adjusted weekly.

To visually observe in-situ, real-time dissolution of Ni precipitates via atomic force microscopy (AFM), cubes of minerals needed to be prepared. Of the solids used in this study, only pyrophyllite fit the mold in terms of purity and size of particles. The talc material was highly contaminated with carbonates and organic matter which were removed when converted into powder form. Gibbsite and silica samples were

received already in powder form. Large pieces of pyrophyllite were cut into one cm^3 cubes, leveled relative to a sample holder, and polished with successively smaller diamond particle pastes (2 μm to 0.25 μm size) to give nearly anatomically flat surfaces. With the flat mineral surfaces, features present after sorption were believed to be solely Ni-Al LDH precipitates. The pyrophyllite cubes were subject to Ni sorption for 14 days under the same reaction conditions mentioned in the previous paragraph before dissolution with EDTA (pH 7.5) or HNO_3 (pH 4.0) via time-resolved AFM analyses, as described later.

Dissolution was carried out by a replenishment technique using 1 mM EDTA at pH 4.0 and 7.5, 3 mM oxalate at pH 4.0, 3 mM acetylacetone at pH 6.0, or HNO_3 at pH 4.0 or 6.0. From the aging Ni/clay mineral suspensions, 30 mL (corresponding to 300 mg of clay) were withdrawn. After centrifuging at 17,000 rpm for 5 minutes, the supernatant was decanted, and 30 mL of the dissolution agent was added to the remaining solids. The suspensions were then placed on a reciprocating shaker at 25° C for 24 hours. The dissolution steps were repeated either 10 times (=10 days) for short-term (aged < 1 month) or 14 days for long-term (aged ≥ 1 month) Ni sorption samples. A disadvantage of the replenishment technique is that there will inevitably be some dissolved Ni entrained in the clay paste and one could argue the formation of Ni-EDTA complexes on the surfaces. However, this accounts for a very small

percentage of the overall Ni released. This is supported by the fact that the rate of dissociation for the Ni-EDTA complexes is slow relative to the residence time of the complexes in solution before replenishment (van den Berg and Nimmo, 1987; Hering and Morel, 1990; Wilkens, 1974). The conditional stability constant (K^{cond}) for Ni-EDTA complexes is approximately 10^{10} M^{-1}. Sorption of Ni-EDTA complexes is also unlikely under the reaction conditions of this study (Nowack and Sigg, 1996; Elliot and Huang, 1979; Elliot and Denneny, 1982; Chang and Ku, 1994) suggesting the complexes prefer to remain in solution once formed. Additionally, the maximum solution concentration of Ni after any given 24 hour replenishment period was 0.46 mM which is far below the saturation point for re-precipitation of Ni under these reaction conditions either on the sorbent or in bulk solution, especially during dissolution with HNO_3 at pH 4.0. ICP-AES or AAS was used to determine Ni and Si in the supernatants during dissolution.

4.3.3 Synthesis of Ni Reference Compounds

An α-Ni hydroxide was prepared by adding 550 mL of 30% ammonia to 500 mL of 1 *M* $Ni(NO_3)_2$ (Génin et al., 1991). The solution was vigorously stirred and purged with N_2. After 2 hours, the suspension was centrifuged and washed with D.I. water in five cycles, shock-freezed in liquid N_2, and freeze-dried. A Ni-Al LDH

sample was prepared by controlled hydrolysis (Taylor, 1984). The amount of Ni and Al (added as $Ni(NO_3)_2 \cdot 9H_2O$ and $Al(NO_3)_3 \cdot 9H_2O$) was adjusted to give an initial Ni/Al ratio in solution of 10. Under vigorous stirring, 450 mL of both solutions were combined. The pH was raised to 6.9 by addition of 2.5 M NaOH and then kept constant for 5 hours using an autotitrator. The precipitate was washed and dried as before. Metal solutions were purged with N_2, and the 2.5 M NaOH was freshly prepared to minimize carbonate uptake by the precipitate. By acid digestion a Ni/Al ratio of 5 was determined. XRD-layer spacings and strong nitrate bands in the IR spectra of the α-Ni hydroxide and the Ni-Al LDH samples confirmed the prevalence of nitrate in the interlayer. Part of both samples was subsequently exchanged with silicate following the method of Depège et al. (1996): 100 mL deionized-distilled H_2O + 0.85 g sodium metasilicate + 0.4 g Ni-Al hydrotalcite, giving a pH of 12.2. The suspensions were heated at 90°C for 24 hours under an N_2 atmosphere, and subsequently aged 2 weeks at 60°C in a sealed vessel (final pH = 12.0). The silicate-for-nitrate exchange was confirmed by FTIR. Further data on these samples are given by Scheinost et al. (1999) and Scheinost and Sparks (1999).

4.4 Spectroscopic, Microscopic, and Thermogravimetric Characterization of Surface Precipitates

Changes in the solid phase Ni speciation during dissolution were periodically assessed via spectroscopic, microscopic, and thermoanalytical techniques. For XAFS and DRS analyses, samples were examined in-situ by centrifuging the suspensions and using the wet clay paste. For HRTGA analyses, the clay pastes were washed three times with D.I. water and freeze-dried before examination. Speciation of dissolution samples in the spectroscopic and thermogravimetric studies was carried out for clay samples aged for one month to ensure that only a negligible part of the Ni was bound as mononuclear surface complexes, and the majority as a precipitate. For AFM analyses, one cm^3 cubes of pyrophyllite were reacted with Ni for 14 days prior to dissolution.

4.4.1 X-Ray Absorption Fine Structure (XAFS) Spectroscopy

XAFS was applied to determine information on the nearest-neighbor chemical environment of Ni such as coordination numbers and atomic distances. Experiments were conducted at the National Synchrotron Light Source (NSLS), Brookhaven National Laboratory (BNL), Upton, New York, on beamline X-11A. The electron

storage ring was operated at 2.528 GeV with beam currents in the 180 - 310 mA range. A 0.5 mm premonochromator slit width and a Si(111) double-crystal monochromator detuned by 25% to reject higher-order harmonics was used. The beam energy was calibrated by assigning the first inflection of the K_α-absorption edge of nickel metal to 8333 eV. The XAFS spectra were collected in fluorescence mode using a Lytle detector. The ionization chamber of the Lytle detector was filled with Ar and the chamber of I_0 was filled with N_2 gas. Samples were positioned at a 45° angle relative to the incident beam and the ionization chamber was situated at 45° off the sample (90° off the incident beam). A Co-3 filter and Soller slits were arranged between the sample and the Lytle detector to reduce scattered X-rays reaching the fluorescence detector. Spectra were collected at 77 K to reduce thermal disorder. Previous studies in our laboratory indicate that Ni speciation does not change by cooling to 77 K versus room temperature (Roberts et al., 1999). Triplicate scans were collected for each sample.

MacXAFS 4.0 (Bouldin et al., 1995) was employed for background subtraction and Fourier filtering. The χ function was extracted from the raw data by using a linear preedge background and a spline postedge background, and by normalizing the edge to unity. The data were next converted from energy to k space and weighted by k^3 to compensate for the dampening of the XAFS amplitude with increasing k. Structural

parameters were extracted with fits to the standard XAFS equation. Using the FEFF6 and ATOMS codes (Zabinsky et al., 1995), *ab initio* amplitude and phase functions for single shells were calculated. A natural takovite ($Ni_6Al_2(OH)_{16}CO_3 \bullet H_2O$) (Kambalda W.A., Australia) and a synthetic β-$Ni(OH)_2$ (Johnson Mattey Co.) were used as reference compounds. Multishell fitting was done in R space over the range $1.104<R<3.129$ Å with $3.2<k<13.6$ $Å^{-1}$ for pyrophyllite samples and $1.104<R<3.191$ Å with $3.2<k<13.6$ $Å^{-1}$ for talc samples. The number of free floating parameters was reduced by one by allowing only equal values for the Debye-Waller factors of the Ni-Ni and Ni-Al shells for pyrophyllite. The R_{Ni-O} and R_{Ni-Ni} values are estimated to be accurate to ±0.02 Å, and the N_{Ni-O} and N_{Ni-Ni} are estimated to be accurate to ±20%. The estimated accuracies for N_{Ni-Al} and R_{Ni-Al} are ±60% and ±0.06 Å, respectively. The accuracy estimates are based on the results of theoretical fits to spectra of the reference compounds of known structure (O'Day et al., 1994b).

4.4.2 Diffuse Reflectance Spectroscopy (DRS)

Although the information provided by DRS is restricted to local symmetry of the first coordination shell, it is more sensitive to changes in the coordination distance of Ni-O (R_{Ni-O}) than XAFS. Therefore, this method proved to be very sensitive in distinguishing between Ni-Al LDH (smaller R_{Ni-O}) and α-Ni hydroxide (larger R_{Ni-O})

by using the energy position of the v2 band which corresponds to the $^3A_{2g} \rightarrow {}^3T_{1g}$ transition (Scheinost et al., 1999). A Perkin Elmer Lambda 9 diffuse reflectance spectrophotometer fitted with a 5 cm Spectralon-coated integrating sphere was employed to collect spectra in the UV-VIS-NIR range. Extraction of the band position was as in Scheinost et al. (1999).

4.4.3 High Resolution Thermogravimetric Analysis (HRTGA)

HRTGA was employed to characterize thermal decomposition reactions attributed to the Ni precipitate phases in the reacted clay mineral samples. Changes in the quantity and temperature of decomposition are indicative of compositional changes in the precipitate. The studies employed a TA Instruments 2950 High-Resolution Thermogravimetric analyzer to examine approximately 15-20 mg samples from sorption and dissolution studies that were previously freeze-dried. The analysis was run under a N_2 atmosphere over a temperature range of 30 to 800 °C. The following high-resolution settings were used: (1) maximum heating rate = 20° C min^{-1}, (2) resolution = 5.0, and (3) sensitivity = 1.0 (Ford and Bertsch, 1999). Data are presented as the derivative of the weight loss curve versus temperature.

4.4.4 Atomic Force Microscopy (AFM)

AFM was employed to investigate the dissolution of Ni-Al LDH precipitates on pyrophyllite aged for 14 days using EDTA (pH 7.5) and HNO_3 (pH 4.0) as dissolution agents. Experiments were conducted in Fluid TappingMode™ on a MultiMode Nanoscope IIIa AFM from Digital Instruments (Santa Barbara, CA) equipped with a fluid flow-through cell. In comparison to normal TappingMode™, similar advantages are realized with Fluid TappingMode™ operation. In this case, however, the fluid medium in the reaction cell tends to dampen the cantilever's normal resonant frequency. Instead of the cantilever's own resonance in Fluid TappingMode™, the entire fluid cell can be oscillated to drive the cantilever into oscillation for optimum scanning. When an appropriate frequency is selected (usually in the range of 5,000 to 40,000 cycles per second), the amplitude of the cantilever will decrease when the tip begins to tap the sample, similar to TappingMode™ operation in air (discussed in Chapter 2).

The use of Fluid TappingMode™ AFM was accomplished by placing a diamond-polished pyrophyllite cube on the sample platform and placing a rubber O-ring on the center of the mineral cube. The microscope head was placed upon the

sample by aligning the groove of the fluid cell with the O-ring on the sample. Once this was completed, the laser was positioned onto the cantilever so that the maximum sum signal occurs. The setup part was then finished and the necessary dissolution agent could then be loaded into the fluid cell at a rate of 0.1 mL min^{-1} with aid of a peristaltic pump with 3/32 inch tubing attached. The tubing with the pump attached was connected onto one of the ports of the fluid cell and another piece of tubing was coupled to the other port for drainage. The solution was slowly pumped into the fluid cell so that strong forces would destroy the tip and cantilever. After this step, the laser was realigned on the photodiode to maximize the sum. Other parameters were adjusted during break times of scanning such as the force curve calibration, gains, scan rate, Z scale and setpoint. Scans were collected at 0 hour (surface unreacted with dissolution agent), 24 hours, and 240 hours. The limited scans ensured few or no artifacts associated with tip dulling. The collected unaltered scans were 1 μm by 1 μm with Z ranges of 60 nm at the maximum resolution of 512 lines and an initial set point of 2 volts. Images are presented in height mode.

4.5 Results

4.5.1 Macroscopic Dissolution Kinetic Data

The large-scale macroscopic dissolution data are presented in Figures 4.1 – 4.5. Dissolution of Ni-Al LDH precipitates on pyrophyllite (Figure 4.1) and gibbsite (Figure 4.3) and α-$Ni(OH)_2$ precipitates on talc (Figure 4.2), amorphous silica (Figure 4.4), and the gibbsite/silica mixture (Figure 4.5) show, that regardless of the dissolution agents, as aging time increases the amount of Ni remaining as a precipitate increases. As expected the ligand-promoted dissolution is more effective than the protolysis by HNO_3 (Bryce and Clark, 1996). The effectiveness of the dissolution agent in removing Ni from the surface, from greatest to least, follows the sequence EDTA (pH 4.0) > EDTA (pH 7.5) ≈ oxalate (pH 4.0) > acetylacetone (pH 6.0) ≈ HNO_3 (pH 4.0) > HNO_3 (pH 6.0). This trend is seen in Table 4.1 for dissolution of 1 month aged sorption samples for each sorbent and dissolution agent after 14 replenishment steps. In Table 4.1, dissolution of Ni-Al LDH precipitates from pyrophyllite resulted in 29, 41, 37, 88, 91, and 97 % of the Ni remaining in the precipitate phase after 14 replenishments steps with EDTA (pH 4.0), EDTA (pH 7.5), oxalate, acetylacetone, HNO_3 (pH 4.0), and HNO_3 (pH 6.0), respectively. This trend

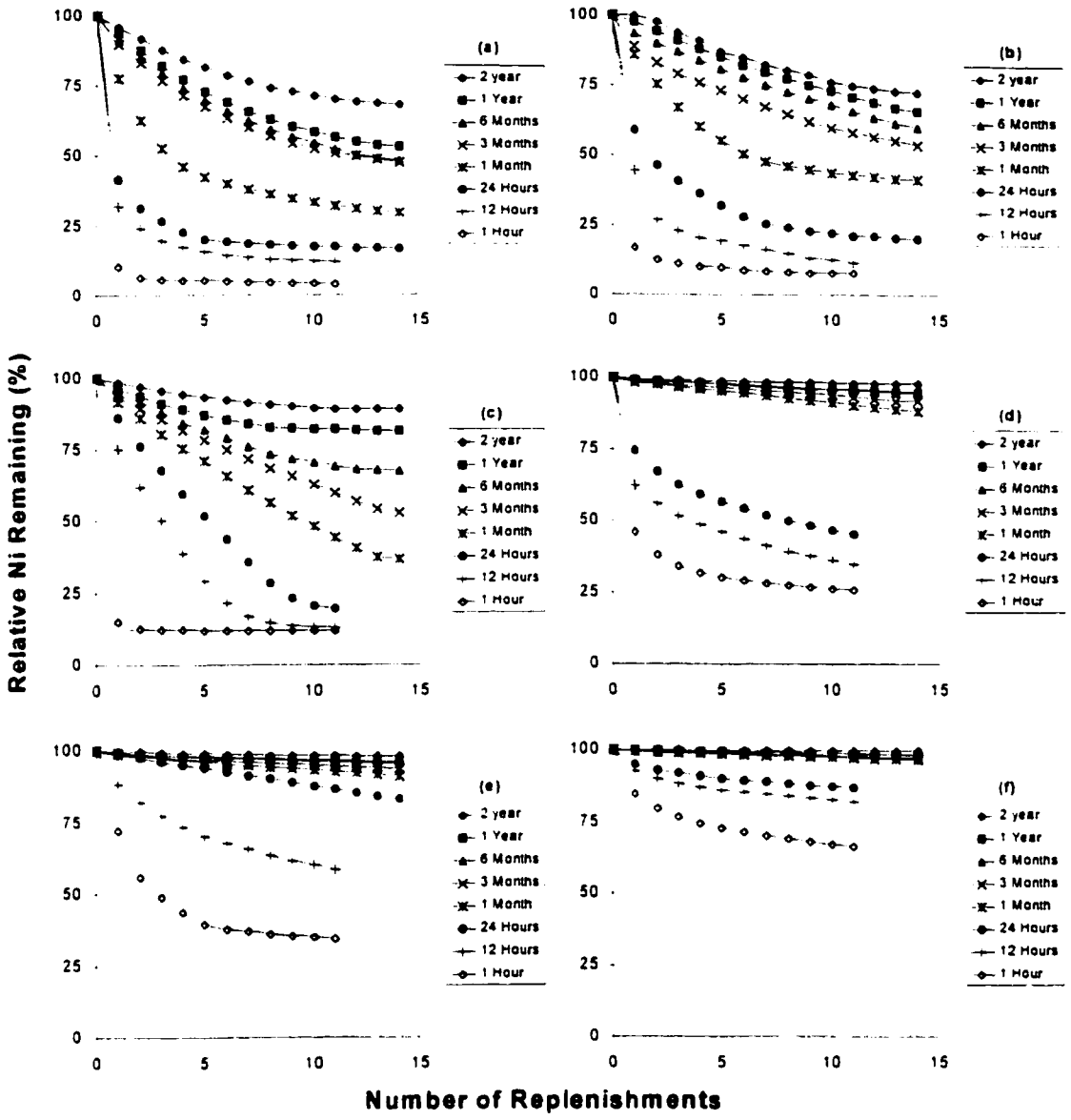

Figure 4.1. Macroscopic dissolution behavior of aged Ni precipitates on pyrophyllite showing the relative amount of Ni remaining on the surface following extraction with (a) 1 mM EDTA at pH 4.0, (b) 1 mM EDTA at pH 7.5, (c) 3 mM oxalate at pH 4.0, (d) 3 mM acetylacetone at pH 6.0, (e) HNO_3 at pH 4.0, and (f) HNO_3 at pH 6.0 plotted against the total number of replenishments. The stability of the Ni precipitates increases with aging time.

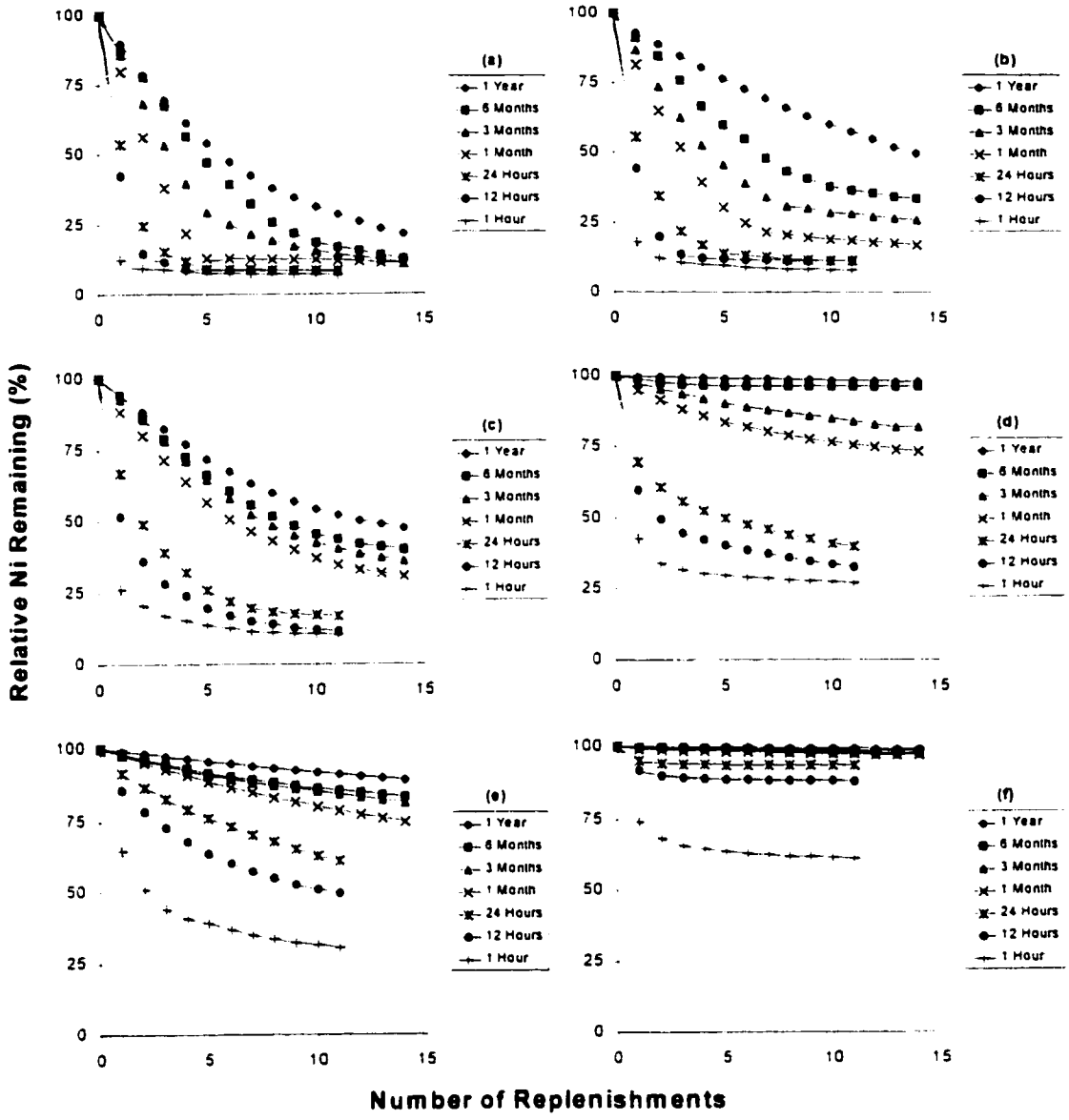

Figure 4.2. Macroscopic dissolution behavior of aged Ni precipitates on talc showing the relative amount of Ni remaining on the surface following extraction with (a) 1 mM EDTA at pH 4.0, (b) 1 mM EDTA at pH 7.5, (c) 3 mM oxalate at pH 4.0, (d) 3 mM acetylacetone at pH 6.0, (e) HNO_3 at pH 4.0, and (f) HNO_3 at pH 6.0 plotted against the total number of replenishments. The stability of the Ni precipitates increases with aging time.

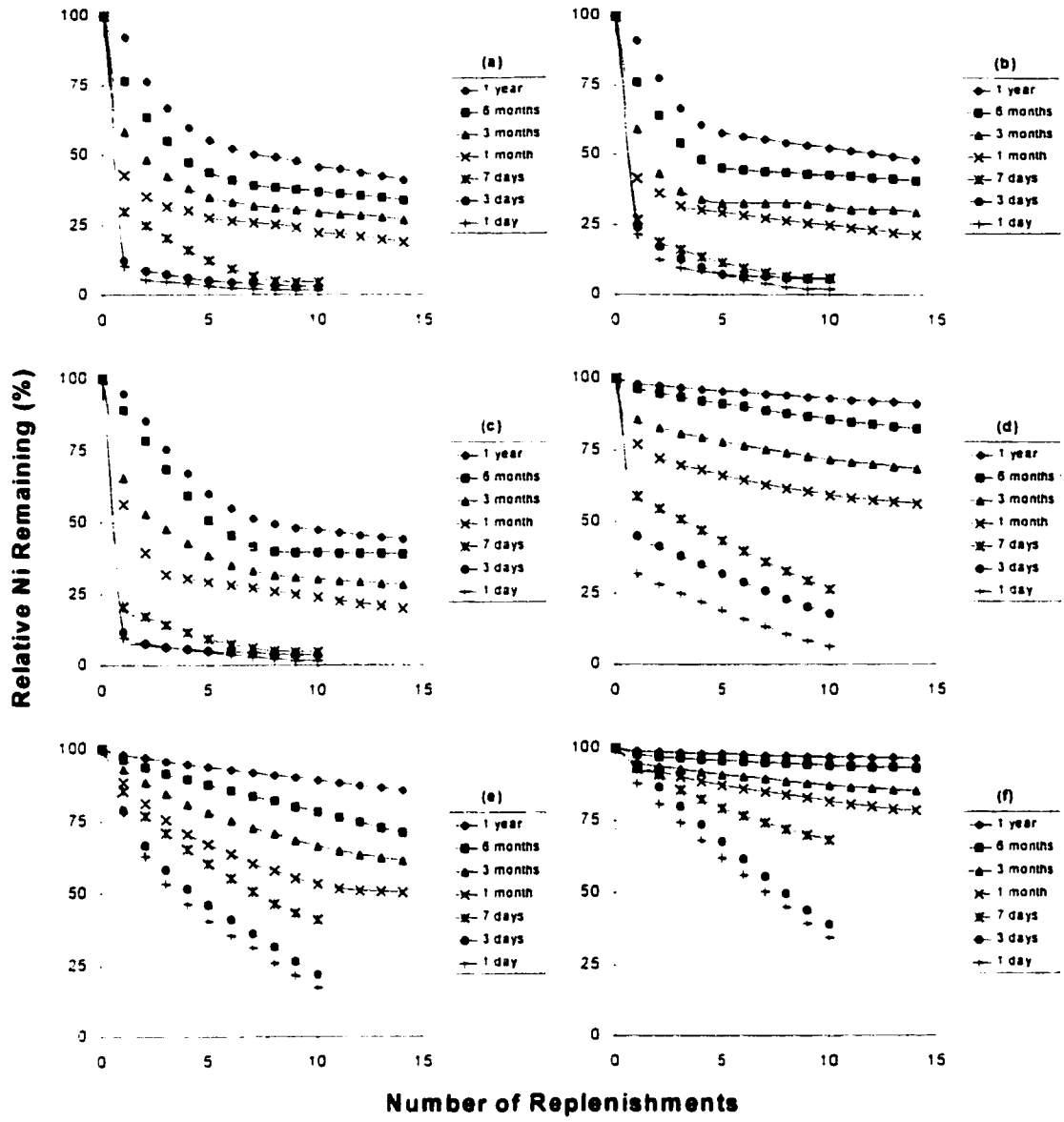

Figure 4.3. Macroscopic dissolution behavior of aged Ni precipitates on gibbsite showing the relative amount of Ni remaining on the surface following extraction with (a) 1 mM EDTA at pH 4.0, (b) 1 mM EDTA at pH 7.5, (c) 3 mM oxalate at pH 4.0, (d) 3 mM acetylacetone at pH 6.0, (e) HNO_3 at pH 4.0, and (f) HNO_3 at pH 6.0 plotted against the total number of replenishments. The stability of the Ni precipitates increases with aging time.

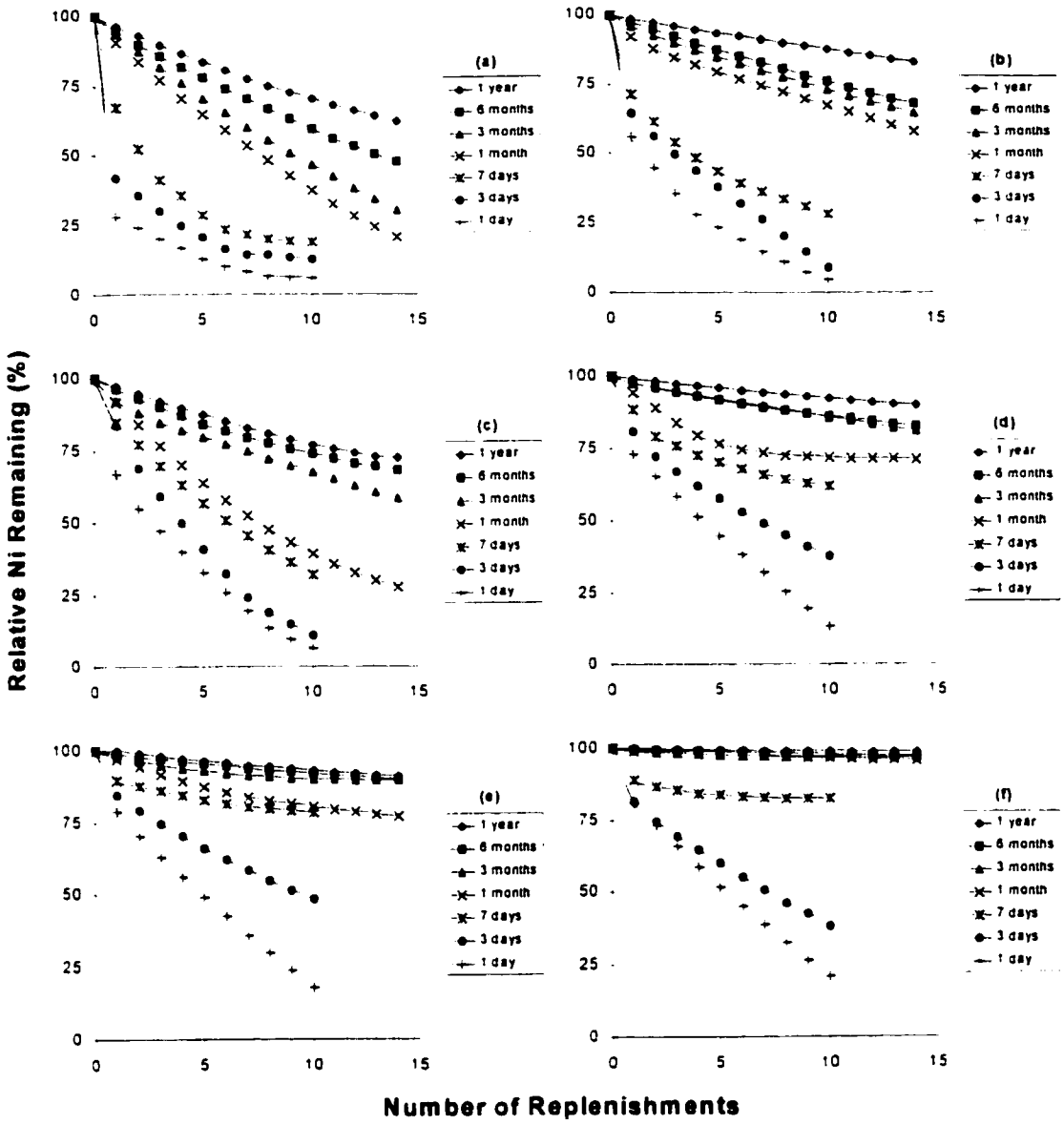

Figure 4.4. Macroscopic dissolution behavior of aged Ni precipitates on silica showing the relative amount of Ni remaining on the surface following extraction with (a) 1 mM EDTA at pH 4.0, (b) 1 mM EDTA at pH 7.5, (c) 3 mM oxalate at pH 4.0, (d) 3 mM acetylacetone at pH 6.0, (e) HNO_3 at pH 4.0, and (f) HNO_3 at pH 6.0 plotted against the total number of replenishments. The stability of the Ni precipitates increases with aging time.

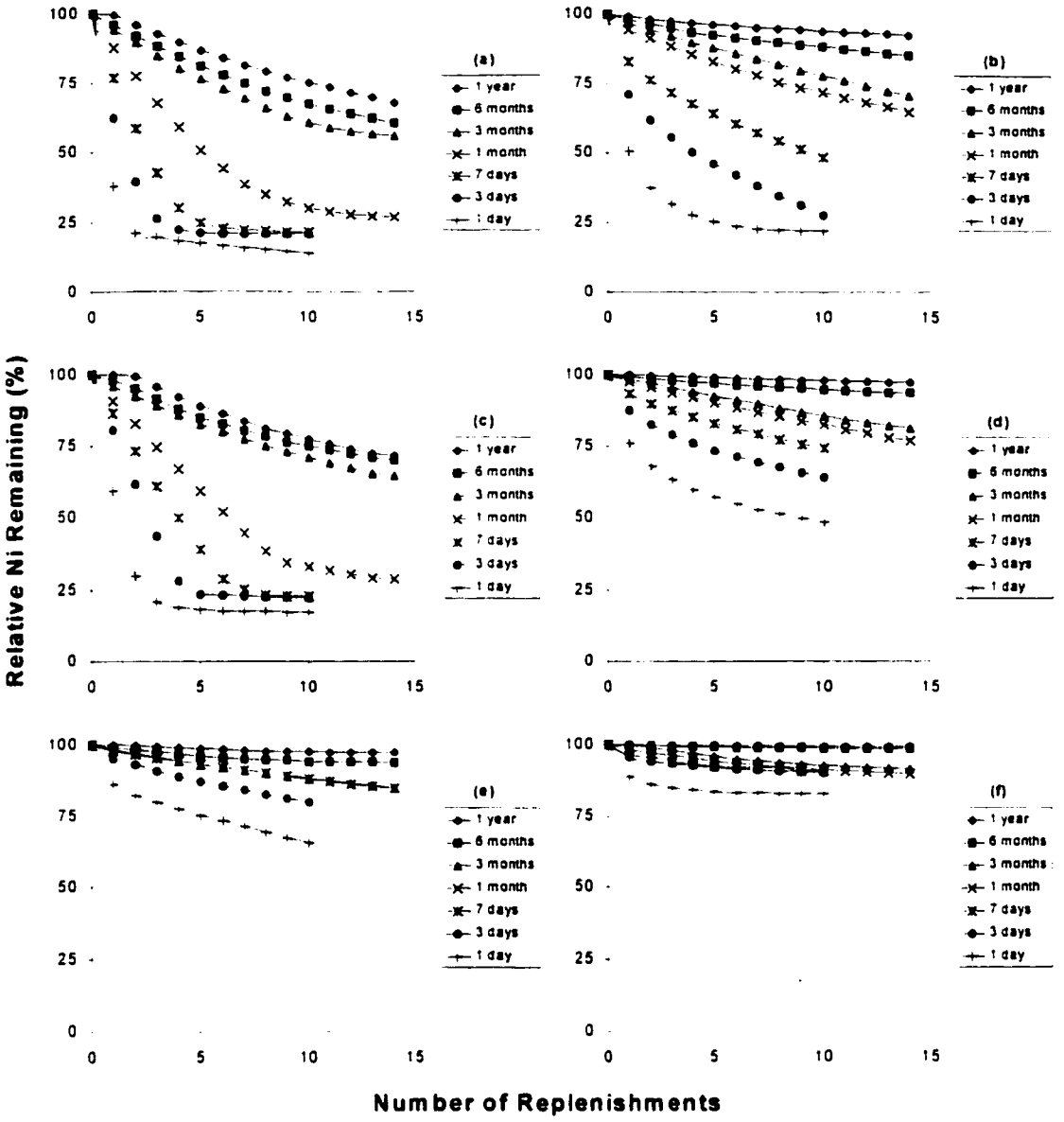

Figure 4.5. Macroscopic dissolution behavior of aged Ni precipitates on gibbsite/silica mixture showing the relative amount of Ni remaining on the mixture surface following extraction with (a) 1 mM EDTA at pH 4.0, (b) 1 mM EDTA at pH 7.5, (c) 3 mM oxalate at pH 4.0, (d) 3 mM acetylacetone at pH 6.0, (e) HNO_3 at pH 4.0, and (f) HNO_3 at pH 6.0 plotted against the total number of replenishments. The stability of the Ni precipitates increases with aging time.

Table 4.1. Relative Ni remaining (%) on one month aged samples after 14 dissolution replenishments.

Sorbent	EDTA (pH 4.0)	EDTA (pH 7.5)	Oxalate	Acetylacetone	HNO3 (pH 4.0)	HNO3 (pH 6.0)
Pyrophyllite	29	41	37	88	91	97
Talc	11	17	31	73	75	97
Gibbsite	19	21	20	56	50	78
Silica	21	58	28	71	77	96
Gibbsite/Silica	27	64	29	77	85	90

was observed for dissolution of Ni precipitates on talc, gibbsite, silica, and the gibbsite/silica mixture with the above dissolution agents as well. This ranking of the dissolution agents may be explained by the species' charge. For example, looking at EDTA (pH 7.5), acetylacetone (pH 6.0), and HNO_3 (pH 6.0) in Figures 4.1-4.5 parts b, d, and f, respectively, one sees that the most negatively charged dissolution agent, EDTA, was more effective in removing the positively charge Ni than the near neutral acetylacetone than the positively charged HNO_3.

While replenishment technique studies are convenient and simple to conduct, the biggest drawback of this method is the failure to remove reaction products that may inhibit further release/dissolution reactions. For comparison, a stirred-flow technique was employed (Figure 4.6) which is useful for desorption/dissolution studies since perfect mixing is effected and reaction products are constantly removed, an advantage over the replenishment and other batch methods, but also more cumbersome (Carski and Sparks, 1985; Bar-Tal et al., 1990). The stirred-flow studies

were conducted in a temperature controlled (25° C) glass-jacketed cylindrical cell (volume 8.5 mL) with the outlet attached to a removable lid and the inlet connected to the bottom of the reaction cell. A 0.22 μm membrane filter was secured to the top of the cell and held in place with the closure of the lid. The filter did not permit the solid fraction to leave the cell but allowed the dissolution agent to move out freely. The solid:solution ratio in the cell was 10 g/L as in the replenishment experiments and stirring within the cell effected complete mixing. The thermostatted dissolution agent was continuously pumped through the cell with the aid of a HPLC pump at a constant flow rate of 0.1 mL min^{-1}. The effluent solution was collected by a fraction collector and analyzed by ICP for Ni.

Only a few dissolution studies were conducted utilizing both the replenishment method and the stirred-flow technique. One such study was the examination of a one-month aged Ni/pyrophyllite sample using EDTA at pH 7.5 and HNO_3 at pH 4.0. For the EDTA dissolution system (Figure 4.6a) at the end of the 5 day study, 45 % of the nickel was removed via the replenishment method while 65 % of the nickel was displaced employing the stirred-flow technique. In the HNO_3 studies (Figure 4.6b), 4% and 25 % of the Ni was removed with the replenishment and stirred-flow techniques, respectively. While the amount of Ni removal is enhanced with the stirred-flow technique, the quantity of EDTA and HNO_3 applied per unit time for the same amount of sorbent is over 17 times greater than that used for the replenishment method. This indicates that although the stirred-flow technique is more effective in

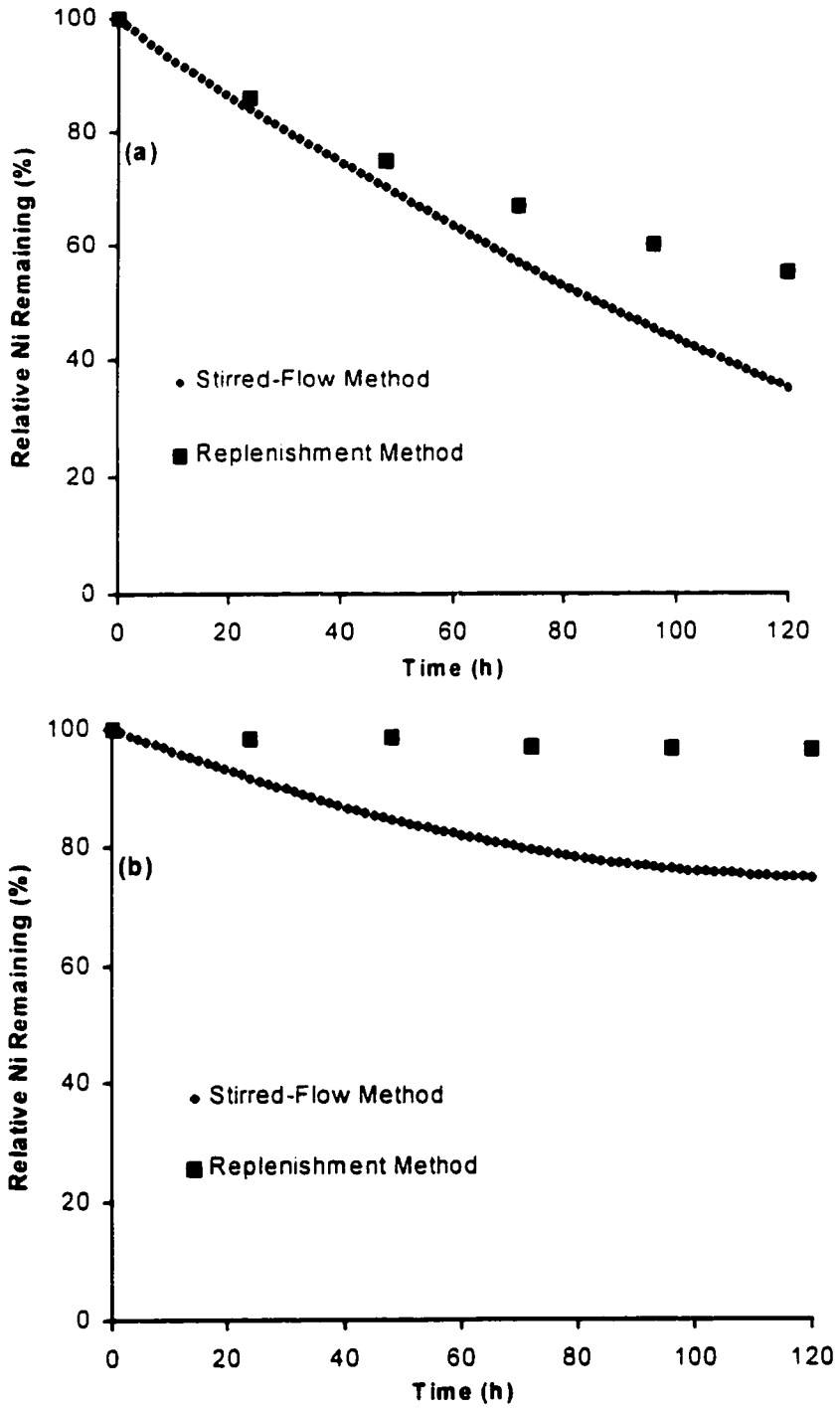

Figure 4.6. Dissolution of one-month aged Ni-Al LDH precipitates on pyrophyllite comparing replenishment and stirred-flow methods using (a) EDTA at pH 7.5 and (b) HNO_3 at pH 4.0.

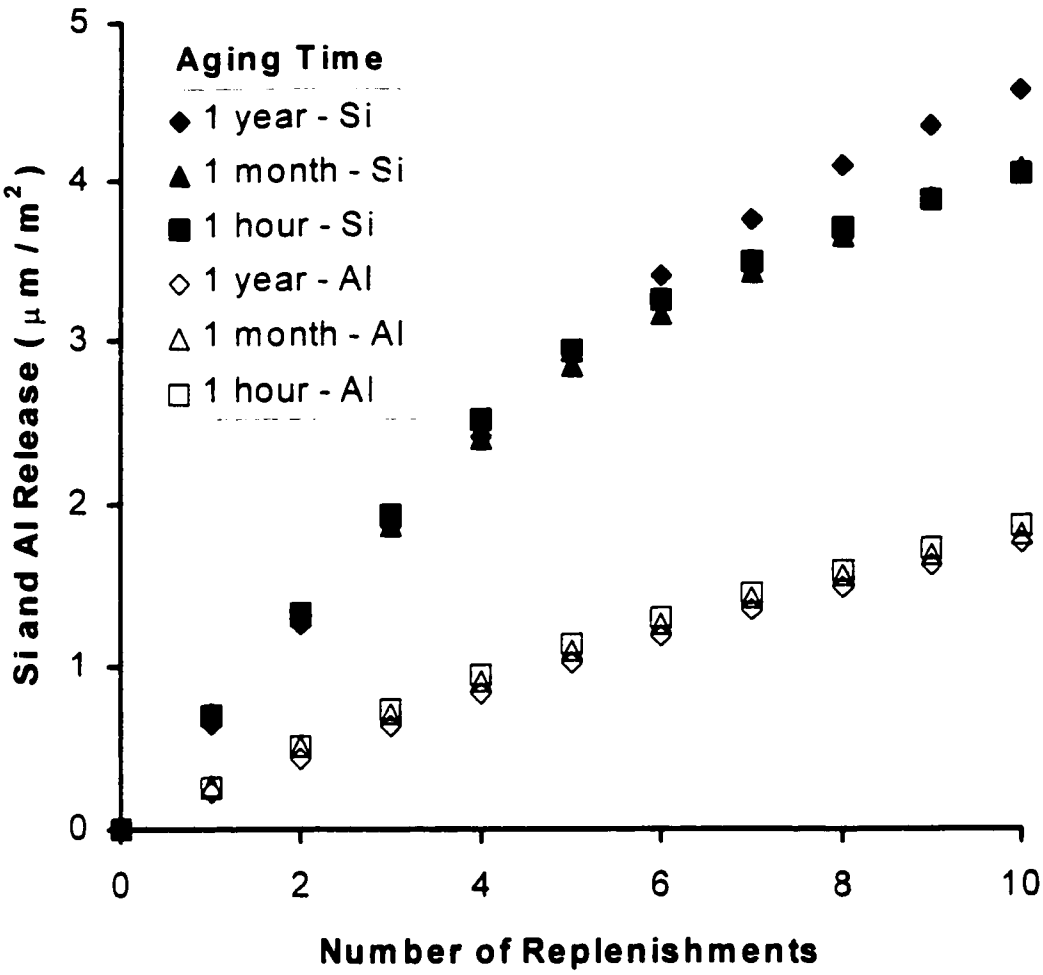

Figure 4.7. Release of Si and Al during dissolution from Ni-Al LDH precipitates on pyrophyllite aged for 1 hour, 1 month, and 1 year using EDTA at pH 7.5.

removing nickel from the surface, the technique would not be economically feasible in a remediation strategy due to the large volume of dissolution agent required.

An important point to consider during the replenishment dissolution experiments is the stability of the sorbent surface. In addition to analyzing for Ni in the dissolution studies, Si was also quantified. Si release during dissolution was comparable regardless of the aging time of the precipitates. Figure 4.7 shows total Si dissolution with EDTA (pH 7.5) from Ni-pyrophyllite samples for sorption aging times of 1 day, 1 month and 1 year. What is believed to be transpiring during the dissolution process is a congruent dissolving of the Ni precipitate in addition to the sorbent surface. This makes it difficult to distinguish Si release from the interlayer of the Ni precipitates and the surface except at early reaction times when very little Si has exchanged into the interlayer.

4.4.2 XAFS Analysis of Dissolution Samples

XAFS spectra were collected for pyrophyllite and talc reacted with Ni for one month, and subsequently subjected to dissolution by EDTA (pH 7.5) for 1 to 7 days (Figure 4.8) and by HNO_3 (pH 4.0) for 1 to 14 days (Figure 4.9). The k^3-weighed χ functions of pyrophyllite (Figures 4.8a and 4.9a) show a beat pattern at 8 $Å^{-1}$

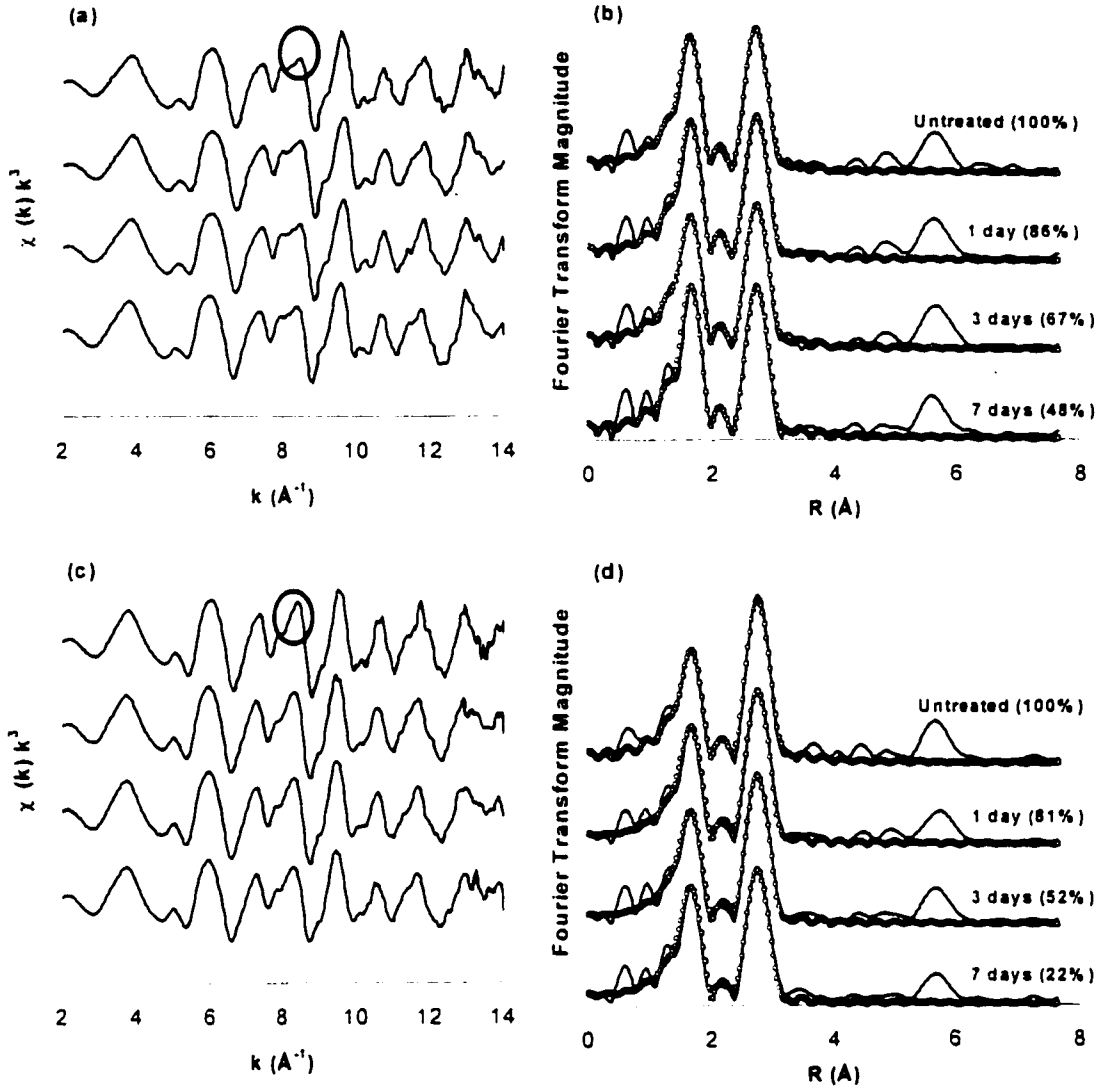

Figure 4.8. Ni-K_α XAFS spectra of pyrophyllite (a and b) and talc (c and d) aged with Ni for one month and subsequently treated with EDTA (pH 7.5) for 1, 3, and 7 days. The k^3 weighted χ functions are shown on the left side, the measured (solid lines) and fitted (dotted lines) radial structure functions on the right side (uncorrected for phase shifts). The circle shows a key identification for Ni-Al LDH versus α-Ni hydroxide.

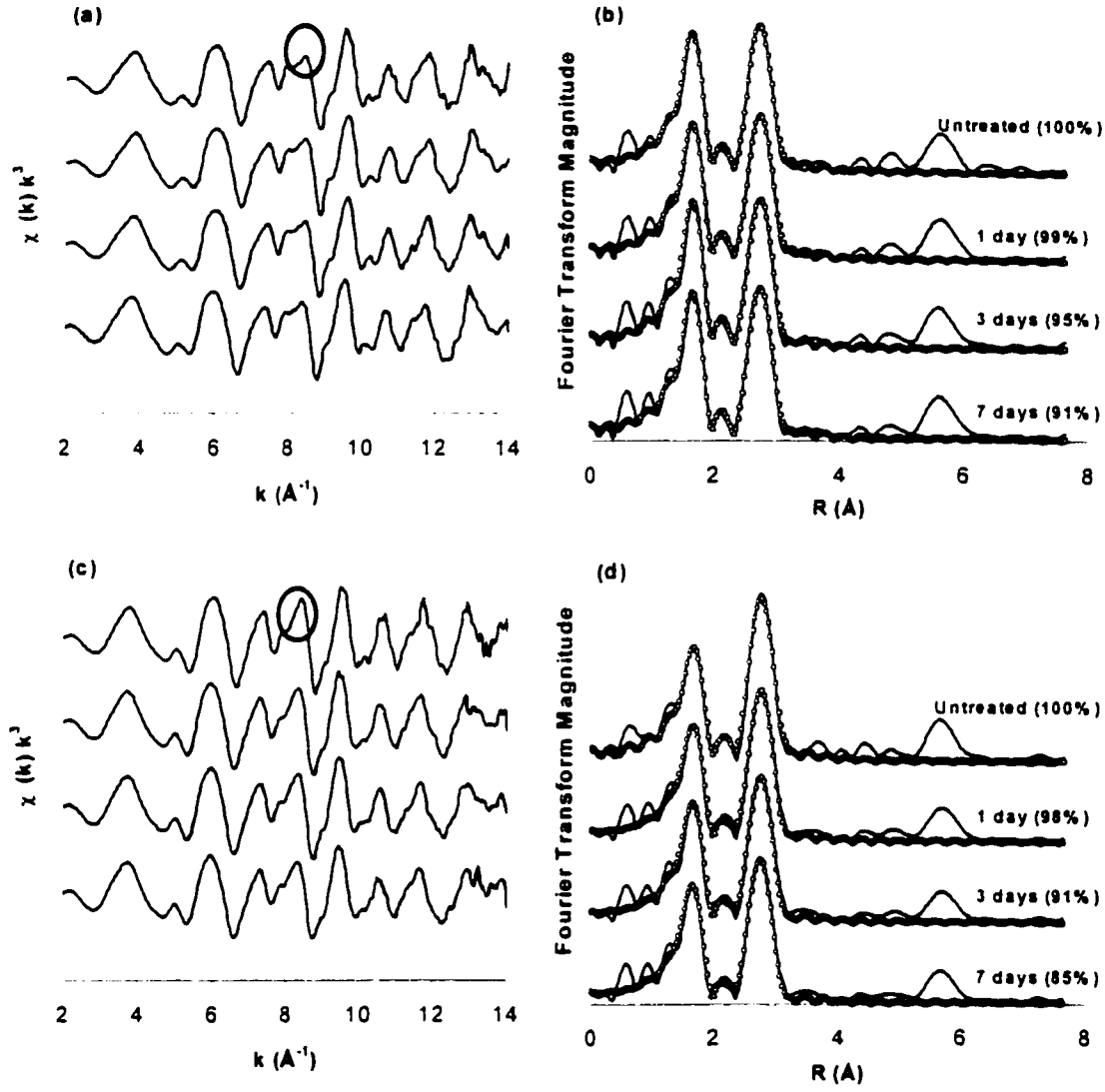

Figure 4.9. Ni-K_α XAFS spectra of pyrophyllite (a and b) and talc (c and d) aged with Ni for one month and subsequently treated with HNO_3 (pH 4.0) for 1, 7, and 14 days. The k^3 weighted χ functions are shown on the left side, the measured (solid lines) and fitted (dotted lines) radial structure functions on the right side (uncorrected for phase shifts). The circle shows a key identification for Ni-Al LDH versus α-Ni hydroxide.

Table 4.2. Structural parameters derived from XAFS analysis for dissolution of nickel precipitates aged for one month on pyrophyllite and talc employing EDTA (pH 7.5) and HNO_3 (pH 4.0).

Sample & Dissolution Time		Ni - O			Ni - Ni			Ni - Al		
	ΔE_0 (eV)	R (Å)[a]	N[b]	σ^2 (Å^2)[c]	R (Å)[a]	N[b]	σ^2 (Å^2)[d]	R (Å)[a]	N[b]	σ^2 (Å^2)[d]
Pyrophyllite										
EDTA										
Untreated	4.7	2.05	6.0	0.003	3.06	4.9	0.003	3.11	1.4	0.003
1 day	3.8	2.05	6.0	0.003	3.06	5.2	0.004	3.12	1.7	0.004
3 days	4.4	2.05	6.0	0.003	3.06	4.9	0.003	3.12	1.2	0.003
7 days	3.9	2.05	6.0	0.002	3.06	5.1	0.003	3.11	1.6	0.003
HNO_3										
Untreated	4.7	2.05	6.0	0.003	3.06	4.9	0.003	3.11	1.4	0.003
1 day	4.0	2.05	6.0	0.003	3.06	5.1	0.003	3.11	1.5	0.003
7 days	4.5	2.05	6.0	0.003	3.06	5.1	0.004	3.10	1.6	0.004
14 days	3.9	2.05	6.0	0.003	3.06	5.2	0.004	3.11	1.4	0.004
Talc										
EDTA										
Untreated	3.6	2.05	6.0	0.003	3.08	6.0	0.003			
1 day	2.9	2.05	6.0	0.003	3.08	5.9	0.004			
3 days	3.0	2.05	6.0	0.004	3.08	6.0	0.005			
7 days	2.7	2.05	6.0	0.003	3.08	5.7	0.005			
HNO_3										
Untreated	3.6	2.05	6.0	0.003	3.08	6.0	0.003			
1 day	2.6	2.05	6.0	0.004	3.08	6.0	0.004			
7days	3.4	2.05	6.0	0.004	3.08	5.9	0.004			
14 days	3.4	2.05	6.0	0.004	3.08	6.1	0.004			

[a] Interatomic Distance; [b] Coordination Number; [c] Debye-Waller factor;
[d] Debye-Waller factors for pyrophyllite (Ni-Ni and Ni-Al) were constrained to be equal

which is characteristic for Ni-Al LDH (Scheinost and Sparks, 1999). This pattern remains unchanged after all dissolution steps, indicating that the initial phase, the dissolved phase and the remaining phase consist predominantly of Ni-Al LDH with about the same Ni/Al ratio. This result is further confirmed by XAFS fits to the radial structure functions (RSFs) (Figures 4.8c and 4.9c). The fit data for pyrophyllite show that Ni is surrounded by 6 O atoms at an average distance of 2.05 Å, by 5 Ni atoms at 3.06 Å, and by 1-2 Al atoms at 3.11 Å (Table 4.2). These local structural data are consistent with those of Ni-Al LDH (Scheidegger et al., 1998; Scheinost and Sparks, 1999), and do not indicate any change with increasing dissolution. The fit data for Ni-reacted talc (Figures 4.8d and 4.9d) show that Ni is surrounded by 6 Ni atoms at 3.08 Å (Table 4.2), which is consistent with α-Ni hydroxide (Pandya et al., 1990; Scheinost and Sparks, 1999). The lack of the characteristic beat pattern at 8 $Å^{-1}$ in the corresponding χ functions confirms the conclusions from the fit (Figure 4.8c and 4.9c). Again, the initial precipitate, the dissolved phase, and the remaining precipitate essentially have an identical local structure.

4.4.3 DRS Analysis of Dissolution Samples

The crystal field splitting of Ni^{2+} in an octahedral O cage is very sensitive to small changes in Ni-O bond distances (Burns, 1993). Therefore, DRS can be used to

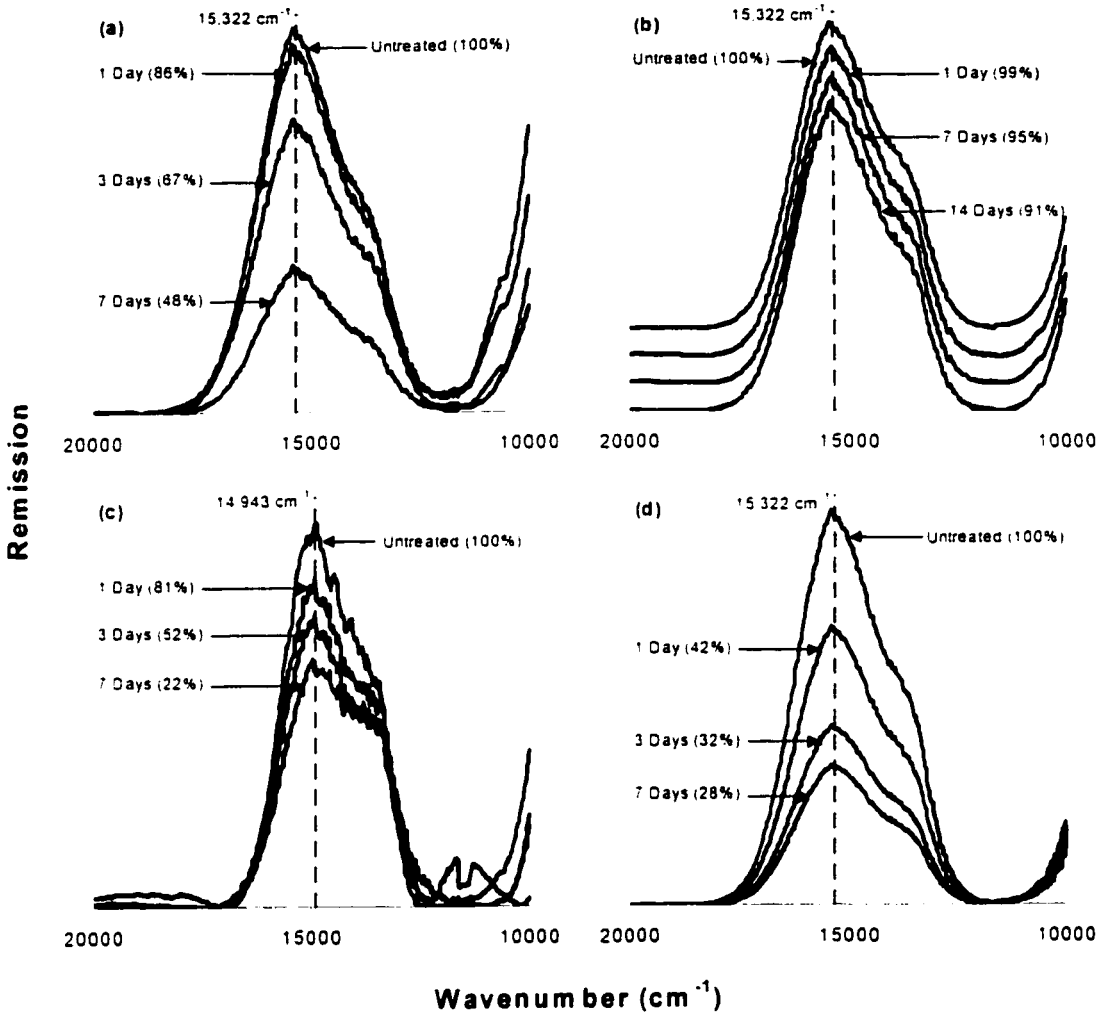

Figure 4.10. The DRS v2 bands for the Ni surface precipitates on (a) pyrophyllite (EDTA pH 7.5), (b) pyrophyllite (HNO_3 pH 4.0), (c) talc (EDTA pH 7.5), and (d) gibbsite (EDTA pH 7.5) aged for one month ("untreated") and subsequently extracted with EDTA for 1, 3, and 7 days or with HNO_3 for 1, 7, and 14 days. The relative amount of Ni remaining on the clay mineral is also given.

distinguish between Ni-Al LDH and α-Ni hydroxide (Scheinost et al., 1999). Consistent with the XAFS results shown before, the ν2 band position of 15,300 cm^{-1} for pyrophyllite (Figures 4.10a and 4.10b) and gibbsite (Figure 4.10d) indicates Ni-Al LDH, and the ν2 band position of 14,900 cm^{-1} for talc (Figure 4.10c) indicates α-Ni hydroxide. In Figures 4.10a and 4.10b, one can compare the difference between EDTA (pH 7.5) and HNO_3 (pH 4.0) promoted dissolution of Ni-Al LDH precipitates on pyrophyllite. The spectra in Figure 4.10b are offset since the curves are nearly identical with only 9 % of the sorbed Ni removed after 14 replenishments with HNO_3. Figures 4.10c and 4.10d show the dissolution of α-$Ni(OH)_2$ on talc and Ni-Al LDH on gibbsite employing EDTA at pH 7.5. In all cases, band positions do not change with increasing dissolution indicating no change in the chemical composition of the precipitate. Because the absorption coefficient of adsorbed mononuclear Ni^{2+} complexes is 2 orders of magnitude lower than that of Ni^{2+} in a three-dimensional, polynuclear structure, band heights are indicative of the amount of Ni present in a precipitate phase (Scheinost et al., 1999). Therefore, the decrease of band heights with increasing Ni removal (Figure 4.10) is clear evidence that the removed Ni is predominantly due to dissolution of the precipitate phases and not due to desorption of adsorbed Ni.

4.4.4 HRTGA Investigation of Dissolution Samples

High-resolution thermogravimetric analysis (HRTGA) was successfully employed to show that Ni-Al LDH (Figure 2.10) and α-$Ni(OH)_2$ precipitates (Figure 2.11) on pyrophyllite and the gibbsite/silica mixture transform into Ni-Al and Ni-phyllosilicate precursors within one year at ambient temperature and pressure, respectively (Ford et al., 1999; Scheckel and Sparks, 2000a). This transformation progresses by silicate-for-nitrate exchange in the interlayer, and the subsequent polymerization of single silicate units which may then become connected with the octahedral hydroxide layers (Depège et al., 1996). This transformation is slightly detectable by DRS and EXFAS (Ford et al., 1999; Scheinost et al., 1999; Scheinost and Sparks, 1999; Scheckel and Sparks, 2000a). Therefore, we employed HRTGA to investigate if a similar transformation has occurred during the one-month aging time on pyrophyllite and the gibbsite/silica mixture, and whether detectable changes of the interlayer composition occur during dissolution. The derivatives of the weight loss curves for pyrophyllite (Figure 4.11) show a maximum at about 280 °C which is due to dehydroxylation of the octahedral layer and the complete collapse of the LDH structure (Bellotto et al., 1996; Ford et al., 1999). However, no weight loss at 220 °C is detectable which would occur due to water and nitrate expulsion (Bellotto et al., 1996; Ford et al., 1999). This indicates that nitrate has been exchanged by silicate in

the Ni-Al LDH interlayer. No change occurs with sequential dissolution steps. HRTGA was also employed to examine the dissolution of the Ni precipitates aged for 1 month on the gibbsite/silica mixture utilizing HNO_3 at pH 4.0 (Figure 4.12). The curve for the mixture unreacted with Ni was subtracted from these curves in order to view only weight loss events for the Ni precipitates. The untreated curve represents a 1 month aged Ni-mixture sample prior to dissolution. The other curves are the result of dissolution with nitric acid for 1, 7, and 14 days or replenishment treatments. The amount of Ni remaining on the mixture surface is noted in the figure legend and as one can see only 15 % of the Ni is released from the surface over the reaction period. The size of each peak is indicative of the amount of each particular phase present on the surface. Decreases in the size of the peaks associated with α-$Ni(OH)_2$ are more pronounced than those in conjunction with the Si-exchanged α-$Ni(OH)_2$ precipitates and very little change in the peaks for Ni phyllosilicate. These results are in line with recent work by Scheckel et al. (2000) that examined dissolution of synthetic α-$Ni(OH)_2$ and Si-exchanged α-$Ni(OH)_2$ precipitates (Figure 4.15) in which the silicated phase was more resistant to dissolution. One could easily hypothesize that the Ni phyllosilicate is even more resistant to dissolution than α-$Ni(OH)_2$ and Si-exchanged α-$Ni(OH)_2$. Therefore, not only the local structure within the octahedral Ni hydroxide

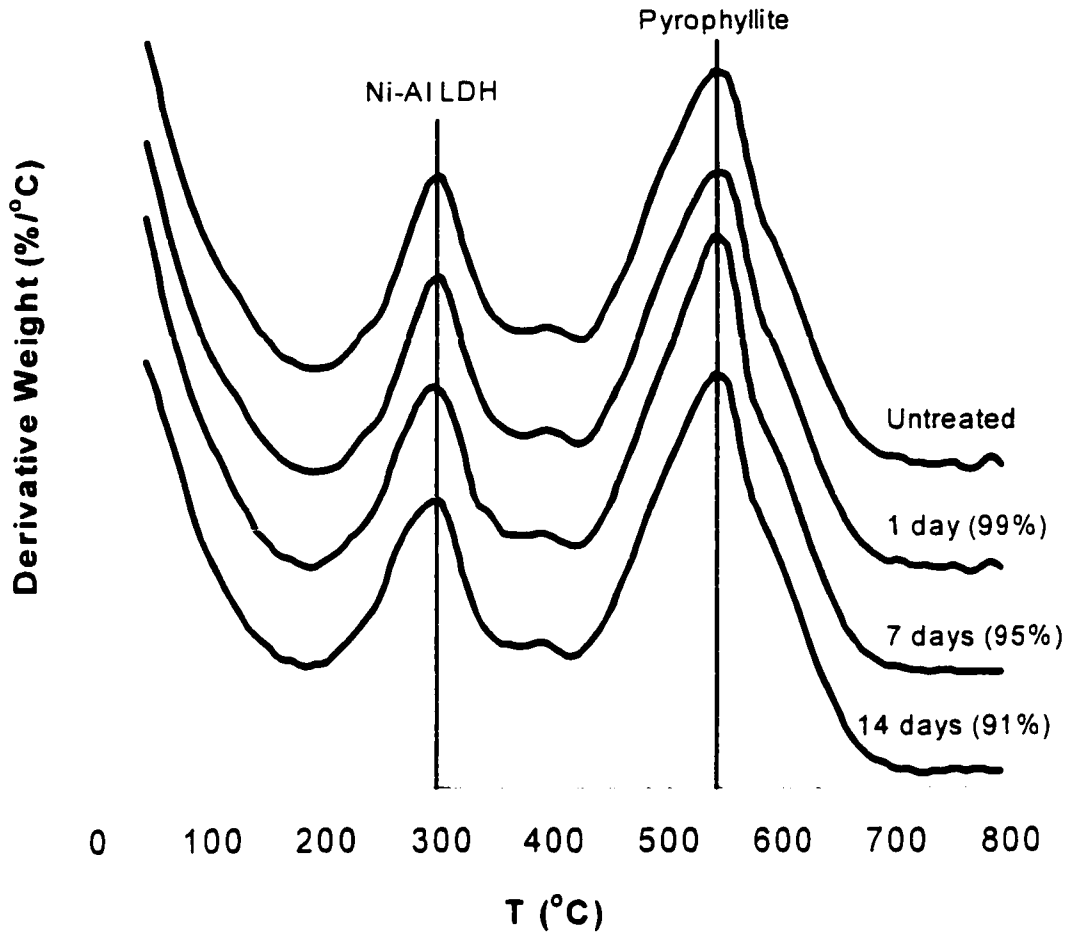

Figure 4.11. High-resolution thermogravimetric analysis (HRTGA) of the Ni surface precipitate on pyrophyllite aged for one month ("untreated") following extraction with HNO_3 (pH 4) for 1, 7, and 14 days. The weight loss event at about 280 °C is indicative of Ni-Al LDH (Ford et al., 1999), while the weight loss between 450 and 600 °C is due to pyrophyllite.

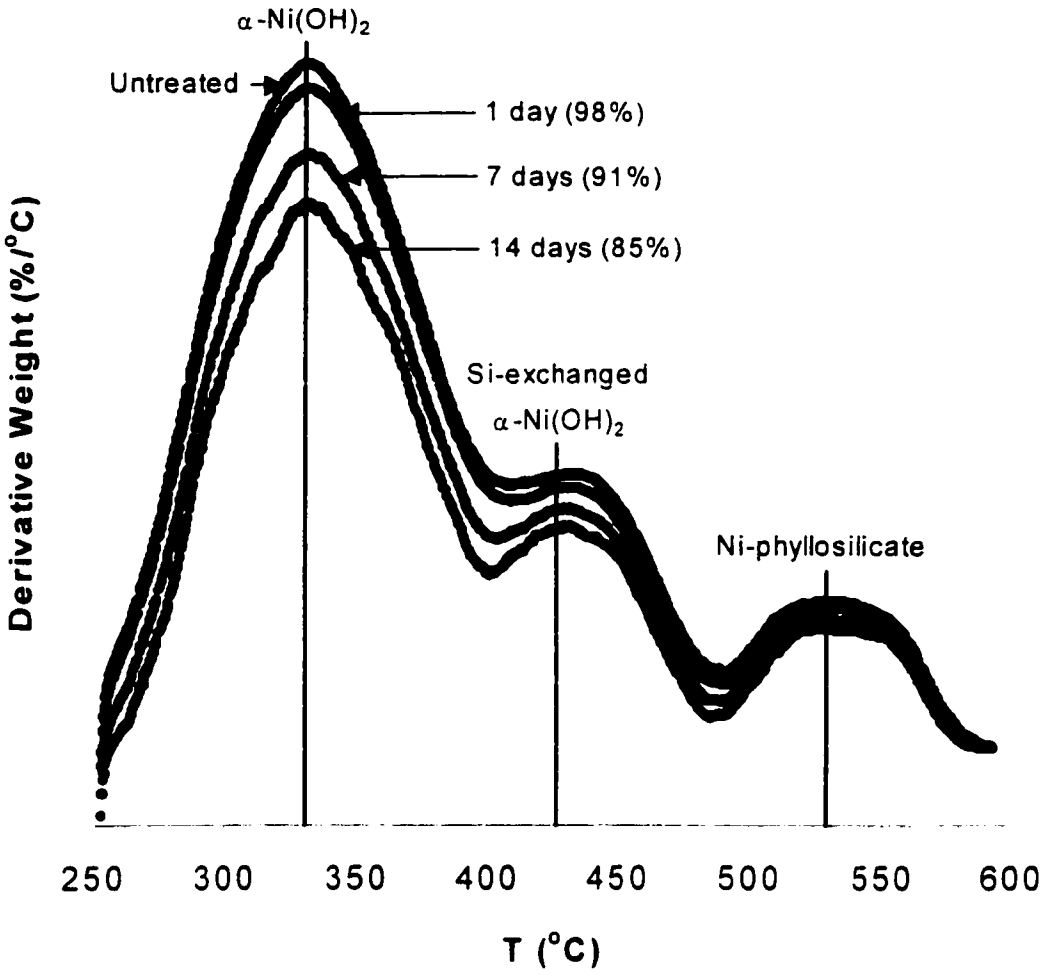

Figure 4.12. Background subtracted HRTGA of Ni surface precipitates on the gibbsite/amorphous silica mixture aged for one month ("untreated") and following extraction with HNO_3 (pH 4) for 1, 7, and 14 days. The weight loss events at about 332, 438, and 533 °C are indicative of α-$Ni(OH)_2$, Si-exchanged α-$Ni(OH)_2$, and Ni phyllosilicate.

layer remains constant with dissolution (XAFS and DRS), but also the interlayer composition.

4.4.5 AFM Analysis of Dissolution Samples

Figure 4.13 shows the ligand-promoted dissolution of 14 day aged Ni-Al LDH precipitates on pyrophyllite after 0 hours (untreated), 24 hours, and 240 hours of treatment with 1 mM EDTA at pH 7.5. The height bar in Figure 4.13 illustrates that lighter colored features on the images are more pronounced on the surface while darker shades indicate smaller features. An arrow marks a particular precipitate peak in the untreated image and follows this feature in the 24 hour and 240 hour images. One can see that as dissolution progresses, the feature marked by the arrow begins to diminish from a bright color to a darker hue indicating that the height of the precipitate is decreasing. This demonstrates that the precipitates are readily dissolving in the presence of EDTA.

Proton-promoted dissolution of 14 day aged Ni precipitates on pyrophyllite after 0 hours (untreated), 24 hours, and 240 hours of treatment with HNO_3 at pH 4.0 is presented in Figure 4.14. Again, an arrow marks a particular precipitate peak in the untreated image and follows this feature in the 24 hour and 240 hour images.

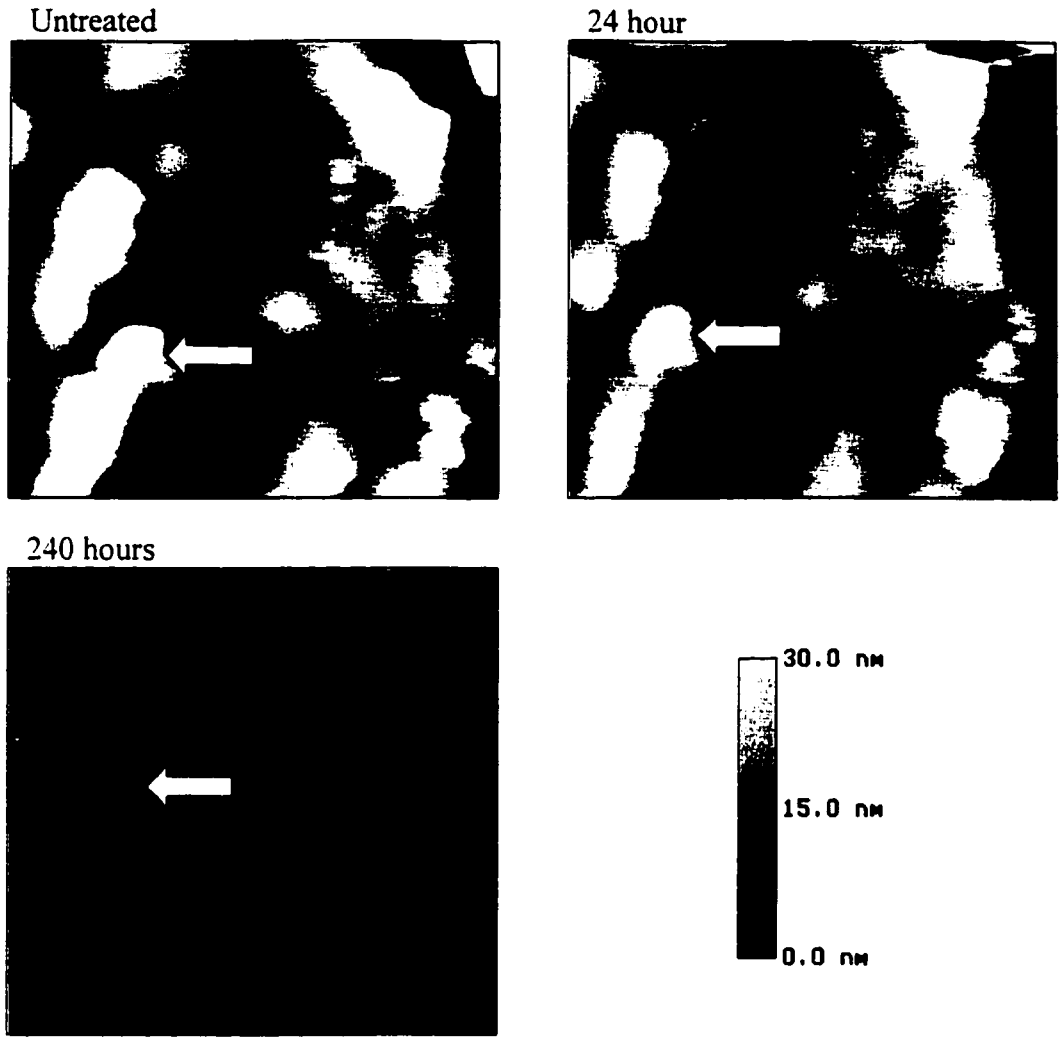

Figure 4.13. Atomic force micrographs (AFM) of pyrophyllite unreacted and reacted with 1 mM EDTA (pH 7.5) for times of 24 and 240 hours. The scan size was 1 μm by 1 μm with a maximum Z-range of 60 nm. The scans were collected in Fluid TappingMode™ AFM.

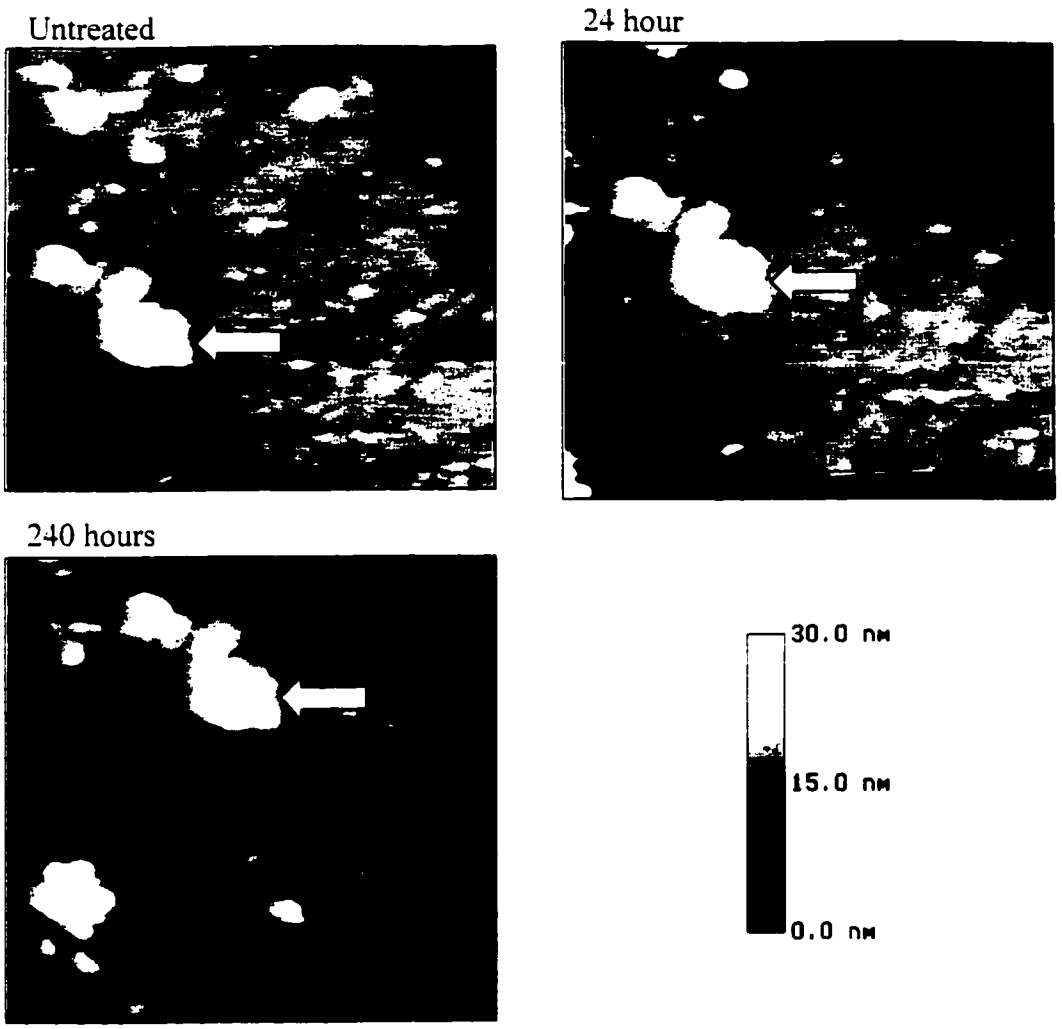

Figure 4.14. Atomic force micrographs (AFM) of pyrophyllite unreacted and reacted with HNO_3 (pH 4.0) for times of 24 and 240 hours. The scan size was 1 μm by 1 μm with a maximum Z-range of 60 nm. The scans were collected in Fluid TappingMode™ AFM.

However, in contrast to dissolution with EDTA in Figure 4.13, the feature marked by the arrow remains relatively unchanged during dissolution with HNO_3 through 240 hours. This is in line with macroscopic and spectroscopic dissolution results which show that nitric acid removes very little Ni from the precipitates.

4.5 Discussion

Former DRS work has shown that detectable amounts of Ni precipitates formed within 5 minutes on pyrophyllite, 7 hours on talc, 24 hours on gibbsite, 24 hours on silica, and 1 hour on gibbsite/silica mixture under similar experimental conditions (Scheinost et al., 1999; Scheckel and Sparks, 2000a). For aging times up to one year, the precipitate phase was a Ni-Al LDH on pyrophyllite and an α-Ni hydroxide on talc, silica, and gibbsite/silica mixture (Scheidegger and Sparks, 1996; Scheinost et al., 1999, Scheckel and Sparks, 2000a). For gibbsite, the initial precipitate phase after 24 hours was predominantly a α-Ni hydroxide, which transformed into a Ni-Al LDH with aging (Scheinost et al., 1999). The DRS and XAFS results on sorbed samples (Chapter 2) are fully consistent with these former results. In all systems, some of the Ni sorbed onto the clay mineral surfaces may have been present as adsorbed Ni. However, this adsorbed Ni constitutes a small fraction of the overall Ni in the system after one-day reaction time (Scheidegger et al., 1997;

Scheidegger et al., 1998; Scheinost et al., 1999). Therefore, removal of Ni from the clay minerals aged for at least one day is prevalently due to dissolution of the two different precipitate phases. This is further substantiated by the decrease of the ν2 band height with sequential dissolution steps (Figure 4.10).

As can be derived from Figures 4.1 – 4.5, the Ni-Al LDH surface precipitates on pyrophyllite are more resistant to dissolution than the α-Ni hydroxide phases on the mixture, talc, and silica, respectively, and the Ni-Al LDH phase on gibbsite. Former work has suggested that Al-containing Ni or Co hydroxides are more resistant to dissolution than the pure metal hydroxides (Scheidegger and Sparks, 1996; Thompson et al., 1999b). However, only part of the observed stability sequence can be explained by this difference between Ni-Al LDH and α-Ni hydroxide. Therefore, the stability of the surface precipitates is determined by more factors than the Al-for-Ni substitution in the hydroxide layers alone. The work by Ford et al. (1999) showed that the stability of a Ni-Al LDH surface precipitate on pyrophyllite was drastically enhanced by exchange of interlayer nitrate by polymerizing silicate (Figure 2.10). The source of the silicate was the dissolution of the pyrophyllite surface during sorption of Ni. Hence, the higher stability of the pyrophyllite Ni-Al LDH may be explained by silication, and the smaller stability of gibbsite Ni-Al LDH by the lack of structural Si. The lack of the 220 °C weight loss event in the HRTGA weight loss curves of Ni-

pyrophyllite indeed supports the silication hypothesis (Figure 4.11). Since the Ni hydroxide layers of α-Ni hydroxide forming under our experimental conditions should also be separated by water and nitrate (Génin et al., 1991; Scheinost and Sparks, 1999), a similar silicate-for-nitrate exchange may occur with the surface precipitate on talc, explaining its greater stability compared to the gibbsite Ni-Al LDH (Figures 4.2 and 4.3).

Table 4.3 lists the transformation sequence of the Ni precipitates associated with each sorbent over initial, short-term, and long-term reaction aging times. The initial period refers to the reaction time in which the primary surface precipitate product formed on the sorbent as distinguished by XAFS, DRS and/or HRTGA. Initial product formation for pyrophyllite, talc, gibbsite, silica, and the mixture were within 5 minutes, 1 hour, 24 hours, 12 hours, and 1 hour, respectively (Scheidegger et al., 1996; Scheidegger et al., 1997; Scheidegger and Sparks, 1996; Scheidegger et al., 1998; Scheinost et al. 1999; Scheinost and Sparks, 1999; Scheckel and Sparks, 2000a). The short-term reaction interval represents reaction times up to about 3 months and the long-term transition period denotes greater than 3 months aging times. The exact times for the short-term and long-term transitions are not fully known since samples were only collected at 1, 3, 6 and 12 months aging periods. Al-for-Ni substitution in the octahedral sheet and/or Si-for-nitrate substitution in the interlayer in which the Al

Table 4.3. Solid-state transformation products of Ni precipitates with aging time.

Sorbent	Precipitate Transition with Time		
	Initial	Short-Term	Long-Term
Pyrophyllite	Ni-Al LDH →	Si-Exchanged Ni-Al LDH →	Ni-Al Phyllosilicate
Talc	α-$Ni(OH)_2$ →	Si-Exchanged α-$Ni(OH)_2$ →	Ni Phyllosilicate
Gibbsite	α-$Ni(OH)_2$ →	Ni-Al LDH →	Ni-Al LDH
Silica	α-$Ni(OH)_2$ →	Si-Exchanged α-$Ni(OH)_2$ →	Ni Phyllosilicate
Gibbsite/Silica Mixture	α-$Ni(OH)_2$ →	Si-Exchanged α-$Ni(OH)_2$ →	Ni Phyllosilicate

and Si are derived from the sorbent, if present, influence the transformations (Ford et al., 1999; Scheckel et al., 2000).

To further substantiate the influence of interlayer silication on the dissolution stability of Ni-Al LDH and α-Ni hydroxide, we investigated the dissolution kinetics of reference compounds where the interlayer composition was verified by FTIR spectroscopy (Figure 4.15). Using HNO_3 at pH 4.0, α-Ni hydroxide dissolved more rapidly than Ni-Al LDH, in line with the results by Scheidegger et al. (1996) and Thompson et al. (1999b). However, Si-exchange of both layered hydroxide phases drastically increased their stability. Note that the Si-exchanged α-Ni hydroxide is even more stable than the original Ni-Al LDH. The observed ranking of the reference

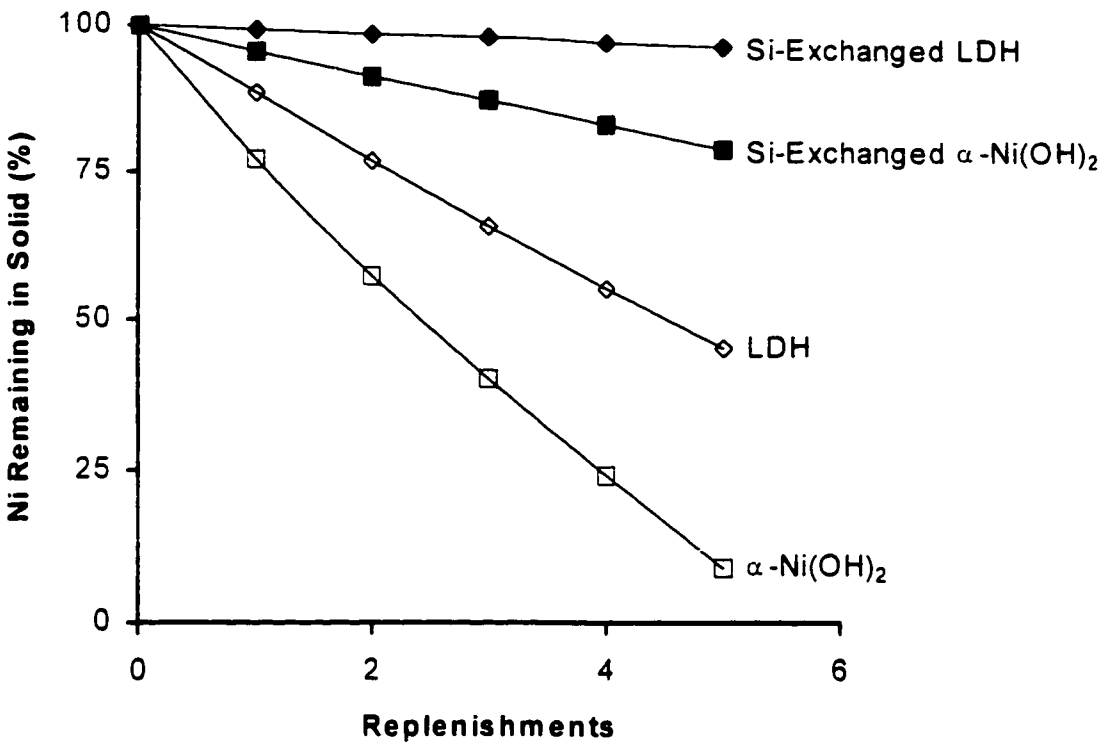

Figure 4.15. Ni release by HNO_3 at pH 4.0 from homogeneous synthetic Ni-Al LDH and α-Ni hydroxide, both with either predominantly nitrate or silicate in the interlayer.

compound stabilities strongly supports the contention that the lower stability of Ni-gibbsite is due to nitrate Ni-Al LDH, while both the α-Ni hydroxide on talc and the Ni-Al LDH on pyrophyllite have silicated interlayers. Therefore, the observed ranking of surface precipitate stabilities (pyrophyllite > mixture > talc > silica > gibbsite) can be explained by a combination of Al-for-Ni substitution within the hydroxide layers and silicate-for-nitrate substitution in the interlayers.

Consequently, the increasing stability of the surface precipitates on pyrophyllite, talc, silica, and mixture with time (Figures 4.1, 4.2, 4.4, and 4.5) can be explained by the silicate-for-nitrate exchange within the first days, and the subsequent silicate polymerization and partial grafting onto the hydroxide layers, in line with the results of Depège et al. (1996) and Ford et al. (1999). However, the LDH phase on gibbsite shows a substantial stabilization against dissolution with aging, too (Figure 4.3). Thus, another factor besides silication must be responsible for this aging effect. This factor could be crystal growth due to Ostwald ripening which could also lead to decrease of dissolution kinetics (Sutheimer et al., 1999). Furthermore, it cannot be excluded that crystal growth may also be responsible for a substantial part of the aging of surface precipitates on pyrophyllite, talc, silica, and the mixture. Further studies are currently underway employing high-resolution transmission electron microscopy (HRTEM) to quantify a possible crystal growth of the surface precipitates with time.

Three techniques, XAFS, DRS and HRTGA, were employed to monitor possible changes in the structure of the surface precipitate of 1-month aged Ni pyrophyllite during dissolution (Figures. 4.8 – 4.12). As no change was observed one could conclude that the precipitate dissolution behavior was analogous to the dissolution of a single phase. That is, the studies did not find evidence that the surface precipitate on pyrophyllite consists of a population of crystals of different composition or structure, where more labile structures would dissolve first and more stable structures would remain.

4.6 Conclusions

In this study, an array of analytical techniques was applied to examine the dissolution of Ni surface precipitates formed on pyrophyllite, talc, gibbsite, silica, and the gibbsite/silica mixture. The macroscopic dissolution studies demonstrated increased stability in Ni surface precipitates with aging. The increase in stability with residence time was attributed to three mechanisms: (1) Al-for-Ni substitution in the octahedral sheets of the brucite-like hydroxide layers, (2) Si-for-nitrate exchange in the interlayers of the precipitates, and (3) Ostwald ripening (size increase) of the precipitate phases. It appeared that the second factor, Si-for-nitrate exchange in the

interlayers, contributed largely to the increase in stability. The Ni-Al LDH precipitates on pyrophyllite, which possessed all three aging factors, resulted in the most stable complexes. However, Ni-Al LDH on gibbsite, which could not undergo Si-for-nitrate exchange in the interlayers, were the least stable precipitates. The α-$Ni(OH)_2$ precipitates on a gibbsite/silica mixture, amorphous silica, and talc fell between pyrophyllite and gibbsite in regards to stability and were probably a result of the degree of interlayer silication.

The ubiquity of metastable Al- and Si-containing minerals in soils and sediments makes the formation of Ni-Al LDH and its transformation into a Ni-Al phyllosilicate precursor at circumneutral and basic pH very likely. The formation of a Ni-Al LDH precipitate has been confirmed after reacting soil clay fractions and a whole soil with Ni at pH > 6.8 (Roberts et al., 1999). The formation of Ni surface precipitates, and the effect of aging on these precipitates, may drastically reduce the ecotoxicity of Ni in soils and sediments.

Chapter 5

CONCLUSIONS

5.1 Summary of Research

The research presented in this dissertation dealt with the sorption and desorption mechanisms of Ni surface precipitates on pyrophyllite, talc, gibbsite, amorphous silica, and a gibbsite/silica mixture. To predict the reaction behavior of metal contaminants, such as Ni, in the environment, basic knowledge of sorption and desorption mechanisms is required. To better understand the kinetics of Ni precipitate formation and dissolution, a number of atomic-level investigative techniques were employed to examine the chemical and physical environments of the precipitates. If the sorbent phase released available Al during the sorption process, the resulting precipitate was a mixed Ni-Al layered double hydroxide (LDH). On the other hand, if Al was not present in solution, resulting from the sorbing material, α-$Ni(OH)_2$ precipitates were observed. As sorption aging time progressed up to two years, the dissolution studies showed that the stability of the Ni precipitates increased. The increase in stability with residence time was attributed to three mechanisms: (1) Al-

for-Ni substitution in the octahedral sheets of the brucite-like hydroxide layers, (2) Si-for-nitrate exchange in the interlayers of the precipitates, and (3) Ostwald ripening (size increase) of the precipitate phases. It appeared that the second factor, Si-for-nitrate exchange in the interlayers, contributed largely to the increase in stability. The Ni-Al LDH precipitates on pyrophyllite, which possessed all three aging factors, resulted in the most stable complexes. However, Ni-Al LDH on gibbsite, which could not undergo Si-for-nitrate exchange in the interlayers, were the least stable precipitates. The α-$Ni(OH)_2$ precipitates on a gibbsite/silica mixture, amorphous silica, and talc fell between pyrophyllite and gibbsite in regards to stability, which was probably a result of the degree of interlayer silication. Thus, the data collected by a combination of macroscopic, spectroscopic, microscopic and thermogravimetric techniques has direct applicability to Ni reactions in soils and the environment that comprise a heterogeneous collection of metastable Al- and Si-containing minerals.

In Chapter 2, the kinetics and mechanisms of Ni sorption on pyrophyllite, talc, gibbsite, amorphous silica, and a gibbsite/silica mixture were investigated. Sorption was shown to involve a fast and slow reaction step regardless of solution pH. The results of the spectroscopic, microscopic, and thermogravimetric studies showed the formation of Ni surface precipitates at relatively short time scales and evidence for conversion of the initial precipitate phase to a phyllosilicate precursor with aging time.

If the sorbent phase released available Al during the sorption process, the resulting precipitate was a mixed Ni-Al layered double hydroxide (LDH). On the other hand, if Al was not present in solution, resulting from the sorbing material, α-$Ni(OH)_2$ precipitates were observed. These results indicate that the formation of metal surface precipitates in soil and sediment environments is quite likely at circumneutral pH.

Chapter 3 investigated the effect of temperature on Ni sorption on the sorbents employed in Chapter 2. As expected, as temperature increased, the rate of Ni sorption increased. Kinetic batch studies conducted at temperatures of 9, 25, and 35 °C yielded apparent first-order forward rate coefficients (k_a). These data were then examined employing the Arrhenius and Eyring equations to determine E_a, A, $\Delta H^{\ddagger}$, $\Delta S^{\ddagger}$, and $\Delta G^{\ddagger}$. Based on values of E_a (93.05 to 123.71 kJ mol^{-1}) and $\Delta S^{\ddagger}$ (-27.51 to -38.70 J mol^{-1}), Ni sorption on these sorbents was surface-controlled and an associative mechanism, respectively. The $\Delta H^{\ddagger}$ values (90.60 to 121.26 kJ mol^{-1}) suggest, as indicated by E_a values, that an energy barrier was present for the system to overcome in order for the reaction to occur. Additionally, the large, positive $\Delta G^{\ddagger}$ suggest that these reactions consume energy. This was the first study to examine metal surface precipitation as a function of temperature. Although metal precipitation can occur in the natural

environment, these results show that temperature plays a large role in the rate of their formation.

The kinetics and mechanisms of Ni precipitate dissolution using a batch replenishment technique were presented in Chapter 4. The two main goals of this study were to examine the influence of aging time on the stability of the Ni precipitates and to investigate, via spectroscopic, microscopic, and thermogravimetric methods, the chemical and physical changes of one-month aged precipitates. An assortment of environmentally important dissolution agents (EDTA, oxalate, acetylacetone, and HNO_3) was employed to observe their ability to dissolve the Ni precipitates. Ligand-promoted dissolution was more effective in removing Ni from the precipitates than proton-promoted dissolution. In the macroscopic dissolution studies, as residence time increased, the amount of Ni removal from the precipitates decreased, indicating an increase in stability with aging. The increase in stability with residence time was attributed to three mechanisms: (1) Al-for-Ni substitution in the octahedral sheets of the brucite-like hydroxide layers, (2) Si-for-nitrate exchange in the interlayers of the precipitates, and (3) Ostwald ripening of the precipitate phases. The observed ranking, in terms of precipitate stability, was as follows: Ni-Al LDH on pyrophyllite > α-$Ni(OH)_2$ on gibbsite/silica mixture > α-$Ni(OH)_2$ on silica > α-$Ni(OH)_2$ on talc > Ni-Al LDH on gibbsite. XAFS, DRS, and HRTGA all showed that

although quantitative changes were evident, the chemical environmental of the Ni precipitates was unchanged. A novel AFM technique, Fluid TappingMode™, was used to visually observe the dissolution of 14-day aged Ni-Al LDH precipitates on pyrophyllite. The AFM study showed the aggressive dissolution behavior of EDTA compared to HNO_3. The information obtained from the research in Chapter 4 definitely proves that Ni precipitate stability increases with residence time and may result in the formation of Ni(-Al) phyllosilicate precursor phases. Research such as this is relatively scarce and more work is required to better understand the fate and potential mobility of metals in these precipitates.

5.2 Future Research

The research presented in this dissertation provides a plethora of information into possible Ni reactions transpiring in the environment through the use of cutting-edge techniques for examining microscopic-level Ni interactions with soils and sediments. However, this work provides only a partial insight to the overall picture in the real world. The work in this dissertation has opened more doors and created more questions than intended but were welcomed. Thus, there is a need to address topics for future research in this area.

One of the most important questions about Ni behavior in the environment is its interaction with inorganic and organic ligands in soils and sediments. Soil organic matter (SOM), organic acids, and chelates have been shown to have a high affinity for metals such as Ni. Could these ligands have inhibitory or enhancement affects on the formation of Ni precipitates?

The research in this dissertation shows that Ni sorption on clay minerals and oxides results in the formation of stable Ni precipitates. While it has contributed an understanding of aging time on formation of surface precipitates, the 1 to 2 year incubation times do not mimic long-term metal contaminated field sites. The influence of aging time on metal sorption and desorption reactions over very long times need to be more intensively studied. The formation of surface precipitates may obviate the need for remediation. However, if this is thought to work, studies will need to be conducted that emphasize the bioavailability of metals to plant and animal life from soil environments contaminated with metal surface precipitates.

There has been limited research done on remediation of metal contaminated sites. One avenue of remediation, that may be advantageous pertaining to cost, for Ni precipitates is phytoremediation. The majority of plants used in phytoremediation are Ni hyperaccumulators. Unfortunately, corporations have patented most of these plants

with little regard to how the hyperaccumulators actually work, just so long as they perform. Determining the exact organic ligand used by the plant for Ni uptake and knowing exactly where the metal is located within the plant may lead to better remediation techniques on a larger scale. Phytoremediation researchers have noted that Ni contaminated soils tend to have elevated levels of Mg after Ni hyperaccumulators are in place. It is thought that an organic ligand, perhaps oxalate, is responsible for Ni uptake by the plant roots and then Ni is translocated to the leaves of the plant to become the central atom in the porphyrin ring of chlorophyll normally occupied by Mg. Researchers have noted the Ni hyperaccumulators often have an olive or dirty-green leaf color after they are established at a Ni contaminated site. Application of phytoremediation to Ni precipitates would be very exciting, cost-effective research that can be accomplished in-situ, thus not requiring the removal of soil for the remediation process.

The temperature sorption studies reported in this dissertation have important implications. It is important to realize that environmental contamination does not often occur at 25 °C. Enhanced sorption and desorption at higher temperatures and retarded sorption and desorption at lower temperatures should be considered when predicting the fate and mobility of metal contaminants. Additionally, effects of

temperature and dehydration on metal sorption/release at different proton and ligand concentrations and residence times merits further study.

The future research needs discussed in this section represent some of the research that need to be examined to obtain a more complete understanding of the reaction behavior of Ni and other metals in the environment. While sorption models are usually designed to describe Ni uptake from solution as adsorption complexes, these models usually do not consider formation of surface precipitates nor do they accurately predict the transformations that take place over time. Incorporation of data on the kinetics and mechanisms of Ni and other metal interactions derived from spectroscopic, microscopic, and thermogravimetric studies will greatly enhance the accuracy and predictive capability of sorption models.

REFERENCES

Ainsworth, C. C., J. L. Pilon, P. L. Gassman, and W. G. Van Der Sluys. 1994. Cobalt, cadmium, and lead sorption to hydrous ferric oxide: Residence time effect. Soil Sci. Soc. Am. J. 58: 1615-1623.

Allmann, R. 1970. Doppelschichtstrukturen mit brucitähnilichen Schichtionen $[Me(II)_{1-x}\ Me(III)_x\ (OH)_2]^{+x}$. Chimia 24: 99-108.

Apel, M. L. and A. E. Torma. 1993. Determination of kinetics and diffusion-coefficients of metal sorption on Ca-alginate beads. Can. J. Chem. Eng. 71: 652-656.

Arrhenius, S. 1889. Ober die Reacktionsgeschwindigkait bei der Inversion von Rohrzucker durch Säuren. Z. physik. Chemie. 4: 226-248.

Atwood, J. D. 1997. Inorganic and organometallic reaction mechanisms. VCH Publishers, New York.

Bargar. J. R., S. N. Towles. G. E. Brown, Jr., and G. A. Parks. 1997. XAFS and bond-valence determination of the structures and compositions of surface functional groups and Pb(II) and Co(II) sorption products on single-crystal α-Al_2O_3. J. Colloid Interface Sci. 185: 473-492.

Bar-Tal, A., D. L. Sparks, J. D. Pesek, and S. Feigenbaum. 1990. Analyses of adsorption kinetics using a stirred-flow chamber: I. Theory and critical tests. Soil Sci. Soc. Am. J. 54: 1273-1278.

Belloto M., B. Rebours , O. Clause, J. Lynch, D. Bazin, E. Elkaim. 1996. Hydrotalcite decomposition mechanisms: A clue to the structure and reactivity of spinel-like mixed oxides. J. Phys. Chem. 100: 8535-8542.

Benjamin, M. M. and J. O. Leckie. 1981. Multi-site adsorption of Cd, Co, Zn, and Pb on amorphous iorn oxyhydroxide. J. Colloid Interface Sci. 79: 209-221.

Biber, M. V., M. Dos Santos Afonso, and W. Stumm. 1994. The coordination chemistry of weathering: IV. Inhibition of the dissoluiton of oxide minerals. Geochim. Cosmochim. Acta 58: 1999-2010.

Bish, D. L. 1980. Anion-exchange in takovite: applications to other hydroxide minerals. Bul. Mineral. 103: 170-175.

Bloom, P. R. and M. S. Erich. 1987. Effect of solution composition on the rate and mechanism of gibbsite dissolution in acid solutions. Soil Sci. Soc. Am. J. 51: 1131-1136.

Bondietti, G., J. Sinniger, and W. Stumm. 1993. The reactivity of Fe(III) (hydr)oxides: effects of ligands in inhibiting the dissolution. Colloid Surf. A: Physicochem. Eng. Asp. 79: 157-167.

Borggaard O. K. 1992. Dissolution of poorly crystalline iron oxides in soils by EDTA and oxalate. Z. Pflanzenernähr. Bodenk. 155: 431-436.

Bouldin C., L. Furenlid, and T. Elam. 1995. MacXAFS - An EXAFS analysis package for the Macintosh. Phys. B. 209: 190-192.

Brady, P. V. and J. V. Walther. 1992. Surface chemistry and silicate dissolution at elevated temperatures. Am. J. Sci. 292: 639-658.

Brindley, G. W. and G. Brown. 1984. Crystal sturctures of clay minerals and their X-ray identification. Mineralogical Society, London.

Brown, T. L., H. E. LeMay, Jr., and B. E. Bursten. 1994. Chemistry, the central science. 6th Ed. Prentice Hall, Englewood Cliffs, NJ.

Brümmer, G. W., J. Gerth and K. G. Tiller. 1988. Reaction kinetics of the adsorption and desorption of nickel, zinc, and cadmium by goethite. I. Adsorption and diffusion of metals. J. Soil Sci. 39: 37-52.

Brusseau, M. L. and P. S. Rao. 1989. Sorption nonideality during organic contaminant transport in porous media. CRC Critical Reviews in Environ. Control 19: 33-39.

Bryce A. L. and S. B. Clark. 1996. Nickel desorption kinetics from hydrous ferric oxide in the presence of EDTA. Colloids and Surfaces 107: 123-130.

Budavari, S., M. J. O'Neil, A. Smith, and P. E. Heckelman. 1989. The Merck index (11th ed.) Merck & Co., Inc., Rahway, NJ.

Bunnett, J. F. 1986. Kinetics in solution. pp. 171-250. *In* Investigations of rates and mechanisms of reactions, C. F. Bernasconi (ed), Wiley, New York.

Burns, R. G. 1976. The uptake of cobalt into ferromanganese nodules, soils, and synthetic manganese (IV) oxides. Geochim. Cosmochim. Acta 40: 95-102.

Burns, R. G. 1993. Mineralogical Applications of Crystal Field Theory. Cambridge University Press, Cambridge, U.K.

Cases, J. and M. François. 1982. Etude des propriétés thermodynamiques de l'eau au voisinage des interfaces. Agronomie. 2: 931-938.

Casey, W. H. and R. R. Westrich. 1992. Control of dissolution rates of orthosilicate minerals by divalent metal-oxygen bonds. Nature 355: 157-159.

Chang, C., and Ku, Y. 1994. Adsorption-kinetics of cadmium chelates on activated carbon. J. Hazard. Mater. 38: 439-451.

Charlet, L. and A. Manceau. 1992. X-ray absorption spectroscopic study of the sorption of Cr(III) at the oxide-water interface. II: Adsorption, co-precipitation and surface precipitation on ferric hydrous oxides. J. Colloid Interface Sci. 148: 443-458.

Chisholm-Brause, C. J., P. A. O'Day, G. E. Brown, Jr. and G. A. Parks. 1990. Evidence for multinuclear metal-ion complexes at solid/water interfaces from x-ray absorption spectroscopy. Nature 348: 528-531.

Chou, L. and R. Wollast. 1984. Study of the weathering of albite at room temperature and pressure with a fluidized bed reactor. Geochim. Cosmochim. Acta 48: 2205-2218.

Clark, C. J., and M. B. McBride. 1984. Chemisorption of Cu(II) and Co(II) on allophanes and imogolite. Clays Clay Miner. 32: 300-310.

Comans, R. N. J., and D. E. Hockney. 1992. Kinetics of cesium sorption on illite. Geochim. Cosmochim. Acta 56: 1157-1164.

Connaughton, D. F., J. R. Stedinger, L. W. Lion, and M. L. Shuler. 1993. Description of time-varying desorption kinetics: Release of naphthalene from contaminated soils. Environ. Sci. Technol. 27: 2397-2403.

Das, A., K., I. M. Pabi, and W. Gust. 1999. Kinetics of the eutectoid transformation in the Cu-In system. J. Mater. Sci. 34: 1815-1821.

Davis, J. A., and J. O. Leckie. 1978. Surface ionization and complexation at the oxide/water interface. J. Colloid Interface Sci. 67: 90-107.

Depège C., E. Z. El Metoui, C. Forano, A. de Roy, J. Dupuis, and J. P. Besse. 1996. Polymerization of silicates in layered double hydroxides. Chem. Mater. 8: 952-960.

d'Espinose de la Caillerie, J. B., M. Kermarec, and O. Clause. 1995. Impregnation of γ-alumina with Ni(II) and Co(II) ions at neutral pH: hydrotalcite-type coprecipitate formation and characterization. J. Amer. Chem. Soc. 117: 11471-11481.

Dutt, M., D. Kameshwari and D. Subbarao. 1998. Size of particle obtained by solution growth technique. Colloids Surf., A. 133: 89-91.

Dzombak, D. A., and F. M. Morel. 1990. Surface complexation modeling; Hydrous ferric oxide. John Wiley & Sons, New York.

Dzombak, D. A., and F. M. Morel. 1986. Sorption of cadmium on hydrous ferric oxide at high sorbate/sorbent ratios: Equilibrium, kinetics and modeling. J. Colloid Interface Sci. 112: 588-598.

Elkatib, E. A., G. M. Elshebiny, G. M. Elsubruiti, and A. M. Balba. 1993. Thermodynamics of lead sorption and desorption in soils. Z. Pflanzenernaehr. Bodenkd. 156: 461-465.

Elliott, H. A., and C. P. Huang. 1979. Adsorption characteristics of Cu(II) in the presence of chelating-agents. J. Colloid Interface Sci. 70: 29-44.

Elliott, H. A., and C.M. Denneny. 1982. Soil adsorption of cadmium from solutions containing organic-ligands. J. Environ. Qual. 11: 658-663.

Elzinga, E. J., and D. L. Sparks. 1999. Nickel sorption mechanisms in a pyrophyllite-montmorillonite mixture. J. Colloid Interface Sci. 213: 506-512.

Evans B. W., and S. Guggenheim. 1988. Talc, pyrophyllite, and related minerals. pp. 225-294. In Hydrous phyllosilicates (exclusive of micas), Vol. 19 (S. W. Bailey, ed.), Mineralogical Society of America, Washington, DC.

Eyring, H. 1935. The activated complex in chemical reactions. J. Chem. Phys. 3: 107.

Farley, K. J., D. A. Dzombak and F. M. Morel. 1985. A surface precipitation model for the sorption of cations on metal oxides. J. Colloid Interface Sci. 106: 226-242.

Fendorf, S. E., L. Guangchao and M. E. Gunter. 1996. Micromorphologies and stabilities of chromium (III) surface precipitates elucidated by scanning force microscopy. Soil Sci. Soc. Am. J. 60: 99-106.

Fendorf, S. E., G. M. Lamble, M. G. Stapleton, M. J. Kelley and D. L. Sparks. 1994. Mechanisms of chromium (III) sorption on silica. I. Cr(III) surface structure derived by extended x-ray absorption fine structure spectroscopy. Environ. Sci. Technol. 28: 284-289.

Fendorf, S. E. and D. L. Sparks. 1994. Mechanisms of chromium (III) sorption on silica. II. Effect of reaction conditions. Environ. Sci. Technol. 28: 290-297.

Ford R. G., A. C. Scheinost, K. G. Scheckel, and D. L. Sparks. 1999. The link between clay mineral weathering and structural transformation in Ni surface precipitates. Environ. Sci. Technol. 33(18): 3140-3144.

Ford R. G. and P. M. Bertsch. 1999. Distinguishing between surface and bulk dehydration-dehydroxylation reactions in synthetic goethites by high-resolution thermogravimetric analysis. Clays Clay Miner. 47(3): 329-337.

Furrer, G. and W. Stumm. 1986. The coordination chemistry of weathering, I. Dissolution kinetics of δ-Al_2O_3 and BeO. Geochim. Cosmochim Acta 50: 1847-1860.

Génin P., A. Delahaye-Vidal, F. Portemer, K. Tekaia-Elhsissen, and M. Figlarz. 1991. Preparation and characterization of α-type nickel hydroxides obtained by chemical precipitation: Study of the anionic species. Eur. J. of Solid State Inorg. Chem. 28: 505-518.

Grandstaff, D. E. 1986. The dissolution rate of forsteritic olivine from Hawaiian beach sand. pp. 41-59. *In* Rates of chemical weathering of rocks and minerals, (S. M. Colman and D. P. Dethier, eds.), Academic Press, New York.

Greenberg, J., and M. Tomson. 1992. Precipitation and dissolution kinetics and equilibrium of aqueous ferrous carbonate vs. temperature. Appl. Geochem. 7: 185-190.

Hansen, H. C. and C. B. Koch. 1998. Reduction of nitrate to ammonium by sulphate green rust: Activation energy and reaction mechanism. Clay Miner. 33: 87-101.

Harvey, D. T., and R. W. Linton. 1984. X-ray photoelectron spectroscopy (XPS) of adsorbed zinc on amorphous hydrous ferric oxide. Colloids and Surfaces 11: 81-96.

Hayes, K. F., A. L. Roe, G. E. Brown, Jr., K. O. Hodgson, J. O. Leckie, and G. A. Parks. 1987. In situ x-ray absorption study of surface complexes: Selenium oxyanions on α-FeOOH. Science 238: 783-786.

Hayes, K. F. 1987. Equilibrium, spectroscopic, and kinetic studies of ion adsorption at the oxide/aqueous interface. Ph.D. Dissertation, Stanford University.

Hering, J. G.; F. M. M. Morel. 1990. Kinetics of trace-metal complexation - ligand-exchange reactions. Environ. Sci. Technol. 24: 242-252.

Hsu, P. H. 1995. Aluminum hydroxides and oxyhydroxides, pp. 331-378, *In* Minerals in Soil Environments, J. B. Dixon and S. B. Weed (eds), Soil Science Society of America, Madison, WI.

James, R. O., and T. W. Healy. 1972. Adsorption of hydrolyzable metal ions at the oxide-water interface. I. Co(II) adsorption on SiO_2 and TiO_2 as model systems. J. Colloid Interface Sci. 40: 42-52.

Jencks, W. P. 1969. Catalysis in chemistry and enzymology. McGraw-Hill, New York.

Johnsson, P. A., M. F. Hochella, Jr., G. A. Parks, A. E. Blum and G. Sposito. 1992. Direct observation of muscovite basal-plane dissolution and secondary phase formation: An XPS, LEED and SFM study. pp. 159-162. *In* Water-Rock Interaction, Y. K. Kharaka and A. S. Maest (eds.). Balkema, Amsterdam.

Junta, J. L., and M. F. Hochella. 1994. Manganese (II) oxidation at mineral surfaces: A micrscopic and spectroscopic study. Geochim. Cosmochim. Acta 58: 4985-4999.

Karickhoff, S. W., and K. R. Morris. 1985. Sorption dynamics of hydrophobic pollutants in sediment suspensions. Environ. Toxicol. Chem. 4: 469-479.

Kamath P. V., and G. H. A. Therese. 1997. On the existence of hydrotalcite-like phases in the absence of trivalent cations. J. Solid State Chem. 128: 38-41.

Khan, S. U. 1973. Equilibrium and kinetic studies on the adsorption of 2,4-D and picloram on humic acid. Can. J. Soil Sci. 53: 429-434.

Kinniburgh, D. G., and M. L. Jackson. 1981. Cation adsorption by hydrous metal oxides and clay. pp. 91-160. *In* Adsorption of inorganics at the solid-liquid interface, M. A. Anderson and A. J. Rubin (eds.), Ann Arbor Sci., Ann Arbor, MI.

Laidler, K. J. 1965. Chemical kinetics. 2nd ed. McGraw-Hill, New York.

Ma, Y. B., and J. F. Liu. 1997. Adsorption kinetics of zinc in a calcareous soil as affected by pH and temperature. Commun. Soil Sci. Plant Anal. 28: 1117-1126.

McBride, M. B., A. R. Fraser, and W. J. McHardy. 1984. Cu^{2+} interaction with microcrystalline gibbsite. Evidence for oriented chemisorbed copper ions. Clays Clay Miner. 32: 12-18.

McBride, M. B. 1985. Influence of glycine on Cu^{2+} adsorption by microcrystalline gibbsite and boehmite. Clays Clay Miner. 33: 397-402.

Mellini, C. 1982. The crystal structure of lizardite 1*T*: Hydrogen bonds and polytypism. Am. Mineral. 67: 587-598.

Noggle, J. H. 1996. Physical chemistry. 3rd ed. HarperCollins Publishers, New York, NY.

Nowack, B., and Sigg, L. J. 1996. Adsorption of EDTA and metal-EDTA complexes onto goethite. Colloid Interface Sci. 177: 106-121.

O'Day, P. A., G. E. Brown, Jr., and G. A. Parks. 1994a. X-ray absorption spectroscopy of cobalt (II) multinuclear surface complexes and surface precipitates on kaolinite. J. Colloid Interface Sci. 165: 269-289.

O'Day P. A., J. J. Rehr, S. I. Zabinsky, and G. E. Brown Jr. 1994b. Extended X-ray absorption fine structure (EXAFS) analysis of disorder and multiple-scattering in complex crystalline solids. J. Amer. Chem. Soc. 116: 2938-2949.

O'Day, P. A., C. J. Chisholm-Brause, S. N. Towle, G. A. Parks, and G. E. Brown, Jr. 1996. X-ray absorption spectroscopy of Co (II) sorption complexes on amorphous silica (α-SiO_2) and rutile (TiO_2). Geochim. Cosmochim. Acta 60: 2515-2532.

Ogwada, R. A., and D. L. Sparks. 1986a. A critical evaluation on the use of kinetics for determining thermodynamics of ion exchange in soils. Soil Sci. Soc. Am. J. 50: 300-305.

Ogwada, R. A., and D. L. Sparks. 1986b. Kinetics of ion exchange on clay minerals and soil. I. Evaluation of methods. Soil Sci. Soc. Am. J. 50: 1158-1162.

Pandya K. I., W. E. O'Grady, D. A. Corrigan, J. McBreen, and R. W. Hoffman. 1990. Extended x-ray absorption fine structure investigation of nickel hydroxides. J. of Phys. Chem. 94: 21-26.

Pignatello, J. J., and B. Xing. 1995. Mechanisms of slow sorption of organic chemicals to natural particles. Environ. Sci. Technol. 30: 1-11.

Roberts D. R., A. M. Scheidegger, and D. L. Sparks. 1999. Kinetics of mixed metal-aluminum precipitate formation on a soil clay fraction. Environ. Sci. Technol. 33: 3749-3754.

Roe, A. L., K. F. Hayes, C. J. Chisholm-Brause, G. E. Brown, Jr., G. A. Parks, K. O. Hodgson. and J. O. Leckie. 1991. In-situ X-ray absorption study of lead ion surface complexes at the goethite/water interface. Langmuir 7: 367-373.

Scheckel. K. G., and D. L. Sparks. 2000a. Kinetics of the formation and dissolution of Ni precipitates in a gibbsite/amorphous silica mixture. J. Colloid Interface Sci. *In press.*

Scheckel. K. G., and D. L. Sparks. 2000b. Macroscopic dissolution of Ni surface precipitates on clay mineral and oxide surfaces. Soil Sci. Soc. Am. J. *In preparation.*

Scheckel. K. G., and D. L. Sparks. 2000c. Temperature affects on Ni sorption kinetics at the mineral/water interface. Soil Sci. Soc. Am. J. *In preparation.*

Scheckel K. G., A. C. Scheinost, R. G. Ford, and D. L. Sparks. 2000. Stability of layered Ni hydroxide surface precipitates – A dissolution kinetics study. Geochim. Cosmochim. Acta. *In press.*

Scheidegger, A. M., G. M. Lamble and D. L. Sparks. 1996a. Investigation of Ni sorption on pyrophyllite: An XAFS study. Environ. Sci. Tech. 30: 548-554.

Scheidegger, A. M., and D. L. Sparks. 1996. Kinetics of the formation and the dissolution of nickel surface precipitates on pyrophyllite. Chem. Goel. 132: 157-164.

Scheidegger, A. M., M. Fendorf and D. L. Sparks. 1996b. Mechanisms of nickel sorption on pyrophyllite: Macroscopic and microscopic approaches. Soil Sci. Soc. Am. J. 60: 1763-1772.

Scheidegger, A. M., G. M. Lamble and D. L. Sparks. 1997. Spectroscopic evidence for the formation of mixed-cation hydroxide phases upon metal sorption on clays and aluminum oxides. J. Colloid Interface Sci. 186: 118-128.

Scheidegger, A. M., G. M. Lamble and D. L. Sparks. 1998. The kinetics of nickel sorption on pyrophyllite as monitered by x-ray absorption fine structure (XAFS) spectroscopy. Geochim. Cosmochim. Acta 62: 2233-2245.

Scheinost, A. C. and D. L. Sparks. 1999. The role of Al in the formation of metal hydroxide precipitates at the clay mineral/water interface: A multiple-scattering XAFS analysis. J. Colloid Interface Sci., *In press*.

Scheinost, A. C., R. G. Ford, and D. L. Sparks. 1999. The role of Al in the formation of secondary Ni precipitates on pyrophyllite, gibbsite, talc, and amorphous silica: A DRS study. Geochim. Cosmochim. Acta, 63(19/20): 3193-3203.

Skopp, J. 1986. Analysis of time dependent chemical processes in soils. J. Environ. Qual. 15: 204-207.

Sparks, D. L. 1985. Kinetics of ionic reactions in clay minerals and soils. Adv. Agron. 38: 231-266.

Sparks, D. L. 1986. Kinetics of reactions in pure and mixed systems. pp. 83-178. *In* Soil physical chemistry. D. L. Sparks (ed.) CRC Press, Boca Raton, FL.

Sparks, D. L. 1989. Kinetics of soil chemical processes. Academic Press, San Diego, CA.

Sparks, D. L. 1991. Chemical kinetics and mass transfer processes in soils and soil constituents. pp. 584-587, *In* Transport processes in porous media. J. Bear and M. Y. Corapcioglu (eds.), Kluwer Academic Publishers, Dordrecht, Netherlands.

Sparks, D. L. 1995. Environmental soil chemistry. Academic Press, San Diego, CA.

Sparks, D. L. 1999. Kinetics of reactions in pure and mixed systems. pp. 83-178. *In* Soil physical chemistry, 2nd Ed., D. L. Sparks (ed.) CRC Press, Boca Raton, FL.

Sparks, D. L., and P. M. Jardine. 1981. Thermodynamics of potassium exchange in soil using a kinetics approach. Soil Sci. Soc. Am. J. 45: 1094-1099.

Sparks, D. L., S. E. Fendorf, P. C. Zhang and L. Tang. 1993. Kinetics and mechanisms of environmentally important reactions on soil colloidal surfaces. pp. 140-143. *In* Migration and fate of pollutants in soils and subsoils. D. Petruzzelli and F. G. Helfferich (eds.), Springer-Verlag, Berlin.

Sparks, D. L., A. M. Scheidegger, D. G. Strawn, and K. G. Scheckel. 1998. Kinetics and mechanisms of metal sorption at the mineral/water interface. pp. 108-135. *In* Mineral-water interfacial reactions; Kinetics and mechanisms. D. L. Sparks and T. J. Grundl (eds.). Am. Chem. Soc., Symp. Ser. 715, Washington, DC.

Sposito, G. 1984. The surface chemistry of soils. Oxford University Press, New York.

Sposito, G. 1986. Distiguishing adsorption from surface precipitation. pp. 217-228, *In* Geochemical processes at mineral surfaces. J. A. Davis and K. F. Hayes (eds.), Am. Chem. Soc., Symp. Ser. 323, Washington, DC.

Sposito, G. 1989. The chemistry of soils. Oxford University Press, New York, NY.

Steinberg, S. M., J. J. Pignatello, and B. L. Sawhney. 1987. Persistence of 1,2-dibromoethane in soils: Entrapment in intraparticle micropores. Environ. Sci. Technol. 21: 1201-1208.

Stern E. A., M. Newville, B. Ravel, Y. Yacoby, and D. Haskel. 1995. The UWXAFS analysis package: Philosophy and details. Phys. B. 209: 117-120.

Strawn, D. G., A. M. Scheidegger and D. L. Sparks. 1998. Kinetics and mechanisms of Pb(II) sorption and desorption at the aluminum oxide water interface. Environ. Sci. Technol. 32: 2596-2601.

Strawn, D. G., and D. L. Sparks. 1999. The use of XAFS to distinguish between inner- and outer-sphere lead adsorption complexes on montmorillonite. J. Colloid Interface Sci. 216: 257-269.

Stumm, W. 1992. Chemistry of the solid-water interface. Wiley, New York.

Stumm, W., and J. J. Morgan. 1981. Aquatic chemistry. Wiley, New York.

Stumm, W., and J. J. Morgan. 1996. Aquatic Chemistry. Wiley, New York.

Stumm, W., and E. Wieland. 1990. Aquatic chemical kinetics. Wiley, New York.

Stumm, W., and R. Wollast. 1990. Coordination chemistry of weathering: Kinetics of the surface-controlled dissolution of oxide minerals. Rev. in Geophysics 28: 53-69.

Sutheimer S. H., P. A. Maurice, and Q. Zhou. 1999. Dissolution of well and poorly crystallized kaolinites: Al speciation and effects of surface characteristics. Am. Mineral. 84: 620-628.

Tanahashi, M., T. Kokubo and T. Matsuda. 1996. Quantitative assessment of apatite formation via a biomimetic method using quartz crystal microbalance. J. Biomed. Mater. Res. 31: 243-249.

Taylor, R. M. 1984. The rapid formation of crystalline double hydroxy salts and other compounds by controlled hydrolysis. Clay Miner. 19: 591-603.

Taylor R. M., and R. M. McKenzie. 1980. The influence of aluminum on iron oxides. VI. The formation of Fe(II)-Al(III) hydroxy-chlorides, -sulfates, and -carbonates as new members of the pyroaurite group and their significance in soils. Clays Clay Miner. 28(3): 179-187.

Thompson, H. A. 1998. Dynamic ion partitioning among dissolved, adsorbed, and precipitated phases in aging cobalt(II)/kaolinite/water systems. Ph.D., Stanford University.

Thompson H. A., G. A. Parks, and G. E. Brown, Jr. 1999a. Dynamic interactions of dissolution, surface adsorption, and precipitation in an aging cobalt(II)-clay-water system Geochim. Cosmochim. Acta. 63: 1767-1779.

Thompson H. A., G. A. Parks, and G. E. Brown, Jr. 1999b. Ambient-temperature synthesis, evolution, and characterization of cobalt-aluminum hydrotalcite-like solids. Clays Clay Miner. 47: 425-438.

Torrent, J. 1991. Activation-energy of the slow reaction between phosphate and goethites of different morphology. Aus. J. Soil Research. 29: 69-74.

Towle, S. N., J. R. Bargar, G. E. Brown, Jr., and G. A. Parks. 1997. Surface precipitation of $Co(II)_{(aq)}$ on Al_2O_3. J. Colloid Interface Sci. 187: 62-68.

van den Berg, C. M. G., and M. Nimmo. 1987. Determination of interactions of nickel with dissolved organic material in seawater using cathodic stripping voltammetry. Sci. Total Environ. 60: 185-195.

van't Hoff, J. H. 1884. Etudes de Dynamique Chimique. F. Muller & Co., Amsterdam.

Wilkins, R. 1974. The study of kinetics and mechanisms of reactions of transition metal complexes. Allyn and Bacon: Boston, MA.

Xia, K., A. Mehadi, R. W. Taylor, and W. F. Bleam. 1997. X-ray absorption and electron paramagnetic resonance studies of Cu(II) sorbed to silica: Surface-induced precipitation at low surface coverages. J. Colloid Interface Sci. 185: 252-257.

Zabinsky S. I., J. J. Rehr, A. Ankudinov, R. C. Albers, and M. J. Eller. 1997. Multiple-scattering calculations of X-ray-absorption spectra. Phys. Rev. B. 52: 2995-3009.

Zhang, P. C. and D. L. Sparks. 1990. Kinetics and mechanisms of sulfate adsorption/desorption on geothite using pressure-jump relaxation. Soil Sci. Soc. Am. J. 54: 1266-1273.

Zinder, B., G. Furrer and W. Stumm. 1986. The coordination chemistry of weathering. II. Dissolution of Fe (III) oxides. Geochim. Cosmochim. Acta 50: 1861-1869.